University of Naples “Federico II”
Departement of Physics

PhD Thesis in
Novel Technologies for materials sensors and imaging

New hollow core fiber design and porphyrin thin film deposition method towards enhanced optical fiber sensors

April 2013

Author: Abolfazl Bahrampour

Tutor: Prof. Antonello Cutolo
Prof. Antonello Andreone
Prof. Agostino Iadicicco
Co-tutor: Prof. Giovanna De Luca

New hollow core fiber design and porphyrin thin film deposition method towards enhanced optical fiber sensors

By

Abolfazl Bahrampour

Spring 2013

To first teacher, professor and spiritual master, my father

To the source of strength and patient my lovely Mother

And

Memory of My lovely sister “Mahboube”

Napoli Napoli!

Quando osservo Napoli da Castel Sant'Elmo, non c'è posto che vedo che non mi faccia sentire a casa. E mi sovviene il ricordo di quando appena arrivato qui la gente mi diceva "quando qualcuno viene a Napoli, arriva piangendo e va via piangendo".
Non sono d'accordo: ora che parto semplicemente non ho parole.

Di nuovo da Sant'Elmo, guardando Spaccanapoli, il ricordo del giorno in cui ci camminai p' 'a primma vòta, non potendo evitare di fissare ogni cosa a partire da Montesanto, passando per Santa Chiara, Piazza San Domenico Maggiore, fino alla chiesa del Duomo, il tutto accompagnato dalla migliore persona che io conosca, Guido. A cui non basta dire grazie perchè non ci sono parole che esprimano bene la sua gentilezza. Se le espressioni della lingua vengono fuori dal ripetersi delle esperienze degli uomini, sono sempre state troppo poche quelle esperienze capaci di creare le parole adatte a descrivere una persona unica come lui. ***Guido*** *per favore accetta dal profondo del mio cuore i miei ringraziamenti senza parole.*
Ancora Spaccanapoli, camminando verso Via dei Tribunali, questa volta con un amico, camminando quasi a caso:"Napoli è il posto per un random walk non solo nei calcoli matematici o nella fisica quantistica credimi!". Ogni punto di questa città t'fà ascì pàzz'! Ho fatto esperienza della gente di Napoli prima con lui, ***Danilo,*** *ormai un mio fratello.*
A Napoli la Storia vive ancora: camminarci dentro significa camminare nella sua storia, dagli antichi greci ai romani, fino all'ultima guerra mondiale e ai juorn' nuost'! Sì Napoli è ancora tutto questo. Quì le persone

hanno imparato a costruire non a distruggere. Qui hanno costruito una città sotterranea per costruire la città esistente.
E ancora camminando, ora sul lungomare d' 'e part' a' Caracciolo fino a Margellina, la Luna piena mi ricorda "E 'a Luna Rossa me parl' 'e te!". Così cerco un posto per sedermi e parlare con la Luna! Qui anche la Luna è tua amica.

Ah! Napoli! Napoli!
Ogni tanto fare solo un giro per il centro, ascoltare la mia musica preferita, raggiungere il Caffè del Professore, e un fantastico caffè che mi ricorda "ah che bell'ò cafè!": jàmm' sentimmancella!
Oppure camminare da Piazza Bellini fino al Kestè e turnà addèret', parlare di cultura e della vita, con un'amica speciale che risponde alle mie domande sulla città della cultura, dell'arte, dell'università, dalla grande folla, dal grande vulcano, e d' 'o paese d' 'o Sòle! ***Daniela,*** *mi fai amare Napoli.*
Ah! Napoli! Napoli!
Ogni volta che vado via da questa città, è come dire: "E io dico: i' parto, addio!". E tu dici "Torna a Napoli. Tiene 'o core 'e nun turnà?"

Abolfazl Bahrampour
Marzo/2013

Acknowledgments

This thesis would have been remained a dream without the help and support of some people whom I wish to address this acknowledgment. It gives me great pleasure in acknowledging the support and help of my tutors Prof. Antonello Cutolo, Prof. Antonello Andreone and Prof. Agostino Iadicicco and my co-tutor Prof. Giovanna De Luca.

It is too difficult to express my gratitude. I cannot find words to express my gratitude to Prof. Cutolo, for introducing me to two amazing scientist and friend Agostino and Giovanna.

It gives me great pleasure in acknowledging, kindness, support and help of Professor Andreone in every situation.

Agostino, my tutor and moreover a good friend, three years of my life, every day meeting, email and phone calls even , if I was in Iran, discussing on project. Thank you Agostino for being supportive and compassionate. I consider it an honor to work with you.

Giovanna, I will never forget hours of explaining chemistry in your amazing style of descriptions, it has always a super impact on me, Thank you for all. I will never forget your supports and kindness.

I would like to thanks Prof. Cusano for all scientific ideas and important hints during collaboration in both part of my thesis with him, also, I am delighted to acknowledge, Armando for the effort in helping me in some computational tricks. Thank you Prof. Michele Giordano for the nice collaboration and letting me to work in IMCB," a friendly environment and brilliant works". Here I would like to thank my friends which I was used to meet them daily, In IMCB, Gabriella, Domenico, Angelo.

Napoli gives me amazing life, I would like to thank Piero for being a good friend, and it was always nice when you open the door of lab and offering some minutes of coffee break.

Napoli brought to my life friends for "life time". There are friends in Napoli, which they just made my life as happy as I wanted, Fatima and Sergei, whom I wish I can

always meet them frequently. Thanks to you for one single thing, "being the friends I look for whole my life".

Sara, “The Dearests”, whenever I felt upset, either on my mobile phone or Facebook I could find, a call or a left message by you, I think you and your presence were a chance for making life smooth for me.

Liuji for all advices, and hours of speaking about everything, my wise friend!

Napoli, and three years here without thinking of you my dear friend Faran, is not possible for all helps and fun we had together.

I am indebted to my many colleagues who supported me, Alberto and his fiancé Sara, Behzad, Deborah, Nitin ,Ehsan, Mohadeseh, Karo, Zahra, Arash, Mariano (and his amazing helps Napolitano-Italiano translation), Ndubiusi, Alan, Oktay, Laleh and Ali thanks to you for all the moments of being and being effective.

I can’t speak about Italy and forget the name of Simeone and Minturno, the family I love here, please accept my profoundest “Ringraziamenti”.

I owe my deepest gratitude to my brother and sister, the lovely couple of physics department (In Napoli and Now of course In Ottawa), and who supported me to find my life in Napoli. Who hosted me long time in their house, and teach me how to live in Napoli, I can’t forget and I won’t forget kindness and moments of being with you. From playing games to cooking “Kaleh Pache”. Ebrahim and Rahil, it is simply bad I can’t head to your office for taking a tea or asking to come for lunch. No way to forget you. Napoli without you “Yaeni Hasrat”.

Writing acknowledgement is difficult and writing about beloved Sisters and Brother, is the most difficult one. “Thank you”, “thanks you”, “thank you”, not only for last three years, but for all the time we spent and you were close in happiness and sad supporting and caring. Maryam, Azadeh and Mohammad-Javad thanks with all love.

I share the credit of my work with my father, for letting me to spent my last year of PhD in his group at Sharif University of technology, moreover for being the best.

And no words can express my thoughts and feelings for thanking you, My Mother.

Table of contents:

NAPOLI NAPOLI!.....4

ACKNOWLEDGMENTS.....6

TABLE OF CONTENTS: 8

LIST OF FIGURES 11

LIST OF TABLES 14

THESIS ABSTRACT AND STRUCTURE.....16

SECTION I.....22

CHAPTER 1 CHEMICAL SENSORS FOR ENVIRONMENTAL MONITORING ...23

1.1 Introduction 23

1.2 Optical fiber sensor 27
1.2.1 Reflectometric configuration.....28
1.2.2 Evanescent wave fiber optic sensor.....29
1.2.3 Functional material.....30
1.2.4 Applications 30

1.3 Summary 33

Bibliography 34

CHAPTER 2 UV INDUCED DEPOSITION TECHNIQUE: A SIMPLE APPROACH TO INTEGRATE OPTICAL FIBER WITH FUNCTIONALIZED THIN FILM 40

2.1 Introduction 40

2.2 UV Induced deposition technique on planar silica substrate 41

2.3 UV induced deposition technique on fiber end 43
2.3.1 Integration of TPyP (4) on the fiber tip 44
2.3.2 Deposition of tetrakis (4-sulfonatophenyl) porphyrin (TPPS) molecule on the fiber end.....48
2.3.3 Silver deposition on the optical fiber structures 52

2.4 Summary **55**

Bibliography **56**

CHAPTER 3 SENSING CAPABILITIES OF TPPS COATED OPTICAL FIBER SENSORS 59

3.1 Introduction **59**

3.2 Deposition process: TPPS film deposition **61**

3.3 Reflectance Spectra analysis **62**

3.4 Sensing capability to detect acid vapor **65**

3.5 Dynamic response of the sensor **67**

3.6 Fluorescence Spectroscopy **69**

3.7 Microscopic results for Acid and Base vapor exposed films **71**

3.8 Summary **73**

Bibliography **74**

SECTION II 77

CHAPTER 4 INTRODUCTION TO PHOTONIC CRYSTAL FIBERS 78

4.1 Introduction **78**

4.2 The Light confinement mechanism **80**
4.2.1 Modified total internal reflection 81
4.2.2 Photonic bandgap guidance 81

4.3 Properties and applications **90**

4.4 Loss mechanisms **91**
4.4.1 Intrinsic loss of solid core PCF 91
4.4.2 Intrinsic loss for Hollow-core fibers 93
4.4.3 Confinement loss of PCFs 94

4.5 Fabrication process of photonic crystal fibers **95**
4.5.1 Stack-and-draw technique 96
4.5.2 Extrusion fabrication process 97

4.6 Summary and some considerations **98**

Bobliography **98**

CHAPTER 5 INTRODUCTION TO PHOTONIC QUASICRYSTALS 103

5.1 Introduction **103**

5.2 Mathematics and generation Algorithms of Quasicrystal patterns 104

5.2.1 Periodicity to Aperiodicity: historical remarks 104

5.2.2Algorithms to generate quasicrystal structures 105
5.2.2.1 8-fold symmetry 105
5.2.2.2 10-fold symmetry 106
5.2.2.3 12-fold symmetry 107

5.3 Photonic properties of quasicrystals 108
5.3.1 Light propagation in 2D photonic quasicrystals and localization 108
5.3.2 Plasmonics in metallic photonic quasicrystals 108
5.3.3 Laser action in aperiodic structures 109
5.3.4 Negative refraction 110

5.4 Quasicrystal band analysis 110
5.4.1 Band analysis of 12-fold 112
5.4.2 Band analysis of 8-fold Ammann-Beenker 116

5.5 Summary 119

Bibliography 120

CHAPTER 6 HOLLOW CORE PHOTONIC QUASICRYSTAL FIBER 123

6.1 Introduction 123

6.2 Band and modal study of 12-fold air hollow core quasi crystal fiber 124
6.2.1 Primitive cell and bandgap calculation of 12-fold 126
6.2.2 Modal analysis and results of 12-fold HC-PQF 129
6.2.3 Electromagnetic field profile for 12-fold 130
6.2.4 Confinement loss for 12-fold HC-PQF 132

6.3 8-fold challenges and solution 132
6.3.1 Geometry for a Modified 8-fold structure 133
6.3.2 Band gap calculation for M8-fold design 136
6.3.3 Modal analysis and results of M8-fold HCPQF 139
6.3.4 Electromagnetic field profile for M8-fold 139
6.3.5 Confinement loss for M8-fold HC-PQF 140

6.4 Summary 141

Bibliography 141

CHAPTER 7 CONCLUSION 143

LIST OF PUBLICATIONS AND SCIENTIFIC PRODUCTION 146

List of figures

Figure 1. 1: Schematic representation of a chemical sensor array system (from [2]). 25
Figure 1. 2: Schematic view of the Fabry-Perot-based configuration. 28
Figure 1. 3: A schematic of chemical sensor based on fiber coupled evanescent wave. 29

Figure 2. 1: The schematic setup of UV induced deposition technique on planar surface. 42
Figure 2. 2 The schematic setup of UV-induced deposition technique on the optical fiber, (inset) a photo of experimental setup. 43
Figure 2. 3: (a) optical fiber transversal section with 200 μm core (properly cleaved); (b) cleaver for optical fiber with diameter up to 250 μm. 44
Figure 2. 4: The schematic of Tetra (4-pyridyl) porphin molecule and Pyridyl as radical. 45
Figure 2. 5: Schematically drawing of deposited Porphyrin film on optical fiber. 45
Figure 2. 6: Optical fiber cross section in different status: (a) Bare fiber; (b) deposited film after 30 minutes UV exposure; and (c) deposited film after two hours UV exposure. 46
Figure 2. 7: The spectroscopy setup and inset, represents the mechanism reflectance analysis. 47
Figure 2. 8: Reflectance spectra of deposited fibers as function of the UV exposure time (all curve are normalized to the bare fiber spectrum): The blue curve refers to non-deposited fiber (as reference value 100%), red curve, pink, black and cyan represent reflectance spectra of deposited fibers with 30 minutes, 1, 2 and 3 hours UV exposure, respectively. 48
Figure 2. 9: The Tetrakis (4-sulfonatophenyl) porphyrin. 49
Figure 2. 10: The cleaved fiber by appropriate cleaver with 200 μm core diameter. 50
Figure 2. 11: Representation of the TPPS porphyrin thin film on the fiber. 50
Figure 2. 12: Reflectance spectra of TPPS deposited on the fiber end the bare fiber normalized reflectance (blue curve) the deposited fiber in 1 hour of UV irradiation (green curve) the black curve presenting the spectrum of TPPS film after 2 hours of deposition, an d a three hours deposited film(red curve). 51
Figure 2. 13: (a) the cleaved fiber (b) silver deposited thin film with respect to 30 minutes of UV irradiation in a 2mg/l concentration. 53
Figure 2. 14: SEM observation of the deposited region on the fiber end from the pink rounded region. 54
Figure 2. 15: The statistical graph of chemical species. 54

Figure 3. 1: (a) deposited optical fiber, as optical fiber sensor (b) the cartoon presentation of H- and J aggregation of TPPS molecule 60
Figure 3. 2: (a) bare fiber (b) the deposited optical fiber tip. 62
Figure 3. 3: Spectroscopy setup for reflectance analysis of acid and base exposure with sensing aim 63
Figure 3. 4: the normalized bare fiber dotted blue curve and TPPS coated film on fiber end (dashed black curve). 64
Figure 3. 5: the post deposition treatment on the fiber tip. 65
Figure 3. 6: Comparison of the reflectance spectra of the fiber tip in different statuses. 66
Figure 3. 7: The amplitude of the reflected signal at 490 nm vs. exposure cycles. 67
Figure 3. 8: The green curve presenting the acid form and the base form is presented in red curve the important wavelengths are shown by vertical lines. 68

Figure 3. 9: Amplitude of the reflected signal at fixed wavelength 489nm versus time during (a) base exposure and (b) acid exposure. 69
Figure 3. 10: Presenting the optical setup to achieve fluorescence spectrum of acid vapor or alkaline sensor. 70
Figure 3. 11: The deposited film without any treatment black line, the TPPS coated film treated by acid (blue curve) and base exposed TPPS coated film (red curve). 71
Figure 3. 12: (a) Acid exposed film deposited on the optical fiber (b) base exposed thin film on the optical fiber. 72
Figure 3. 13: (a) acid exposed thin film (b) base exposed thin film. 72
Figure 3. 14: The film treated by acid just after base and second round with base. 73

Figure 4. 1 (a) Solid core PCF, (b) Bragg fiber schematic, (c) Hollow core PCF. 80
Figure 4. 2: Is presenting the triangular lattice. And its fabrication. The microscopic photography is kindly provided by Optoelectronic group university of Naples "Parthenope". 82
Figure 4. 3: The schematic presentation of the HC-PCF problem. 83
Figure 4. 4: (a) The triangular lattice (b) unitcell to define lattice. 85
Figure 4. 5: The band diagram versus in-plane wave vector in the irreducible B-zone (inset) at the out of plane$kz\ \Lambda/2\pi\ = 0.05$. 85
Figure 4. 6: Is representing the band diagram versus in plan wave vector in the Irreducible B-zone at kz $\Lambda/2\pi$ =0.5. 86
Figure 4. 7: Band diagram versus in plane wave vector at kz $\Lambda/2\pi$ =0.5. 86
Figure 4. 8: The projected band gap as function of out of plane wave vector. 87
Figure 4. 9: Representation of the band gap a function of effective index vs. normalized wavelength. 88
Figure 4. 10: The optical fiber with a hollow core of diameter of R formed by triangular periodic structure 88
Figure 4. 11: The representation of dispersion relation for the fundamental mode of the hollow core. 89
Figure 4. 12: The Intensity patterns ($ez \bullet\ Re[E\hat{}* \times H]$) of the Hollow-core fiber, corresponding to (a) λ/Λ=0.63 (b) λ/Λ=0.67(c) λ/Λ=0.71 90
Figure 4. 13: The electric field representation of the fundamental mod at λ/Λ=067. 90
Figure 4. 14: The drawing and stack process 96

Figure 5. 1: 2-D Ammann-Beenker tiling with 8-fold symmetry, (a) the sizes and geometrical specification, and (b) decorating process by canonical substitution. 106
Figure 5. 2: 10-fold geometry structure. 107
Figure 5. 3: (a) the generator (b), (c) off-spring dodecagon type I, II respectively. 107
Figure 5. 4: 12-fold structure and approximant for band calculation 111
Figure 5. 5: (a) decagonal repeating portion, (b) 8-fold different portion 112
Figure 5. 6: Band structure of 12-fold quasi crystal calculated by FEM in presence of (a) $kz\ \Lambda/2\pi = 0.4\ , b\ kz\Lambda/2\pi\ = 0.6\ and\ ckz\ \Lambda/2\pi = 1$. 114
Figure 5. 7: Electromagnetic field profile calculated for a structure with 7 cylinders of r/Λ=0.49 as approximant. The fields are corresponding to eigenfrequency of (a) $\omega\Lambda/2\pi c$=0.6, (b) $\omega\Lambda/2\pi c$=0.61, (c) $\omega\Lambda/2\pi c$=0.6105, (d) $\omega\Lambda/2\pi c$=0.64, (e) $\omega\Lambda/2\pi c$=0.68, (f) $\omega\Lambda/2\pi c$=0.68 115
Figure 5. 8: approximant for 8-fold and Bravias vectors. 116
Figure 5. 9: Band structure of a 2-D, 8-fold symmetry with employing a square approximant for different out of plane wave vector, (a)$kz\ \Lambda 2\pi = 0.2(b)\ \ (kz\ \Lambda)/2\pi = 0.4, (c)\ \ (kz\ \Lambda)/2\pi = 0.8$. 117

Figure 5. 10: Electromagnetic field profile calculated for a structure with 14 cylinders of r/Λ=0.37 in the approximant. The field profiles is belong to eigenfrequencies of (a) ωΛ/2πc=0.52055, (b) ωΛ/2πc=0.5205, (c) ωΛ/2πc=0.5202, (d) ωΛ/2πc=0.5201, (e) ωΛ/2πc=0 119

Figure 6. 1: A big portion of 12-fold generated by stampifli algorithm. 125
Figure 6. 2: the 12-fold HC-PQF cross section with a core of (a) 7 holes integrated (b) 19 holes integrated. 126
Figure 6. 3: Bandgap map of the 12-fold structure as a function of out of plane wave vector, investigation between 10 bands. 127
Figure 6. 4: Band diagram calculated for 12-fold considering 20 bands where (a) $(kz\ \Lambda)/2\pi = 1.6, (b)(kz\ \Lambda)/2\pi = 1.7$. 128
Figure 6. 5: Band diagram of 12-fold structure as effective index vs. normalized wavelength, (inset) band gap as function of out of plane wave vector(two gaps is shown by violet and black error bars). 129
Figure 6. 6: Effective index of fundamental mode of fiber with core of R=2.05Λ black line and fiber with core R=1.38Λ blue solid line. 130
Figure 6. 7: The electromagnetic field profile of 12-fold HC-PQF in case where R=2.05Λ at (a) λ/Λ=0.5, (b) λ/Λ=0.55. 131
Figure 6. 8: The electromagnetic field profile of 12-fold HC-PQF in case where R=1.38Λ at (a) λ/Λ=0.51, (b) λ/Λ=0.55. 131
Figure 6. 9: Represents confinement loss for 12-fold HC-PQF for R=1.38Λ. 132
Figure 6. 10: Representing the bandgap map of 8-fold. 133
Figure 6. 11: (a) Ammann–Beenker structure and (b) a modification approach as dotted red circles. 134
Figure 6. 12: (a) overlap of Ammann-Beenker structure (red dotted lines), and M8-fold as solid black structure. (b) Geometrical details of M8-fold and M8-fold approximant. 135
Figure 6. 13: Cross section of M8-fold HC-PQF, with core radius of R=1.38Λ. 136
Figure 6. 14: Band structure of a 2-D, M8-fold symmetry with employing a square approximant for different out of plane wave vector, (a)$kz\ \Lambda 2\pi = 1.45(b)\ (kz\ \Lambda)/2\pi = 1.65.$ 137
Figure 6. 15: Electromagnetic field profile calculated for a structure with 14 cylinders with $SAFF = 82\%$. the field profiles are belong to eigenfrequencies of (a) ωΛ/2πc=2.19, (b) ωΛ/2πc=1.92, (c) ωΛ/2πc=2.04 at certain reciprocal vector k=(0.5,0.5,1.9). 138
Figure 6. 16: The band map as a function of effective index and (inset) band map with eigenfrequeny presentation (blue and red error bars represent bandgap). 139
Figure 6. 17: Represent effective index of fundamental mode of M 8-fold HC-PQF. 139
Figure 6. 18: The field profile of the fundamental mode in case of M8-fold fiber at (a) λ/Λ=0.628, (b) λ/Λ =0.671. 140
Figure 6. 19: represents confinement loss for M8-fold HC-PQF. 141

List of tables

Table 2. 1: The chemical contents of the deposited film. 55

Table 6. 1: The comparison of position and radius of geometrical component of 8-fold structure and M8-fold lattice. 136

Thesis Abstract and structure

In last decades, optoelectronic components and in particular fiber optic based devices have received great attention for their advantages in several fields. For instance, fiber optic technology is with a short history but with very rapid development in the past and now its impact in all aspects of communication field is well evident whereas fiber–optic sensors (FOSs) provide the potential to create very sensitive and selective measurements. Enhanced FOSs are typical achievement by combining the versatility of the optical transducer and an intelligent design of the active materials. An appropriate sensitive material permits to reach a high sensitivity and selectivity towards specific chemicals [1] while an optimized transducer enhances the interaction between guided light and sensitive materials itself.

In this scenario, the present PhD work is focused on two main aspects.

a) In the first two years we experimentally investigated simple method to integrate an appealing class of functional material with optical fiber transducer. Due to strong multidisciplinary nature of this activity, it was principally provided at Institute for Composite and Biomedical Materials *(IMCB) of the CNR,* Napoli, in cooperation with Giovanna De Luca and Michele Giordano (both with IMCB-CNR).
b) In the third year of this thesis, during my collaboration with photonic research group in Sharif University of Technology, Tehran, the research activity was principally focused on the design of novel hollow core quasi-crystal fiber via theoretical/numerical analysis for their appealing features in sensing and communications fields.

In following, please permit us to briefly introduce both topics. Among different functional materials as possible candidates to realize novel sensors, porphyrin derivatives have received great attentions [2]. Therefore recently a novel UV-induced technique for deposition of porphyrin molecules on planar substrates/devices has been widely investigated [3]. The main aim of this work is to integrate porphyrin molecules with non-conventional substrate such optical fiber end via UV-assisted procedure. We experimentally demonstrated that different porphyrin molecules such as TpyP (4) (meso-tetra (4-pyridyl) porphyrin) and tetrakis (4-sulfonatophenyl) (TPPS) present their compatibility to this technique. Finally an extent of stated method represents

ability to integrate silver on optical fiber, taking the photophysical benefits of silver salts. In all results of mentioned coating method a thin film completely aligned in the core of fiber has been obtained. Additionally sensing potentialities of TPPS coated optical fiber for environmental monitoring in the detection of acid vapor was experimentally investigated by spectral measurements of the reflected signal. TPPS self-assembled film can switch from H to J aggregate as a response to presence of base and acid gases and thus different spectral features can be observed in the reflected spectrum as consequence of probe exposure. In the base (deprotonated) form of TPPS film four Q-bands is observable according to H-form of aggregation whereas in acid treated film very narrow and intense peak (bandwidth of ~14 nm), around 490 nm is visible. This particular feature indicate the presence of very ordered J-aggregates [3]. In this work spectral analysis and dynamic time response are investigated and reported [4] demonstrating very appealing sensing features in the detection of acid and basic vapors.

During the last year coinciding with the staying in Photonic research group of Sharif university of technology in Tehran (Iran) and keeping direct and frequent contact with prof. Iadicicco (Univ. Naples Parthenope), the research activity was principally focused on the design of novel quasi-crystal hollow core fiber via numerical analysis based on FEM analysis. Photonic crystal fibers (PCFs) is refering to a new class of optical fibers that have wavelength-scale morphological microstructure running down their length [5]. They, according to their guiding mechanisms, may be divided into index-guiding PCFs (IG-PCFs) and photonic band-gap fibers (PBFs). In light of their composite nature, PCFs enable a plenty of possibilities and functionalities hitherto not possible. In the last decade, particular attention has been focused on PBFs due to the lattice assisted light propagation within the hollow core (HC) [6] and thus named hollow core PCFs (HC-PCFs). As matter of fact in an HC-PCF, light is confined and guided by a PBG in the air core. This particular feature has a number of advantages such as lower Rayleigh scattering, reduced nonlinearity, novel dispersion characteristics, and potentially lower loss compared to conventional optical fibers [7, 8]. In addition, the HC-PCFs also enable enhanced light/material interaction (in the core region), thus providing a valuable technological platform for ultra-sensitive and distributed biochemical sensors [9, 10]. For instance the ability to host material in the hollow core permits to integrate HC-PCFs with fluorescent molecules [10]. Hence the HC-PCF integration with functional material can lead to promising high sensitivity sensors.

It is worth noting that in past all HC-PCFs and IG-PCFs focused on the periodic structure (such as the PBGs generated by holes of various shapes arranged on a triangular, square, honeycomb, or Kagome periodic arrays lattice) [7,11,12]. Recently a few works are focused on new fiber design based on photonic quasi crystals (PQs) [13-14]. PQs are a special class of aperiodic crystals having long-range order but lacking periodicity. Several research demonstrates that PQs can produce interesting photonic properties [15-17]. For example, the PQs can offer higher rotational symmetries, more isotropic Brillion zone, and hence potentially can open more uniform PBGs at a lower dielectric contrast [15]. On this concept IG-PQFs based on PQs are proposed since 2010 [14]. Sun et al. proposed a HC-PQF based on 12-fold symmetric PQs [14]. It is shown that this type of fiber provides two PBGs enabling simultaneous guidance in two wavelength regions. Here our attention relies on the design of novel hollow core photonic quasi crystal fibers via theoretical/numerical analysis employing finite element method (FEM). The FEM allows the PCF cross-section in the transverse x – y plane to be divided into a patchwork of triangular elements, which can be of different sizes, shapes, and refractive indices. In particular, we first studied HC-PCF with triangular lattice, and then we focused quasi-crystal fiber involving 12-fold, and 8-fold structures. Successively a modified 8-fold structure was designed and investigated to improve guided band gaps and dispersion properties of pristine 8-fold.
In conclusion this work is organized in two sections, each one including three chapters. Here we briefly present the chapter's contents of both sections.

Section I:

Chapter 1. An introduction to chemical sensing and chemical optical fiber sensor is provided, and we present fiber's abilities and its advantages as chemical sensor. Followed, by an approach to optical fiber modification and employing functional material to enhance sensing characteristic of optical fiber sensors.

Chapter 2. A UV-Induced deposition technique for coating of different porphyrin molecules is introduced. The results for adoption this technique on the optical fiber technology with aim to fabricate new class of fiber devices is presented and analyses. We studied different Porphyrin molecules and the extension of technique to molecules such as silver in this chapter.

Chapter 3. The integration of a tetrakis (4-sulfonatophenyl) porphyrin (TPPS) thin film with optical fiber technology is obtained via UV-induced deposition. This leads to the growth of TPPS thin films the potential of porphyrins as functional

materials, enable the design of novel active and passive in-fiber devices. Here, the presence of intense and narrow band in the reflected spectra is successfully exploited to detect corrosive or toxic vapors, such as strong volatile acids and bases, at room temperature and pressure. Florescence analysis and reflectometry for detection of volatile acid and base is presented and stability and dynamic response of new device as chemical optical fiber sensor is discussed.

Section II :

Chapter 4. The fundamental principles of operation of Photonic crystal fibers (PCF) are discussed. First of all a general introduction to PCF is given. Then the attention is focused on the derivation and the physical interpretation of the band structure and guiding mode. The concept of loss will be discussed completely and finally fabrication process for the new class of optical fiber is presented.

Chapter 5. We introduce Photonic quasicrystal structures, several optical properties and novel applications of quasicrystals will be discussed. Different methods of quasicrystal analysis will be named. Finally, we study band structure and field distribution of 2 dimensional, 8-fold (Ammann-Beenker) and 12-fold symmetry with employing finite element method. We came to results of appearing band gap in such a low refractive index contrast of 1:1.46 with increasing the out of plane wave vector.

Chapter 6. The fundamental principles to introduce Hollow core photonic Quasicrystal fibers is presented. Comparative study of different symmetries for study of Hollow core Photonic quasicrystal fiber (HC-PQF) is obtainable. Band gap for different structures of 12-fold and 8-fold will be calculated .we propose a new geometry which is called modified 8-fold with idea of attaining enhanced hollow core photonic quasi crystal. Expectedly Modified 8-fold represents extraordinary gap profile at $\frac{\lambda}{\Lambda} < 1$ permitting simultaneous propagation in two spectral windows. The results of bandgap are in agreement with fundamental mode dispersion relation and loss of the proposed HC-PQF.

Conclusion, conclude this work with a discussion of achievement and ongoing activities and an outline of the main conclusions.

Bibliography:

1. M. Giordano, M. Russo, A. Cusano, A. Cutolo, G. Mensitieri, and L. Nicolais, “Optical sensor based on ultrathin films of δ-form syndiotactic polystyrene for fast and high resolution detection of chloroform,” Appl. Phys. Lett 85, 5349 (2004).
2. G. De Luca, G. Pollicino, A. Romeo, S. Patane, and L. Monsù Scolaro, “Control Over the Optical and Morphological Properties of UV-Deposited Porphyrins Structures,” Chem. Mater 18, 5429-5436 (2006).
3. Monsu ScolaroL, RomeoA, CastricianoM, De Luca G, Patane S, MicaliN.,"Porphyrin deposition induced by UV irradiation" Journal oftheAmerican Chemical Society 2003;125:2040–1,(2003).
4. Abolfazl Bahrampour, Agostino Iadicicco, Giovanna De Luca, Michele Giordano, Anna Borriello, Antonello Cutolo, Andrea Cusano, Luigi Monsù Scolaro,"Porphyrin thin films on fiber optic probes through UV-light induced deposition", Optics & Laser Technology 49, 279-283,(2013).
5. .R.F. Cregan, B.J. Mangan, J.C. Knight, T.A. Birks, P.St.J. Russell, P.J. Roberts, D.C. Allan, "Single-mode photonic bandgap guidance of light in air," Science 285, 1537-1539, (1999).
6. P. Russel, "Photonic Crystal Fibers," Science 299, 358-362, 2003.
7. L. Vincetti, F. Poli, and S. Selleri, “Confinement loss and nonlinearity analysis of air-guiding modified honeycomb photonic bandgap fibers,” IEEE Photon. Technol. Lett., vol. 18, no. 3, pp. 508–510, Feb. 1, (2006).
8. K. Saitoh and M. Koshiba, “Leakage loss and group velocity dispersion in air-core photonic bandgap fibers,” Opt. Express 11, 3100-3109 (2003),
9. Petru Ghenuche, Hervé Rigneault, and Jérôme Wenger,"Hollow-core photonic crystal fiber probe for remote fluorescence sensing with single molecule sensitivity,"Optics Express Vol. 20, Iss. 27, pp. 28379–28387 (2012).
10. Huang CG, Zhu L,"Enhanced optical forces in 2D hybrid and plasmonic waveguides: OPTICS LETTERS, 35, 10, 1563-1565 (2010).
11. M. Yan, P. Shum, and J. Hu, "Design of air-guiding honeycomb photonic bandgap fiber," Optics Letters, Vol. 30, Issue 5, pp. 465-467 (2005).
12. F. Poletti and D. J. Richardson, "Hollow-core photonic bandgap fibers based on a square lattice cladding," Opt. Lett. 32, 2282-2284 (2007).

13. H. Zhao, R. Proietti Zaccaria, P. Verma, J. Song, H. Sun,"Single-mode operation regime for 12-fold index-guiding quasicrystal optical fibers",Applied Physics B,100, 3,499-503,(2010).
14. Xiwen Sun; Hu, D.J.J., "Air Guiding With Photonic Quasi-Crystal Fiber," Photonics Technology Letters, IEEE , vol.22, no.9, pp.607,609, May1, (2010)
15. Y.S Chan, C.T. Chan and Z.Y. Liu,"Photonic Band Gaps in Two Dimensional Photonic Quasi-Crystals", Phys. Rev. Lett. 80, 956 (1998).
16. M. E. Zoorob, M. D. B. Charlton, G. J. Parker, J. J. Baumberg & M. C. Netti,"Complete photonic bandgaps in 12-fold symmetric quasicrystals," Nature 404, 740-743, (2000)
17. A. Ricciardi, I. Gallina, S. Campopiano, G. Castaldi, M. Pisco, V. Galdi, and A. Cusano, “Guided resonances in photonic quasicrystals,” Opt. Express 17(8), 6335–6346 (2009).

Section I

Chapter 1

Chemical sensors for environmental monitoring

1.1 Introduction

The ability to detect, quickly and efficiently, the presence of specific chemicals can be a matter of life or death. Leaks of toxic or explosive gases, monitoring of glucose or anesthetics in the bloodstream, examining for harmful compounds in foods, all needs selective, sensitive, fast and reliable chemical sensing devices.

Chemical sensors in most cases can be schematically described as composed of a sensitive and a transducer. The sensitive part interacts with the surrounding environment, collects and concentrate molecules at or within the surface undergoing physical changes. Instead transducer converts physical or chemical occurrence into an interpretable and quantifiable term. The heart of the chemical sensor is the sensitive element which is the interface between the transducer and external environment so that the nature, the selectivity and sensitivity of the sensor depends upon these interactive materials.

Suitable materials to use as sensing part should optimize specific interactions with a target analyte or narrow class of analytes, should provide a fast and reversible diffusion of the penetrants, small recovery times and should maintain the physical state so as the geometry over several cycles of use, in order to avoid hysteretic effects, and thus to ensure the reproducibility [1]. Candidate materials for chemical sensors include polymers, organic monolayers, ceramics, metals semiconductors, nanostructured and porous materials (nanomaterials, molecular sieves, sol-gels, and aerogels), biomolecules and combination of them. Of course, adequate and detailed physical, chemical and structural characterizations of the exploited sensing materials are essential for a deep understanding of their properties and for a rational design of the whole chemical sensor and of its performances.

The natural step following the selective recognition of an analyte from the sensitive layer is the signal transduction, and thus the choice of an opportune technique to read the physical or chemical changes occurring at the sensing part. Transducing approaches can include mechanical (acoustic wave, micromechanical), electrochemical, optical, thermal, and electronic types. Each has strengths and weaknesses relative to the particular application. Each transduction principle can be implemented in a variety of configurations, and fabricated by multiple approaches, resulting in many different sensing platforms. Unfortunately, does not exist a unique, best approach for the developing of a reliable, robust, sensitive and selective chemical sensor or sensing system. In fact, the appropriate choice of the sensitive material and transducing technique depends upon a number of factors, among which:

• The environmental conditions in which the sensor will operate, such as temperature, presence or absence of possible chemical interferences, harsh or corrosive conditions, electromagnetic interferences

• Application needs, which include the desired limit of detection, dynamic range, precision, stability, selectivity and lifetime (aging).

• Power, size and weight requirements

• Cost and ease of use

• Safety in the measurement environment

In addition, many applications may be best addressed using not a single chemical sensor but chemical sensors arrays, a schematic representation of which, reported in figure 1.1, evidences the steps from analyte collection to response output [2].

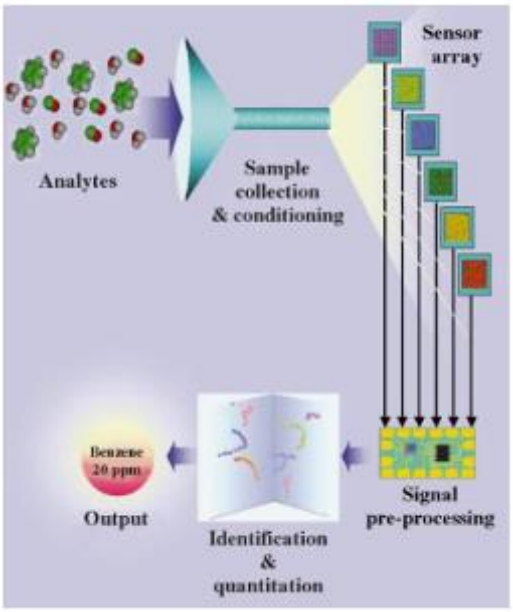

Figure 1. 1: Schematic representation of a chemical sensor array system (from [2]).

The generic "sensor array" can be composed by a few to tens of sensors, either based upon a single material class on a single type of transducer, or various type of materials combined with one or even more transducers (with different operating principles). The "sample collection and conditioning" step may include preconcentration and/or preseparation. To provide greater accuracy and robustness of the system responses, the array may sometimes include some proportion of intentionally redundant (nominally identical) sensors. A "signal pre-processing" is also necessary not only for analog-to-digital conversions, filtering of noise, and multiplexing, but also to streamline the output from the sensors by averaging identical elements, eliminating "out of range" responses, normalization, scaling, etc. The "identification & quantitation" steps typically utilize some forms of pattern recognition to classify the response as one of the "known" (previously measured and calibrated) analyte; better methods can also identify a response pattern that does not match any known analytes, rather than making an incorrect identification. Depending on the method chosen, quantitation can be performed simultaneously, or as a separate step following analyte identification. "Output" can take many forms, from a simple indicator light or alarm to the display of analyte identities, concentrations, probability that the identification is accurate, and related information.

The advantage of using multiple sensor devices hinges on the relaxed selectivity of the individual chemically-sensitive coatings. However, the cost of simpler coatings comes

in the form of more complex mathematical analysis requirements (for example to select the optimal sensor elements from a menu of many possibilities, or/and to interpret the results of multi-element arrays by means of appropriate pattern-recognition algorithms) and the increased power required to run such recognition algorithms on suitable processors. In the following paragraph the most exploited chemical sensors for environmental monitoring are introduced with particular attention to the optical fiber sensors, which in the last decades demonstrated to be very attractive for a wide range of chemical sensing applications.

A number of chemical sensors have been developed for environmental monitoring applications [3], a classification of which can be carried out upon their principal physics and operating mechanisms. The most exploited transduction principles in chemical sensing are the mass change and the resistivity/conductivity change of the sensitive element occurring upon the exposure to and consequent sorption of the molecules of target environmental analytes. The first physical parameter in many cases is determmined by shift in the resonant frequency of an oscillating piezoelectric crystal. Depending on the kind of the vibrational wave propagated in the crystal, a mass sensor can be classified as Quartz Crystal Microbalance (QCM) or Surface Acoustic Wave (SAW) sensors [4-7]. They typically use a thin polymeric film as sensitive layer [8], however SAW and QCM-based chemical sensors using other sensitive coatings have been studied [9, 10]. Instead, resistivity/conductivity changes are typically detected by conductometric measurement carried out on sensitive materials (mainly semiconducting metal oxides and conjugated polymers) deposited between two electrodes. That sensor technologies are called Metal Oxide Semiconductors (MOS) and Conductive Organic Polymer (COP) sensors [11]. During the last two decades, however, a remarkable interest has been also focused on optical transduction principles for the measurement of chemical and biological quantities [12]. Since the development of the first optical sensors for the measurement of CO2 and O2 concentration [13], a large variety of devices based upon optical methods have been used in chemical sensors and biosensors including ellipsometry, spectroscopy (luminescence, phosphorescence, fluorescence, Raman), interferometry (white light interferometry, modal interferometry in optical waveguide structures), spectroscopy of guided modes in optical waveguide structures (grating coupler, resonant mirror), and surface plasmon resonance. In these sensors a desired quantity is determined by measuring the refractive index, absorbance

and fluorescence properties of analyte molecules or of a chemo-optical transducing medium [14-24].

1.2 Optical fiber sensor

Optical fiber sensors are very attractive in chemical sensing applications, due to unique characteristics deriving by the use of optical fibers. The most outstanding property of optical fibers is their ability to transmit optical signal over large distant with minimum loss permitting an optical fiber sensor remotely located from the instrumentation. Beside what have mentioned small size, light weight, high flexibility and, temperature variation resistant make optical fibers suitable candidates for chemical measurement in harsh situation or where hazardous chemicals may be present or extremes in temperature occur. Since optical power density can be controlled from the source to be kept in certain limits optical fiber sensors in compare to their electronic counterpart are extremely safer, therefore preferred in explosive environments.

As a sort of benefit, Optical signals are immune to electrical and magnetic interference, so the optical signal which contains measurement information won't be effected by power lines or electrical machinery.

Fiber optic sensing is very versatile, since the absorbance, reflectance, fluorescence, fluorescence quenching, evanescent wave, surface plasmon resonance, and luminescence, can all be exploited as measurements parameters, and several wavelengths launched in the same fiber in either direction form independent signals. This can be an approach for monitoring of several chemicals with a single fiber sensor and also simultaneously monitoring of environment parameters variations which could dramatically affect the chemicals concentration measurements, such as the temperature of the fiber.

Basically, a challenge remains from the very beginning of this discussion, the motivation of optical fibers is to protect the light from environment. Therefor a suitable modification on the fiber is needed permitting light interaction with medium in a controllable manner. The mentioned change is usually in two aspects one is geometrical modification of the fiber and the second is regarding to integration of a functional material. Geometrical modification enhance light interaction with medium while functional material take the role of selectivity of sensor. Indeed functional material basically acts as translator for chemical to optical signals. In the following we study

different arrangement of optical fiber sensors and some issues in functional materials and finally some applications of chemical fiber sensors will be mentioned.

1.2.1 Reflectometric configuration

The reflectometric arrangement is fundamentally based on a low quality and extrinsic Fabry-Perot interferometer and, as schematically shown in figure 1.2, uses a thin sensitive film deposited at the fiber end suitably cleaved and prepared, to produce a Fabry-Prot cavity. The thin film acts accordingly as an optical cavity where the first mirror is given by the fiber-thin film layer interface while the second one is given by the sensitive layer-air medium interface.

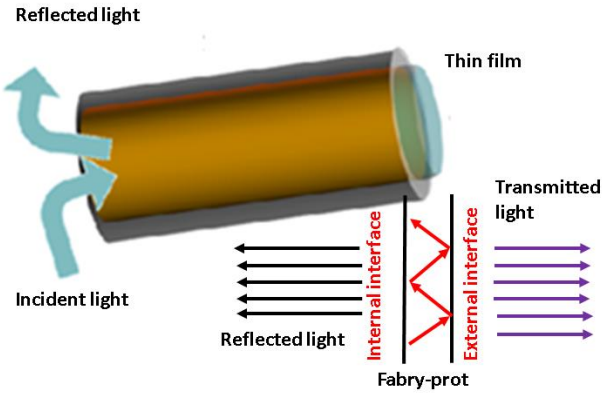

Figure 1. 2: Schematic view of the Fabry-Perot-based configuration.

First described in 1899 by Fabry and Perot [25], the interferometer known by their names makes use of multiple reflections between two closely spaced surfaces. In fact the light is partially reflected each time it reaches the second surface, resulting in multiple offset beams which can interfere with each other (see Figure 1.2).

The amount of light reflected at the first interface can be calculated as the sum of the multiple reflected beams and is strongly influenced even by very small changes of the distance between the two surfaces (cavity) or its optical properties [26]. This explains the massive use of such configuration in fiber optic-based sensing in the two past decades, especially for the detection and measurements of various physical, chemical and biomedical parameters [27, 28]. All these characteristics, combined with the possibility to integrate a number of sensitive materials with the optical fibers by means of very simple, low cost and versatile deposition techniques make it one of the most attractive and useful optoelectronic configuration especially suitable for practical

applications. The key point of the reflectometric configuration is thus the dependence of the reflectance at the fiber/film interface on the optical and geometrical properties of the sensitive materials.

1.2.2 Evanescent wave fiber optic sensor

Optrodes or reflectometry technique use the light delivered to the terminal end of the fiber to generate a signal near the fiber end terminal, while evanescent wave sensors exploit the electromagnetic wave of the penetrated light at the surface between the fiber core and the fiber cladding. The evanescent wave is able to interact with analytes within the penetration depth (where light penetrate in cladding during TIR process), therefore, material placed in this region, can be detected due to either, the absorption of propagating light or generation of fluorescence during the exposing of analytes can be detected. The main benefit of evanescent wave technique rely on the ability to couple electromagnetic waves out of the fiber into the surrounding medium, which opens a large interaction medium with materials far as it is shown in figure 1.3.

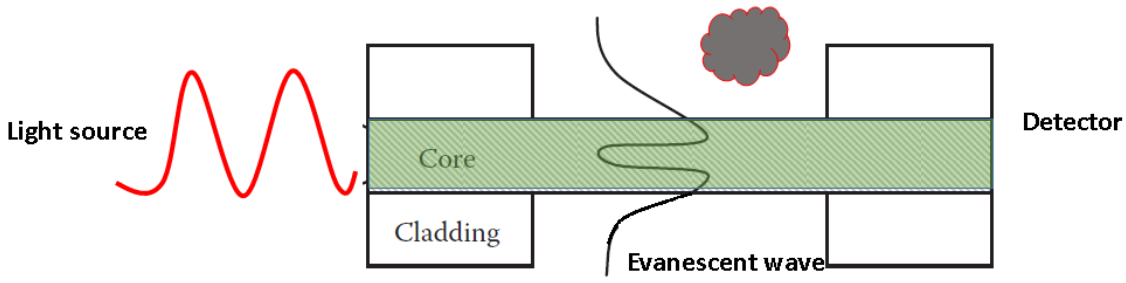

Figure 1. 3: A schematic of chemical sensor based on fiber coupled evanescent wave.

Therefore, higher sensitivity is expected. Several approach is mentioned to employ, evanescent field based sensors include attenuated total reflection type sensors and total internal reflection fluorescence sensors. In the first case, the evanescent wave produces a net flow of energy across the reflecting surface in the surrounding medium. The energy transfer can lead to attenuation in reflectance that depends on the absorption of the evanescent waves. In TIRF, when the evanescent light selectively excites a fluorophore, the fluorescence emitted by the fluorophore can be coupled back into the fiber and guided all the way to the detector. Several arrangement to enhance these sensor sensitivity and better interaction with environment has been proposed such as

D-shaped optical fibers or holey fibers for evanescent base chemical optical fiber sensors [29, 30].

1.2.3 Functional material

Generally, selectivity of sensor is defined based on the ability of sensor to intelligently recognize the target's optical features. This can be managed with employing, functional materials integrated on the fiber. Therefore such functional material might be chosen carefully and integrated on the optical fiber. An intelligent optical setup will play important rule to connect the chemical reaction to optical signal. In a good optical fiber sensor the functional material should response only on the concentration change of the target. The other requirement for selectivity is, the optical signal must be dedicated to the target not for other chemical or physical effect around optical fiber sensor. Therefore, the selection of material with specific optical functionality during interaction with target is important

Over the past decades porphyrin derivatives have been extensively employed as functional materials for optical sensing, due to their capabilities to interact with different chemical species and to translate this binding through changes of their characteristic photophysical properties [31, 32]. The relative easiness of the synthetic protocols resulting to these molecules permits to design porphyrins having a good processability, and recent results have shown that porphyrin derivatives are well suited for integration with optical fiber technology, critical for remote sensing within hazardous environments. For instance, fluorescence quenching or observation of signature band sin the absorbance spectra of properly selected porphyrins and has been recently reported in the literature [33–35]. Also a gas sensor able to detect ammonia emitted from human skin has been obtained through coating an unclad fiber with a multi layered porphyrin film with exploiting Evanescent wave technique [36, 37]. Hence a careful selection of functional material alongside of an intelligent design of optical setup can lead to a selective and sensitive optical fiber sensor.

1.2.4 Applications

Humidity and pH Sensors

One of the most important measurand in the environmental monitoring is the humidity level. Humidity measurement is essential for several fields, including meteorological services, chemical processing, food industry, construction fields, air-conditioning, computer and electronic industries. Optical fiber humidity sensors with taking the unique advantages of optical fiber got more precision in compare with the electronic counterpart.

Basically fiber optics humidity sensors function on the basis of water-sensitive materials (intelligently) coated on fiber to modulate optical signal propagating in fiber [38].

Another important measurand that need high attention is the pH value. Actually measurement of pH can be the matter of death or life. Practically in several application fields such as medicine, environmental sciences, agriculture, food and oil and gas to measure pH is an important concern. For instant a pH sensor was developed on the basis of a pH-sensitive fluorescence dye-doped cellulose acetate thin-film modified polymer fiber [39], approving the ability of tailoring the pH response range through doping a surfactant in the sensing film.

Environmental Gas sensors

Most of Industries create gaseous releases as a result of the production process. From chemical processing to energy production industries, all produce different amount and category of gases emission. Therefore control and monitoring gas level during the production process and in the post processing is necessary.

Consequently, it is of importance to study and develop gas sensing techniques that are selective, quantitative and fast acting. To satisfy these requirements optical fibers in different class are exploited. Since optical fiber sensors are very attractive for fast, real time detection and measurement gases.

With development of optical fiber and appearing photonic crystal fiber, gas and liquid sensing got huge impact.as cladding holes run along the optical fiber and the presence (or change) of such molecules is visible in the air holes of the fiber since a loss appears in the transmission spectrum for the characteristic wavelengths of the particular gas species. The first approach to this technique was through the use of a solid core hexagonal lattice PCF [40]. Acetylene sensing was also demonstrated by exploiting HC-PCFs. Gas diffusion inside of a hollow core PCF was successfully monitored by measuring the attenuation of the guided light through the fiber due to absorption of light by the gas sample [41]. A methane sensor functioning at 1670 nm was developed

through absorption spectroscopy for gas concentration inside of a hollow core fiber, with a minimum of detection of 10 ppmv [42]. A hydrogen sensor was reported based in a tapered fiber with coated with thin layers and evanescent field, could be absorbed with gas-permeable thin films [43]. The detection of volatile organic compounds was verified through a reflectometer [44]. Oxygen and nitrogen detection was performed by spontaneous Raman backscattering [45].

Molecular Sensors

This class of sensors is very attractive and important for applications such as biochemistry or biomedicine for detection of molecules like DNA, proteins and cancer cells. Optical fibers are very appropriate for such applications, given that they can be used to control the interaction between guided light and target simultaneously acting as a tiny sample chamber.

DNA Introducing PCFs instead of glass chips can lead to a significant improvement of the sensitivity, with respect to the present technology. DNA sensors based in HC-PCFs were reported: by using a highly efficient evanescent-wave detection of fluorophore-labeled biomolecule in aqueous solutions positioned in the air holes of the microstructured part of the PCF [46]

Protein Sensors, Detection of quantum-dot-labeled proteins was reported using a soft-glass fiber and near-infrared light. The protein concentration was measured using this fluorescence capture approach, with a detection limit of 1 nM and extremely small sample volume (of order of 10 pl) [47]. The rendering of biologically glass three hole fiber via immobilization of antibodies within the holes of the fiber cross-section was demonstrated for detection of proteins [48]. The recognition of the proteins that bind to the antibodies is made through fluorescence labeling, opening up the possibility for measurement of multiple biomolecules via immobilization of multiple antibodies. Using Surface plasmon resonance in a fiber with silver nanoparticles cluster the detection of 4-mercaptobenzoic acid was reported [49]. Evanescent-field sensing is a very used technique in molecular detection: inserting Methylene Blue in the cladding holes of a solid core PCF its absorption spectrum was measured [50] a salinity sensor was also developed using a polyimide-coated High birefringence Sagnac interferometer based on coating-induced radial swelling [51]. This sensor achieved a salinity sensitivity of 0.742 nm/ (mol/L.

More chemicals sensing

Besides the chemicals mentioned in previous sections, many other chemical compounds can also be detected by using fiber optic chemical sensors. For example, nitro aromatics in water can also be sensed by using a mid-IR spectrum based fiber-optic sensor and ozone can be detected by using an ultraviolet (UV) evanescent wave sensor [52]. In an ozone sensor, the sensing probe is made of gas-permeable silicone cladding; the output signal shows a linear response to ozone over the range of 0.02–0.35 vol% with a response time of about 1 min. Furthermore, pesticide analysis can be realized by using surface plasmon-resonance (SPR) biosensors. For example, a gold-coated waveguide SPR sensor can be used to monitor the attachment of biotin–avidin layers to the surface of the sensor in an aqueous environment, which enables the detection of the pesticide simazine [53]. Finally, there are numerous other types of fiber optic chemical sensors for monitoring acid, wastes, ground water, toxicity, and heavy metals [54-56].

Clinical Sensing

The fast development of bio-reflect meters has also enabled the potential clinical applications, which effected from both the healthcare and economic points of view. For instant, an optical fluorescence biosensor has been investigated for blood gaseous contaminant analysis, which is used to measure blood gases and pH via fluorescence measurements [57]. Fiber optic biosensors have also been employed for blood fatty (cholesterol measurement. The sensor is based on the use of a cholesterol oxidizer and oxygen transduction. The signal is obtained by the oxygen sensitive complex immobilized in the bioactive layer. Hence, the signal can be correlated to the cholesterol concentration [58], and in situ glucose monitoring has been developed by luminesce quenching method ruthenium diimine [59].

Finally, fiber optic biosensors is also used to monitor drug delivery. Here the drug dissolution level is monitored by a UV/vis spectral analysis [60].

1.3 Summary

In this chapter we have shown different classes of optical fiber sensors are developing and they lead to very high performance in sensing capabilities. Functional materials and especially porphyrin molecules as class of good functional material have been

introduced. In this chapter we have shown that optical fiber and Porphyrin molecules are able to provide outstanding potential respecting to sensing aims, the amount of papers in chemistry of Porphyrin and patents of photonic crystal fiber chemical sensors are the witness of this statement. Therefore an intelligent design of functional material, optical setup and transducer will lead to a selective, accurate and real time and in situ, remote sensor.

In the next chapters we will study experimentally the possibility to use porphyrin molecules as functional material and their integration with optical fiber technologies to realize novel in-fiber device for sensing applications. In particular we will analyze non-conventional UV-assisted deposition technique to selectively integrate different porphyrin molecules onto core region of fiber optic ends. Successively investigation on sensing properties in environmental monitoring field of novel fiber devices will be reported and discussed. Here acid vapor detection was successfully demonstrated by very simple and low cost total in-fiber devices.

Bibliography

1. J. W. Grate, M. H. Abraham, ““Solubility interactions and the selection of sorbent coating materials for chemical*sensors* and *sensor* arrays,” ”Sensors and Actuators, B 3, 85–111, (1991).

2. J. Ricco, R. M. Crooks, and J. Janata, “Chemical Sensors: A Perspective of the Present and Future ”The Electrochemical Society Interface, Vol. 7, No. 4, p. 18, Winter 1998,

3. O. S. Wolfbeis, Anal. Chem., ““Fiber-optic chemical sensors and biosensors,”” 76(12) pp 3269 – 3284, (2004).

4. L.J. Kepley, R.M. Crooks, A.J. Ricco, “Self Assembled, Composite Monolayer: A New Paradigm for Sensor Design,”Anal. Chem. 643191, (1992).

5. M Consales, S Campopiano, A Cutolo, M Penza, P Aversa, G.Cassano, M Giordano and A Cusano, Sensors and Actuators B, 118 (2006) 232–242.

6. M.Penza, G.Cassano, P.Aversa, A.Cusano, M.Consales, M.Giordano, L.Nicolais, ““Carbon nanotubes thin films fiber optic and acoustic VOCs sensors: Performances analysis,” IEEE Sensors Journal, Vol. 6, No. 4. pp: 867-875, (2006).

7. J. Hartmann, J. Auge and P. Hauptmann, “Possibilities of *chemical sensing* at the semiconductor/electrolyte interface” Sensors and Actuators B: Chemical, Volume 19, Issues 1-3, Pages 429-433, (1994).

8. J. W. Grate, Chemical Society Reviews 100(7), “"Acoustic Wave Microsensor Arrays for Vapor Sensing."” 2627-2647, (2000).

9. M.Penza, G.Cassano, P.Aversa, F.Antolini, A.Cusano, M.Consales, M.Giordano, L.Nicolais, “Carbon nanotubes coated multi-transducing sensors for VOCs detection” Sensors and Actuators B, 111-112, 171-180, (2005).

10. J. Zhang, J. Hu, Z.Q. Zhu, H. Gong, S.J. O’Shea, “. Quartz crystal microbalance coated with sol–gel-derived indium–tin oxide thin films as gas sensor for NO detection.” Colloids and Surfaces A: Physicochemical and Engineering Aspects Volume: 236, Issue: 1-3, April 1, 2004, pp. 23-30

11. D. James, S. M. Scott, Z. Ali, and W. T. O’Hare, “Chemical sensors for electronic nose systems”, Microchip. Acta 149, 1–17 (2005)

12. F. Baldini, North Atlantic Treaty Organization, “Optical chemical sensors”, Springer, 2006, ISBN 1402046103

13. D.W.Lubbers, N.Opitz, “Eine neue pCO 2 -bzw: pO 2 -Messonde zur Messung des pCO 2 Oder pO 2 von Gasen und Flüssigkeiten,”Zeitschrift Fur Naturforschung C 30, 532–533, (1975).

14. I. Zudans, W.R. Heineman and C. J. Seliskar, “In situ measurements of chemical sensor film dynamics by spectroscopic ellipsometry. Three case studies” Thin Solid Films, Volumes 455-456, 710-715, (2004).

15. I.M. Steinberg, A. Lobnik, O.S. Wolfbeis, “Characterisation of an optical sensor membrane based on the metal ion indicator Pyrocatechol Violet” Sensors and actuators. B, Chemical, vol. 90, pp. 230-235, (2003).

16. G. Orellana, Analytical and Bioanalytical Chemistry Volume 379, (2004).

17. J. Homola, S. S. Yee, G. Gauglitz, “Surface plasmon resonance sensors: review,” Sensors and Actuators B 54, pp. 3-15, (1999).

18. A. G. Mignani, L.Ciaccheri, A.Cimato, C. Attilio, P.R. Smith, “Surface plasmon resonance*sensors*: review”, Sensors and Actuators B 111–112, 363–369, (2005).

19. A. G. Mignani, Andrea A. Mencaglia, Leonardo Fiaccheri, Proceedings of the SPIE, Volume 5952, pp. 89-99 (2005).

20. F. J. Arregui, I.R. Matias, R.O. Claus, “Nanofilms on Hollow Core Fiber-Based Structures: An Optical Study”, IEEE Sensors Journal, Vol.3, No.1, February (2003).

21. O.S. Wolfbeis, “Fiber Optic Chemical Sensors and Biosensors” Boca Raton, CRC Press, (1991).

22. A. Brecht, G. Gauglitz, Bioelectron. “Optical probes and transducers” 10, 923–936, (1995).

23. G. Gauglitz, “Optochemical *Sensors* in *Sensors*: A Comprehensive Survey”Sensor Update vol. 1, VCH Verlagsgesellschaft, Weinheim, (1996).

24. G. Boisde, A. Harmer, “Chemical and biochemical sensing with optical fibers and waveguides” Artech House, Boston (1996).

25. Fabry C and Perot A, "Theory et applications d'une nouvelle méthode de spectroscopie interférentielle" Ann. Chim. Phys., Paris 16 115-44, (1899).

26. Angus Macleod,"The early days of optical coatings”, J. Opt. A: Pure Appl. Opt., 1,799 (1999).

27. Dakin, J. and Culshaw, B. (ed. by), Optical Fiber Sensors: Principles and Components, Artech House, Boston, (1988).

28. Jackson, D. A." Monomode optical fiber interferometers for precision measurement". J. Phys. E: Sci. Instrum., 18, 981–1001, (1985).

29. Y. L. Hoo, W. Jin, H. L. Ho, D. N. Wang and R. S. Windeler, Evanescent-wave gas sensing using microstructure fiber, Opt. Eng., 41, 1, pp. 8–9, (2002).

30. D. L. Wise and L. B. Wingard, Biosensors with Fiberoptics, Humana Press, Clifton, NJ, pp. 1–300, 19917. W. Jin, G. Stewart, M. Wilkinson, B. Culshaw, F. Muhammad, S. Murray, and J. O. W. Norris, Compensation for surface contamination in a D-fiber evanescent wave methane sensor, J. Lightwave Technol., 13, 6, (1995).

31. S.H. Lim, L. Feng, J.W. Kemling, C.J. Musto, K.S. Suslick, "An optoelectronic nose for detection of toxic gases, Nature Chemistry, 1,562–567, (2009).

32. K.M. Kadish, K.M. Smith, R. Guilard (Eds.), the porphyrin handbook, vol. 6Academic Press, New York (2000)

33. X.B. Zhang, Z.Z. Lib, C.C. Guoa, S.H. Chena, G.L. Shena, R.Q. Yua, "Porphyrin–metalloporphyrin composite based optical fiber sensor for the determination of berberine," Analytica Chimica Acta, 439, 65–71 (2001),

34. X.B. Zhang, C.C. Guo, Z.Z. Li, G.L. Shen, R.Q. Yu, "An optical fiber chemical sensor for mercury ions based on a porphyrin dimer", Analytical Chemistry, 74 , 821–825,(2002).

35.R. Ni, R.B. Tong, C.C. Guo, G.L. Shen, R.Q. Yu ,"An anthracene/porphyrin dimer fluorescence energy transfer sensing system for picric acid", Talanta, 251–257, 63 (2004),

36. G. Huyang, J. Canning, M.L. Åslund, D. Stocks, T. Khoury, M.J. Crossley," Evaluation of optical fiber microcell reactor for use in remote acid sensing", Optics Letters, 817–819,35, (2010).

37. S. Roman, K. Sergiy, Y. Wataru, L. Seung-Woo,"A preliminary test for skin gas assessment using a porphyrin based evanescent wave optical fiber sensor Sensors & Transducers, 54–67,125 ,(2011).

38. Ana M. R. Pinto and Manuel Lopez-Amo,"Review Article Photonic Crystal Fibers for Sensing Applications", Journal of Sensors ,Volume 2012, Article ID 598178, 21 pages, (2012).

39. X. H. Yang and L. L. Wang, "Fluorescence ph probe based on microstructured polymer optical fiber," Optics Express, vol. 15, no. 25, pp. 16478–16483, (2007).

40. Y. L. Hoo, W. Jin, H. L. Ho, D. N. Wang, and R. S. Windeler, "Evanescent-wave gas sensing using microstructure fiber," Optical Engineering, vol. 41, no. 1, pp. 8–9, (2002).

41. Y. L. Hoo, W. Jin, H. L. Ho, J. Ju, and D. N. Wang, "Gas diffusion measurement using hollow-core photonic bandgap fiber," Sensors and Actuators B, vol. 105, no. 2, pp. 183–186, (2005).

42. E. Austin, A. van Brakel, M. N. Petrovich, and D. J. Richardson, "Fibre optical sensor for c2h2 gas using gas-filled photonic bandgap fibre reference cell," Sensors and Actuators B, vol. 139, no. 1, pp. 30–34, (2009).

43. V. P. Minkovich, D. Monzón-Hernández, J. Villatoro, and G. Badenes, "Microstructured optical fiber coated with thin films for gas and chemical sensing," Optics Express, vol. 14, no. 18, pp. 8413–8418, (2006).

44. J. Villatoro, M. P. Kreuzer, R. Jha et al., "Photonic crystal fiber interferometer for chemical vapor detection with high sensitivity," Optics Express, vol. 17, no. 3, pp. 1447–1453, (2009).

45. M. P. Buric, K. P. Chen, J. Falk, and S. D. Woodruff, "Improved sensitivity gas detection by spontaneous Raman scattering," Applied Optics, vol. 48, no. 22, pp. 4424–4429, (2009).

46. J. B. Jensen, L. H. Pedersen, P. E. Hoiby et al., "Photonic crystal fiber based evanescent-wave sensor for detection of biomolecules in aqueous solutions," Optics Letters, vol. 29, no. 17, pp. 1974–1976, (2004).

47.Y. Ruan, E. P. Schartner, H. Ebendorff-Heidepriem, P. Hoffmann, and T. M. Monro, "Detection of quantum-dot labeled proteins using soft glass microstructured optical fibers," Optics Express, vol. 15, no. 26, pp. 17819–17826, (2007).

48. Y. Ruan, T. C. Foo, S. Warren-Smith et al., "Antibody immobilization within glass microstructured fibers: a route to sensitive and selective biosensors," Optics Express, vol. 16, no. 22, pp. 18514–18523, (2008).

49. Z. Xie, Y. Lu, H. Wei, J. Yan, P. Wang, and H. Ming, "Broad spectral photonic crystal fiber surface enhanced Raman scattering probe," Applied Physics B, vol. 95, no. 4, pp. 751–755, (2009).

50. C. M. B. Cordeiro, M. A. R. Franco, G. Chesini et al., "Microstructured-core optical fibre for evanescent sensing applications," Optics Express, vol. 14, no. 26, pp. 13056–13066, (2006).

51. C. Wu, B. O. Guan, C. Lu, and H. Y. Tam, "Salinity sensor based on polyimide-coated photonic crystal fiber," Optics Express, vol. 19, no. 21, pp. 20003–20008, (2011).

52. R. A. Potyrailo, S. E. Hobbs, and G. M. Hieftje, Optical waveguide sensors in analytical chemistry: Today's instrumentation, applications and trends for future development, Anal. Chem., 48, p. 456, (1998).

53. R. D. Harris, B. J. Luff, J. S. Wilkinson, R. Wilson, D. J. Schiffrin, J. Piehler, A. Brecht, R. A. Abuknesha, and C. Mouvet, Integrated optical surface plasmon resonance biosensor for pesticide analysis, IEEE Colloquium on Optical Techniques for Environmental Monitoring (1995/182), p. 6, London, (1995).

54. K. J. Kuhn and J. T. Dyke, A renewable-reagent fiber-optic sensor for measurement of high acidities, Anal. Chem., 68, 2890, (1996).

55. R. B. Thompson, Z. Ge, M. Patchan, C. Chin-Huang, and C. A. Fierke, Fiber optic biosensor for Co (II) and Cu (II) based on fluorescence energy transfer with an enzyme transducer, Biosens. Bioelectron. 11, p. 557, (1996).

56. CMSTCP (Characterization, Monitoring & Sensor Technology Crosscutting Program), Technology Catalog-HaloSnif- Optic Spectrochemical Sensor, http:// www.cmst.org/cmst/Tech_Cat.text/6.1.html (1998).

60. P. J. Gemperline, J. Cho, B. Baker, B. Batchelor, and D. S. Walker, Determination of multicomponent dissolution profiles of pharmaceutical products by in situ fiber-optic UV measurements Anal. Chim. Acta, 345, p. 155, (1997).

Chapter 2

UV induced deposition technique: A simple approach to integrate optical fiber with functionalized thin film

2.1 Introduction

Chemical optical fiber sensors as one of the most intriguing applications of optical fiber has got attention from scientific community. Different structures and configurations in order to obtain a selective and accurate sensor already presented in chapter one. In between the geometrical justification of optical fiber to facilitate the interaction of propagated light with measurand seems compulsory, and different works reported different approach to this aim[1-2].

Furthermore a chemical sensor, cannot be efficient and valuable if it cannot present suitable selectivity. To improve the selectivity of sensor, different approach to integrate functional material in fiber is reported.

Different coating techniques in controllable fashion, has been reported and developed on the optical fiber. For instant the Langmuir–Blodgett (LB) technique [3-5] has been reported and developed for deposition of materials on the optical fiber as well as different substrate, this techniques needs a careful and complicated preparation of the optical fiber substrate. The Electrostatic self-assembly ESA is another technique for the deposition of multilayered films of magnetic [6], electrically conductive [7], and non-linear optical materials [8] onto a substrate, the critical point is the ESA technique is limited to small class for chemical spices such as polymers. On the other hand new class of porphyrin molecules due to their fascinating optical and photophysical abilities are well known molecules. Which with their linear and nonlinear optical properties and their functionalities in the wide range of materials taking an important role in

fabrication of optical sensors. In this aim many works shows their compatibility, sensibility on the optical fiber platform [11, 12].

In this chapter our attention is devoted to a new technique of deposition taking the advantages of acid formation in a halogenated solvent by a UV induced technique and we developed the extensibility of technique in different porphyrin molecules and consequently we step forward to performing and preliminary analysis of silver coating on the optical fiber with the same technique.

Optical microscopic analysis with aim to morphological study is employed for all the deposited structures. The deposited film is characterized and studied in light of an in-fiber reflectometry technique.

2.2 UV Induced deposition technique on planar silica substrate

In this section deposition of porphyrin molecule on planar substrate with a simple UV irradiation of porphyrin molecule is reported. This process is due photochemical decomposition of a chlorinated solvent of porphyrin solvent [13].

Experimental setup of this method is arranged as follow; they used a deuterium lamp as the UV light source and a diluted solvent (order of $10^{-5}\ mol\ L^{-1}$) of porphyrin molecules like tetrakis (4-sulfonatophenyl) porphyrin (TPPS) or Tpyp4 in dichloromethane. A schematic plot of the deposition setup is plotted in figure 2.1 where an optical aperture is used to control the light beam power of deuterium lamp. The violet surface inside the cuvette (transparent chemical container) is showing the region which dye molecule will be deposited. With employing the Optical Aperture a complete control on UV irradiation level in unit of time is achievable. Cuvette is used playing role as holder of the halogenated solvent and it also play the rule of substrate, while we already know pure silica is transparent for UV light and typical holder of solvent in optical chemistry. On the other hand use of cuvette open the possibility of absorption spectral analysis of deposited film.

To understand morphological and geometrical control of the deposited film, a deep understanding of deposition procedure is obligatory. Therefore first of all our attention is to explain the deposition mechanism.

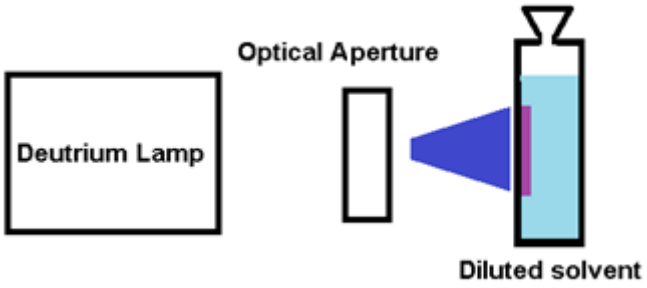

Figure 2. 1: The schematic setup of UV induced deposition technique on planar surface.

Film formation mechanism of the deposition technique is described as bellow:

1. First of all the decomposition of the halogenated solvent will happen in exposure with UV light. A localized formation of the hydrochloric acid (HCL) will happen. (This formation of HCl is one of the key points of this deposition process).
2. Presence of HCl, which cause the consequent protonation of the dye molecules on the substrate and of course lead to reduction in their solubility. It is worth nothing that due to local formation of HCl the local reduction in solubility is happening.
3. Deposition of dye molecules right at the surface of substrate is done. And the deposited film as reported is in agreement with the geometry of light spot [12, 13].

In the deposition process the control of several parameter is important, we can name the, optical source power, wavelength range, concentration of dye in dichloromethane alongside of the UV irradiation time, which are playing clear rules. As we've mentioned the process of deposition is started by local decomposition of halogenated solvent so keep and controlling of the UV power is of interest. The effort is to keep the UV power in low level, which is why in the UV induced method (in planar substrate and deuterium lamp) they design and employ a controllable aperture to control the light power and exposure of light in average time unit. The consequence of high UV power will be forming Hydrochloric acid in all the solvent which lead a total precipitation of dye molecules in the cuvette (not locally, and on the silica substrate). On other hand the decomposition of Halogenated solvent can be happened in certain energy level which is completely dependent to wavelength of the light, of course the light source should cover that wavelength as well. The concentration of the solvent is also been mentioned, and playing important role while, with increasing the deposition time consequently thickness of film will increase. But of course it is limited to the concentration level of halogenated solvent. The film thickness increase represents a

saturation level due to reduction of transparency (for UV) due to increase of deposited film.

2.3 UV induced deposition technique on fiber end

In this work our attention is on extent of UV induced deposition of different porphyrin molecules on the optical fiber end. The deposition of dye molecule film is achieved by dipping the well cleaved tip of a multimodal fiber in a deposit-able solution in dichloromethane (CH2Cl2) with a concentration (~5×10^{-5} molL^{-1}) and by the subsequent irradiation with UV light coupled to the fiber optics. Figure 2.2 is depicting the deposition setup schematically and photo of setup is presented inset figure 2.2.

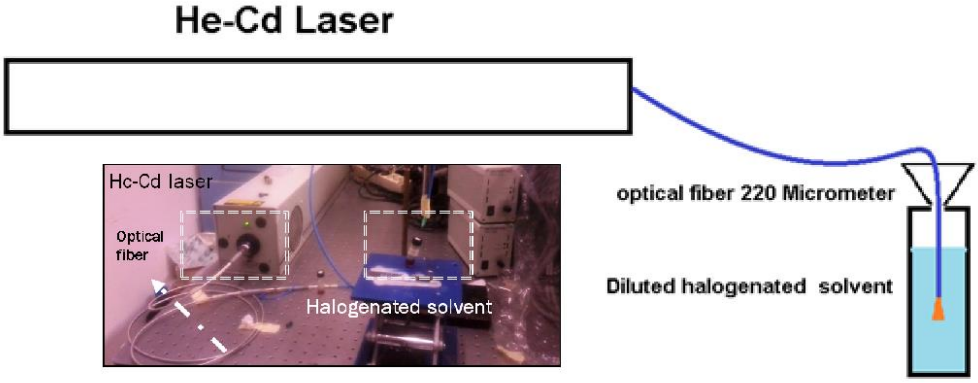

Figure 2. 2 The schematic setup of UV-induced deposition technique on the optical fiber, (inset) a photo of experimental setup.

The mechanism of film formation, [13, and 14] can be reported as follow:

1. The slow decomposition of the halogenated solvent by UV photons, with the localized formation of hydrochloric acid (HCl) near the fiber end.
2. The consequent protonation of the dye molecules by the tip with a reduction in their solubility;
3. The deposition of the protonated dyes as self-assembled thin film right at the surface of the fiber tip.

As optical fibers in last 4 decades played important rule in telecommunication and recently on sensing applications, the techniques for integrating materials with optical fiber are very intriguing. The major improvement in the presented experimental setup lies in the versatility of the fiber optics which plays a multiple role to name some:

I. It permits to guide the UV radiation up to the fiber tip surface triggering the film deposition only on the core region (due to the UV light emission). So due to local precipitation of molecules the deposition forms in the core region of fiber

II. The tip surface acts as support for the sensing material;

III. In the characterization step (see figure 2.7), the optical fiber behaves as waveguide both for the incident (interrogation) radiation and for the backscattered (response) signal in VIS range.

The deposition was performed on non-standard optical fibers (Ocean Optics) with 200 µm core diameter and 220 µm cladding diameter, for their capability to propagate in UV-VIS range. Fiber tips were prepared as illustrated in figure 2.3 (a) using appropriate fiber cleaver as shown in figure2.3. (b).

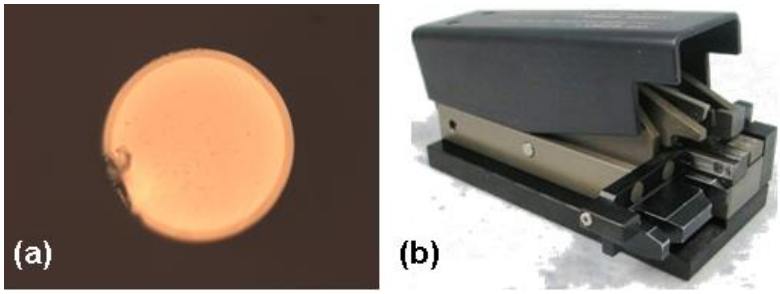

Figure 2. 3: (a) optical fiber transversal section with 200 µm core (properly cleaved); (b) cleaver for optical fiber with diameter up to 250 µm.

And a He-Cd laser (λ = 325 nm; 9.5 mW) was employed as UV source to irradiate a dilute dye molecule solution in CH_2Cl_2 ($\sim 5 \times 10^{-5}\ mol\ L^{-1}$).

It is worth highlighting that even if the laser wavelength falls outside of the strongest absorption range for the solvent (below 240 nm), with a reduced yield of its photochemical decomposition reaction, it still allows a satisfactory deposition. In next sections we will study the deposition of Tpyp4 as the first molecule and in the next step we devote our activity on the study of deposition of other porphyrin molecule TPPS and eventually the extensibility of this technique will go under investigation by study of silver molecule and the deposition of silver molecule on the optical fiber distal end.

2.3.1 Integration of TPyP (4) on the fiber tip

Tetra (4-pyridyl) porphyrin molecule is formed by a structure called porphin which is the simplest form of porphyrin with four radical compounds of pyridyl as shown in figure 2.4.

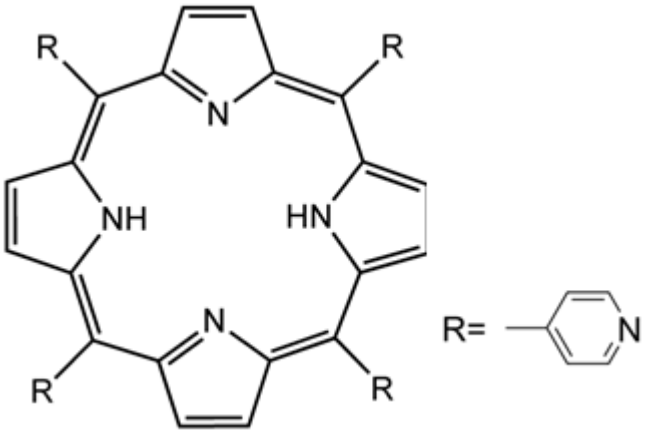

Figure 2. 4: The schematic of Tetra (4-pyridyl) porphin molecule and Pyridyl as radical.

Their photophysical properties (as monomer) has been reported in organic solvent [15-17]. Tetra (4-pyridyl) porphin (TpyP (4), hereafter) is insoluble in aqueous solution, but it is readily soluble under acidic conditions [10]. Its photophysical properties as monomer in organic solvents have been investigated, [11, 12] their elusive nature of aggregates of this molecule in mixed organic-aqueous is proven [18].

In this section our work is devoted to integration of TpyP (4) on the optical fiber end, with aim to have a thin film located to core region of optical fiber. We employed the UV-induced technique of deposition as previously explained.

To start deposition process, respecting to setup mentioned in figure 2.2 we irradiate a UV light with wavelength of 325 nm to solvent TpyP (4) in CH2Cl2, with concentration of ($\sim 5 \times 10^{-5} \frac{M}{L}$) . The light delivery is done by optical fiber with 200 μm of core diameter. During the UV irradiation a trace of pale brown light can be detected in the solvent which is due to fluorescence features of solvent.

At the same time, the optical fiber terminal is subjected to deposition. It is expected a device as schematically illustrated in figure 2. 5.

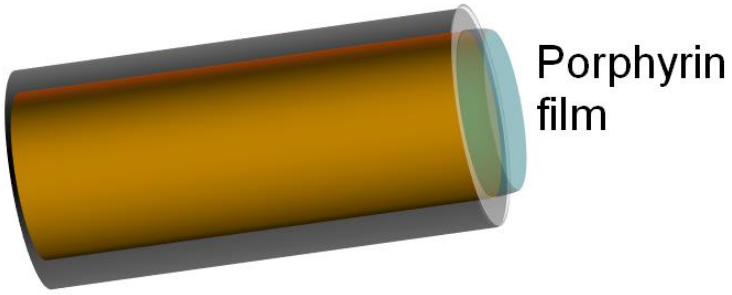

Figure 2. 5: Schematically drawing of deposited Porphyrin film on optical fiber.

The cleaved fiber will provide a planar suitable substrate for deposition of material on the surface. Here we focused our attention on the morphological investigation of results of deposition results.

Microscopic investigation of the bare fiber is presented in figure 2.6. (a) the defect on the left down is due to cleaver's effect a 30 minutes of irradiation UV cause a deposited fiber as the microscopic image is shown in figure 2.6.(b) the deposited TpyP(4) , most likely the core and cladding region is distinguishable and the core is uniformly covered by porphyrin molecules.

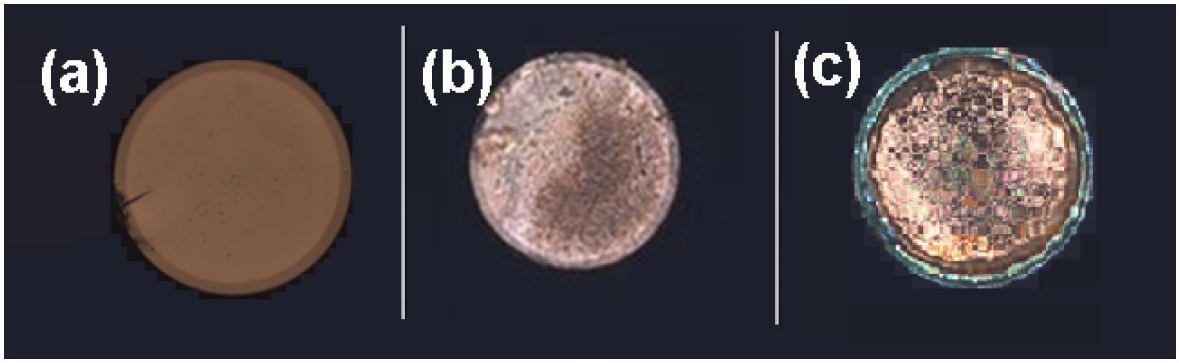

Figure 2. 6: Optical fiber cross section in different status: (a) Bare fiber; (b) deposited film after 30 minutes UV exposure; and (c) deposited film after two hours UV exposure.

We already spoke about the effective parameters on the deposition layer, the irradiation time is good basis of controlling the thin film, and a series of experiment with different irradiation time has been performed and consequently studied by microscopic observation. Following the microscopic temporal study of film for 2 hours of UV irradiation is presented in figure2.6 (c).

Figure 2.6. (b) And (c) representing a comparison of 30 minutes and 2 hours of UV irradiation respectively. The uniformity of presented film in both case with the alignment of film to the core of fiber is remarkable. With increasing the irradiation time a better recognition between cores and clad is possible. The thickness of film on the fiber increases with increasing the irradiation time, but as a result, UV transparency decreases which leads to an eventual saturation level of deposition.

On the other hand for the characterization of the deposited thin film a backscattering analysis is proposed, to this goal we analyze the reflected signal from the fiber end surface through optical fiber. Spectroscopic measurements of the reflected signal by the fiber tip have been performed by coupling the fiber to a broadband light

source emitting in the visible range and to an optical spectrometer (Avantes AvaSpec mod. 2048) through a 2×1 coupler (50% power splitting in both arms) which allows to split the incident and reflected light. Figure 2.7 presenting the spectroscopy setup and inset representing the light path mechanism.

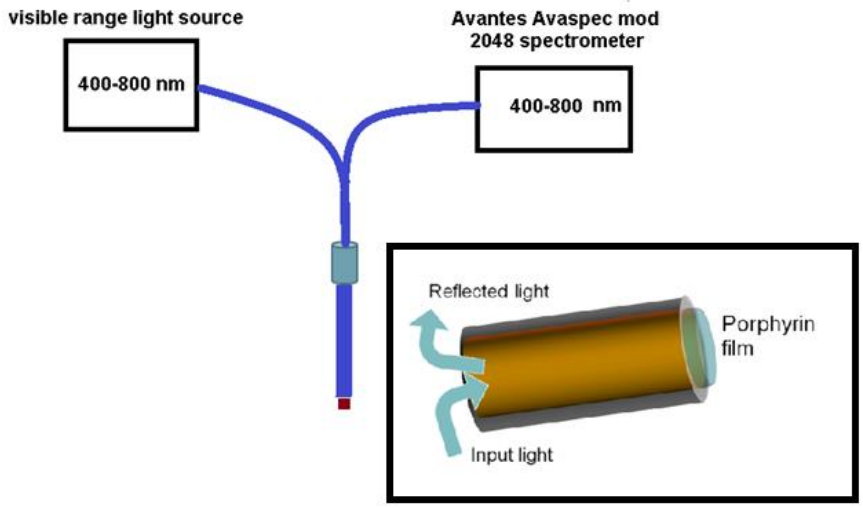

Figure 2. 7: The spectroscopy setup and inset, represents the mechanism reflectance analysis.

The reflectance spectra have been obtained by normalization of all signals to the bare fiber spectrum (just after end cleaving), in order to remove the effects of non-flat source and detector sensitivity across the entire visible range. Figure 2.8 plots the reflectance spectra of the bare fiber the blue graph, a TpyP(4) coated fiber after 30 minutes of deposition (red curve), where the presence of the self-assembled film causes a decrease in reflectance intensity of an average of 35% as compared with the 100% reference value. But spectral features of TPyP(4) like Q-bands of the TpyP (4) porphyrin which are centered about 513, 546, 588, and 648 nm and in the form of planar substrate will have a red shift and only 2 bands around 625 and 670 nm remain in case of planar substrate. In case of optical fiber the spectral results of a film formed by30 minutes UV irradiation depict only one Q-band centered around ~ 570, obviously the spectrum of mentioned film is standing at difference with the deposition obtained onto quartz in a planar arrangement and can be the reason of the red shift belong to one of the smaller bands, [12], which is presented in this curve.

With increasing the irradiation time, the TpyP (4)-coated fiber tip does not exhibit clear spectral features in its reflected spectrum right after film deposition. Figure 2.8 the

pink, black and cyan graphs respectively present coated films after one, two and three hours of irradiation.

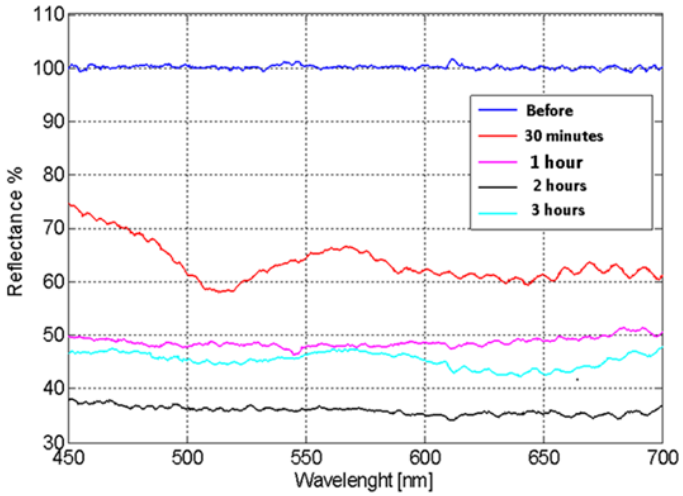

Figure 2. 8: Reflectance spectra of deposited fibers as function of the UV exposure time (all curve are normalized to the bare fiber spectrum): The blue curve refers to non-deposited fiber (as reference value 100%), red curve, pink, black and cyan represent reflectance spectra of deposited fibers with 30 minutes, 1, 2 and 3 hours UV exposure, respectively.

In conclusion in current section with study of deposition of TpyP (4) we admit the possibility of deposition of TpyP (4) on the non-Standard optical fiber-End employing a UV-Induced technique of deposition. Optical microscope investigation of experimental results approve the presence of porphyrin thin film on the fiber surface respecting to different irradiation time (Deposition temporal length) a clear morphological difference has been observed. The deposited film is almost self-aligned to the core site of the optical fiber. on the other hand an spectral analysis of the reflected light from the fiber-end has been performed and the spectral results reporting some evidence of the thin film present on the optical fiber after 30 minutes of deposition while by increasing the irradiation time length the film does not exhibit any clear spectral feature except the decrease on the amplitude of the normalized reflected spectrum.

2.3.2 Deposition of tetrakis (4-sulfonatophenyl) porphyrin (TPPS) molecule on the fiber end

In the previous section, we have demonstrated the possibility of growing discrete porphyrin crystals on an optical fiber-end surface from a dichloromethane solution of tetra (4-pyridyl) porphyrin employing a UV induced technique of deposition and we study the ability of deposition of the Porphyrin thin film on the fiber end.

The photo generation of hydrochloric acid in the interface of the fiber-end and dichloromethane solved in TpyP (4) plays the important rule in the crystallization of porphyrin on the optical fiber end.

Acid formation induced a decrease in solubility of the resulting protonated porphyrin with respect to the neutral parent compound. Which results to a self-assembled layer. In this section a new porphyrin molecule with aim to check extensibility of UV-induced technique and investigation of spectral feature is under investigation.

The Tetrakis (4-sulfonatophenyl) porphyrin (TPPS) is one of Porphyrin spices which is made of a porphin with four sulfatophenyl radical connected as shown in figure 2.9 as a water soluble compound has got numerous attention and widely investigated due to their ability of form different aggregations [16-17].

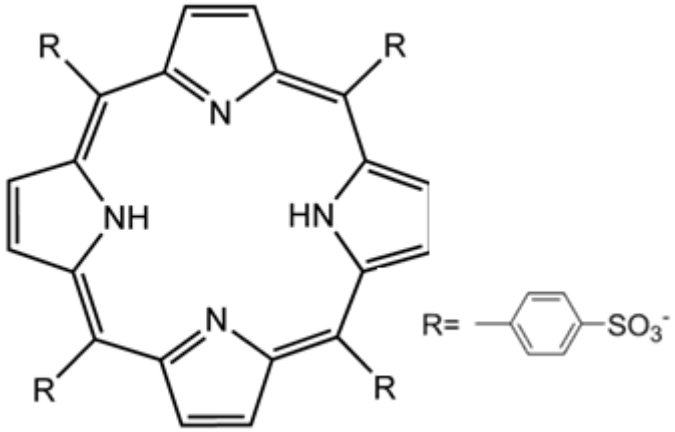

Figure 2. 9: The Tetrakis (4-sulfonatophenyl) porphyrin.

Here we will report on the formation of homogeneous thin films of the titled porphyrin by using the same irradiation technique of the previous section. The deposition setup is the one has been reported in figure 2.2 and the deposition of the porphyrin molecule has been achieved by dipping the end cleaved fiber (figure2.10) while UV irradiation to solvent (tetrabutylammonium salt of TPPS in CH2Cl2).

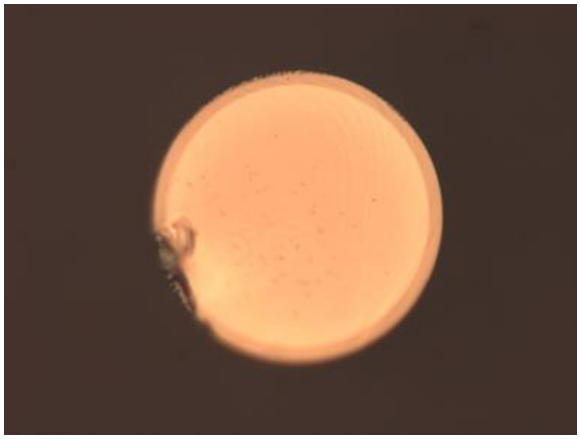

Figure 2. 10: The cleaved fiber by appropriate cleaver with 200 µm core diameter.

The deposition of the porphyrin has been achieved by UV irradiation of a diluted solution of the tetrabutylammonium salt of TPPS in CH2Cl2 (30−40 µmol/L) by using a He-Cd laser (9mW optical power). The irradiation time of 120 minutes was the study case and with this time a uniform thin film of TPPS has been formed on the fiber end, as it is shown in figure 2.11 the self-alignment thin film is very well shown, the separation line is completely matched with the core-clad border line.

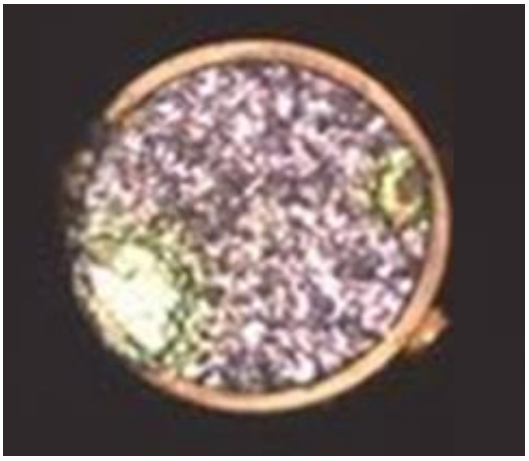

Figure 2. 11: Representation of the TPPS porphyrin thin film on the fiber.

The color difference in the left down of the photo is due to defect caused by cleaver.

A spectroscopic setup for characterization of TPPS deposited optical fiber similar to the one in figure 2.7 is organized. We choose three different deposited film with different deposition time, 1 hour, 2 and 3 hours of UV irradiation. We expect with changing the deposition time the spectroscopy results present the differences in back scattered signal.

The spectral analysis for characterization of thin films has been achieved by normalization of all signals to the bare fiber spectrum, and defining the dark state, in

order to remove the effects of non-flat source and detector sensitivity across the entire visible range. Figure 2.12 plots the reflectance spectra of the bare fiber the blue graph, a TPPS coated fiber after 1 hour of irradiation (green curve), where the presence of the self-assembled film causes a decrease in reflectance intensity of an average of 22.5% as compared with the 100% reference value but the black curve in figure 2.12 depicts the reflectance spectrum of 2 hours deposition (black curve), and finally a 3 hours deposition (red curve) is presented in figure 2.12.

The spectral analysis of the film here is showing the difference on optical amplitude directly with increasing the deposition time and that means the absorption from the surface increases. On the other hand the presence of the Soret band at 420 nm is not observable any more, and no special feature in blue band is observable.

About the Q bands of the TPPS porphyrin at 516, 551, 591, and 646 nm exhibit a red shift, and in the planar substrate form, at the end of the process only two are clearly detectable at 610 and 660 nm. While in the green curve three of the Q-band can be detected with the small bumps and this issue is also applicable in the red graph and it is nice to mention small bumps also are detectable on the red curve near 400 nm (while this region is the border of accuracy of our spectrometer we prefer to not comment about the region.).

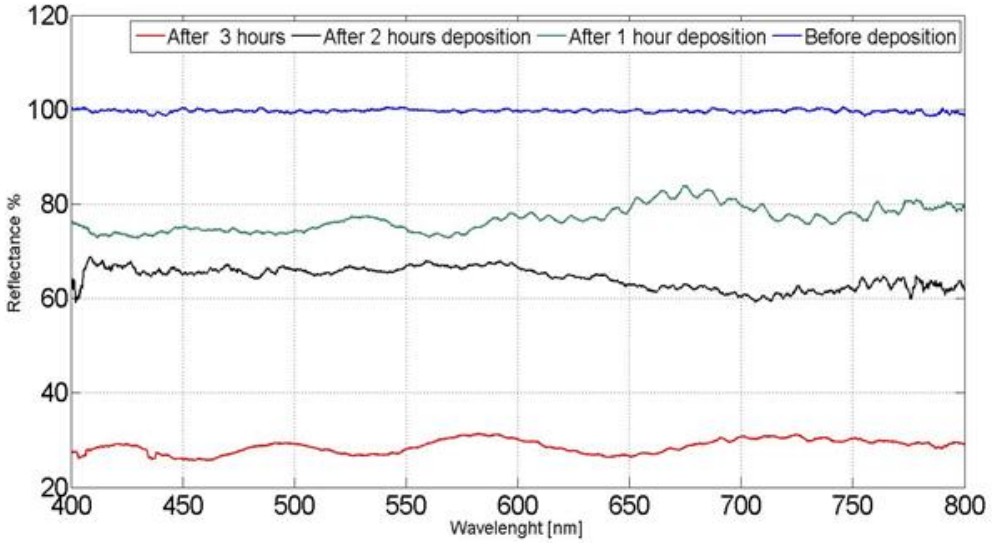

.

Figure 2. 12: Reflectance spectra of TPPS deposited on the fiber end the bare fiber normalized reflectance (blue curve) the deposited fiber in 1 hour of UV irradiation (green curve) the black curve presenting the spectrum of TPPS film after 2 hours of deposition, an d a three hours deposited film(red curve).

In the black curve there is no special feature except the decrease in amplitude. To summarize our study we achieved the ability to deposit new porphyrin molecule on the optical fiber tip employing UV induced technique the morphological and geometrical study of fiber tip with mean of microscopic observation shows very uniform film limited to the fiber core and a clear separation line is showing how the deposition technique is strongly dependent on the delivered UV light. On the other part our attention was devoted to spectrum analysis of the reflectance spectra from the film through the fiber. The analysis show decreases on the amplitude in different deposition time. The spectral investigations illustrated, some spectral feature also in different films. The spectral differences can be explained by the thickness and/or different aggregation forms of the film. This molecule has been mentioned because of their abilities to detect different materials and in chapter 3 the sensing Ability of achieved device will be better studied.

2.3.3 Silver deposition on the optical fiber structures

.

The integration of silver and gold nano particles on the optical fibers is intriguing due to their abilities for increasing the sensing capabilities of chemical optical fibers. The use of silver nanoparticles (Ag-NPs) has advantages when the sensors are placed in high humidity environments due to their antibacterial behavior preventing the bacteria growth. This phenomena is reported in different works and silver is good candidate for biological sensors [20-22] moreover, the Ag-NPs for optical sensors is well-known processed and known to the phenomenon of surface Plasmon Resonance (SPR) as a sensing signal response[23-24].

By the way, the generation of a new class of resonances has been reported which can be supported by thin-film coated optical waveguides.

Therefore it looks intriguing to integrate silver on fiber optics. In this section we report a preliminary study of silver deposition on fiber via UV induced technique, check marking this method to a wider class of molecules.

The name of silver coating has tight relation with the history of photography and Thomas Wedgwood is whom with using the silver salts has got the idea to produce a photo, due to their photo physical possibilities of silver salts and their decomposition in specific wavelengths. In this certain point with combining the idea of traditional

photography and UV-induced technique, we extent the technique to silver molecules as well.

The arrangement of optical setup for deposition is the same as previous ones, with dipping the well cleaved fiber to the solvent of silver bromide and dichloromethane (2mgr/mol) and 30 minutes of UV irradiation. The deposited film is shown as follows in figure 2.13. The film is providing the self-alignment phenomena and moreover a uniform silver film is detectable on the optical fiber-end surface. Comparing with the cleaved fiber. We can report the defects on the thin layer in different parts of core site which can be due to damage on the fiber end.

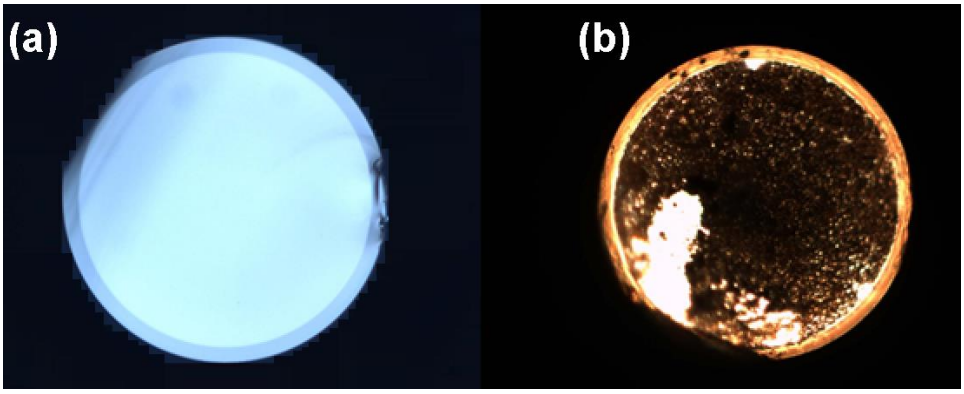

Figure 2. 13: (a) the cleaved fiber (b) silver deposited thin film with respect to 30 minutes of UV irradiation in a 2mg/l concentration.

Scanning electron microscope analysis

Scanning electron microscope (SEM) microscopic observation is representing for a sample with 2 hours of deposition time, a quasi-uniform deposition on the fiber end. The results are the following. Figure 2.14 is illustrating a portion of film.

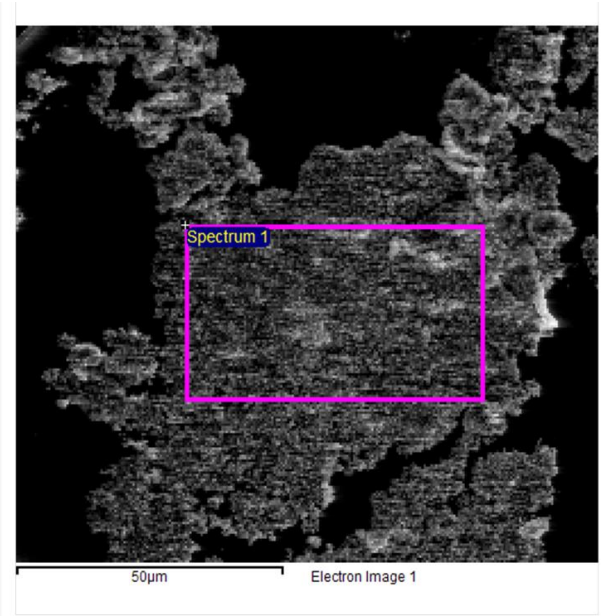

Figure 2. 14: SEM observation of the deposited region on the fiber end from the pink rounded region.

an spectroscopy has performed and the figure 2.15 is depicting the statistical graph for amount of different molecules or atoms on the surface of the fiber as it is clear table 2.1 is presenting the results and it shows an amount near 65% of the surface covered with the silver molecules and almost more than 20% of the structure is made of silica and its derivate which means the substrate as background material.

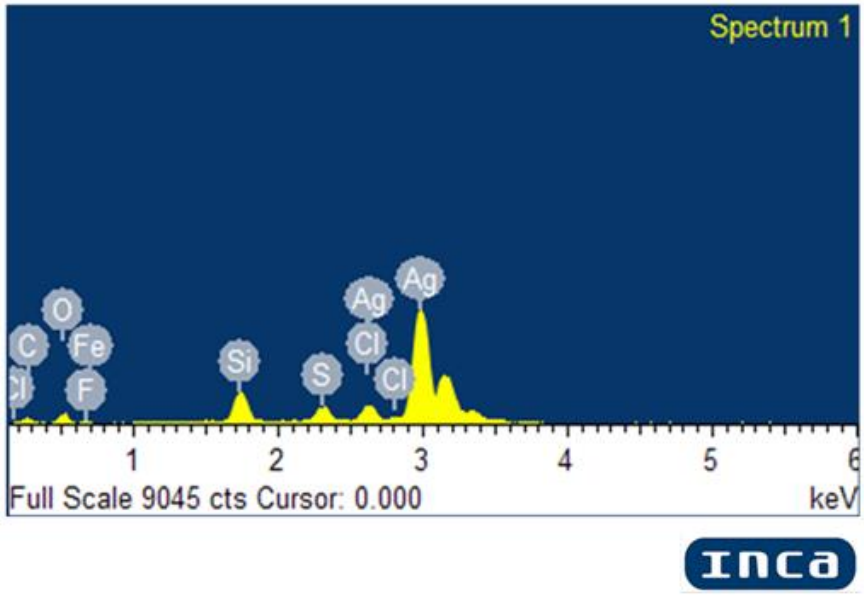

Figure 2. 15: The statistical graph of chemical species.

In Table 2.1 the list of all chemical spices is included and the results are easy to conclude and strongly uniform and dense present of silver is shown here while on the

other hand there are few other spices related to optical fiber surface detected on the fiber.

Element %	Weight%	Atomic %
C K	4.29	13.58
O K	18.08	43.01
F K	3.93	7,87
Si K	5.37	7.27
S K	2.74	3.25
Cl K	2.45	2.63
Fe K	0.45	0.30
Ag L	62.68	22.1

Table 2. 1: The chemical contents of the deposited film.

In summery we have found the possibility of deposition of thin film of silver on the fiber end with studying the film with optical microscopic and SEM one. This study also presents a well uniformed silver layer and high percentage of silver regarding to SEM results. Optical microscopic results very clear presented the presence of silver molecules on the fiber surface and eventually the deposited fiber spectrum analysis has been done and studied.

2.4 Summary

In this chapter our effort was devoted to develop and investigate the ability of deposition of material on the optical fiber. With taking advantages of versatility of optical fibers beside a UV-Induced technique of deposition, this technique for porphyrin molecules have been studied and it is resulting to a self-aligned uniform film on the fiber core. Optical microscopic and a backscattered spectroscopy technique together admitted our claim about thin film. On the other hand an investigation for the development of technique has been done, in order to represent the ability of this technique for deposition of other molecules, to this aim silver molecule is one of the best candidates and the technique is adopted for deposition of silver molecules. The SEM analysis and optical microscopy analysis are representing a uniform thin film of silver on the fiber end.

Bibliography

1. Giordano M, Russo M, Cusano A, Cutolo A, Mensitieri G, Nicolais L," Optical sensor based on ultrathin films of d-form syndiotactic polystyrene for fast and higher solution detection of chloroform", Applied Physics Letters ,85,5349,(2004).

2. Cusano A, Pilla P, Contessa L, Iadicicco A, Campopiano S, Cutolo A , "High sensitivity optical chemosensor based on coated long period gratings for sub-ppm chemical detection in water", Applied Physics Letters, 87, 234105, (2005).

3. R.H. TREDGOLD, "Langmuir-Blodgett films: Organic monolayer imaged", Nature 313, 348 (1985)

4. M. Consales, A. Crescitelli, M. Penza, P. Aversa, M. Giordano, A. Cutolo, A. Cusano, "SWCNTs Based Nano-Composites as Sensitive Coatings for Advanced Fiber Optic Chemical Nano-Sensors," Optical Sensors 2008, Proc. of SPIE Vol. 7003, (2008).

5. R.B. Charters," Continuous fibre optic components utilizing evanescent coupling to organic thin films", PhD Thesis Cranfield University, (1995).

6. Liu Y, Wang Y and Claus R O, "Layer-by-layer electrostatic self-assembly of nanoscale Fe3O4 particles and polyimide precursor on silicon and silica surfaces" Appl. Phys. Lett. 71 2265–7, (1997)

7. Liu Y, Wanga Y and Claus R O, "Layer-by-layer ionic self-assembly of Au colloids into multilayer thin-films with bulk metal conductivity" Chem. Phys. Lett. 298 315–9, (1998)

8. K.M. Lenahan,Y-X Wang,Y Liu,R.O Claus,J.R. Heflin,D. Marciu and C. Figura, "Novel polymer dyes for nonlinear optical applications using ionic self-assembled monolayer technology", Adv. Mater. 10 853–5, (1998)

9. Decher G, Hong J D and Schmitt J "Buildup of ultrathin multilayer films by a self-assembly process: III. Consecutively alternating adsorption of anionic and cationic polyelectrolytes on charged surfaces Thin Solid Films" 210/211 831–5, (1992)

10. A.Rosidian, Y Liu and R. O. Claus, "Ionic self-assembly of ultrahard ZrO2/polymer nanocomposite thin films," Adv. Mater. 10 1087–91], (1998)

11. G. Huyang, J. Canning, M.L. Åslund, D. Stocks, T. Khoury, M.J. Crossley "Evaluation of optical fiber microcell reactor for use in remote acid sensing", Optics Letters, 35 , 817–819,(2010).

12. G. De Luca, G. Pollicino, A. Romeo, L. Monsù Scolaro," Sensing behavior of Tetrakis(4-sulfonatophenyl)porphyrin thin films," Chemistry of Materials, 18, pp. 2005–2007, (2006)

13. L. Monsù Scolaro, A. Romeo, M. Castriciano, G. De Luca, S. Patanè, N. Micali," Porphyrin deposition induced by UVirradiation", Journal of the American Chemical Society, 125 , 2040–2041,(2003)

14. Abolfazl Bahrampour, Agostino Iadicicco, , Giovanna De Luca, , Michele Giordano, Anna Borriello, Antonello Cutolo, Andrea Cusano, Luigi Monsù Scolaro,"Porphyrin thin films on fiber optic probes through UV-light induced deposition", Optics & Laser Technology, 49, 279-283,(2013)

15. D.L.Akins, H.R Zhu, C. Guo," Absorption and raman-scattering by aggregated meso-tetrakis (p-sulfonatophenyl) porphine," J Phys Chem, 98, 3612-3618, (1994)

16. N. C. Maiti, M. Ravikanth, S. Mazumdar, and N. J. Periasamy, J. Chem. ," Fluorescence dynamics of non-covalently linked porphyrin dimers and Aggregates", Phys. 99,17192,(1995)

17. O. Ohno, Y. Kaizu, H. J. Kobayashi, Chem. Phys., "J-aggregate formation of a water-soluble porphyrin in acidic aqueous media"1993, 99, 4128, (1993).

Pasternack,

18. Maria Angela Castriciano, Andrea Romeo, Giovanna De Luca , Valentina Villari , Luigi Monsù Scolaro, and Norberto Micali ,"Scaling the Chirality in Porphyrin J-Nanoaggregates",J. Am. Chem. Soc., 133 (4), 765–767, (2011)

19. A. Bahrampour, A. Iadicicco, G. De Luca, M. Giordano, A. Cutolo, L. Monsù Scolaro, and A. Cusano, "Sensing Characteristics to Acid Vapors of a TPPS Coated Fiber Optic: a Preliminary Analysis", Proceeding, World Academy of Science, Engineering and Technology,, 71,venice 2012

20. P.J. Rivero, A. Urrutia, J. Goicoechea, C.R.Zamarreño, F.J. Arregui, I.R. Matías, NanoscaleRes. Lett. 6, 1-7 (2011).

21. A. Urrutia, P.J. Rivero, L. Ruete, J. Goicoechea,F.J. Arregui, I.R. Matías, "An antibacterial surface coating composed of PAH/SiO2 nanostructurated films by layer by layer",Phys. StatusSolidi C 7, 2774-2777. (2010),

22. M.E. Yazdanshenas, M.R. Nateghi,"Assessment of silver nanoparticles and its application in conservation and restoration of cultural and historic objects", Cellulose 16, 1147-1157 (2009),

23. Luis M. Liz-Marzán, Langmuir,"Tailoring Surface Plasmons through the Morphology and Assembly of Metal Nanoparticles", 22, 32–41, (2006).

24. P.J.G. Goulet, G.R. Bourret, R.B. Lennox, "Facile Phase Transfer of Large, Water-Soluble Metal Nanoparticles to Nonpolar Solvents", Langmuir 28, 2909-2913 (2012).

Chapter 3

Sensing capabilities of TPPS coated optical fiber sensors

3.1 Introduction

Measure and control the levels of toxic and/or aggressive vapors is very important in many fields ranging from environmental science to oil and gas industries, e.g. to ensure the safety of the working environment. In this context, fiber–optic sensors provide the potential to create very sensitive and selective measurements by combining the versatility of the optical transducer and an intelligent design of the active materials to reach a high sensitivity and selectivity towards specific chemicals [1, 2]. Over the past decades porphyrin derivatives have been extensively employed as functional materials for optical sensing, due to their ability to interact with many different chemical species and to report this binding through changes of their distinctive photophysical properties [3, 4]. The relative simplicity of the synthetic protocols leading to these molecules, allows to design porphyrins having a good processability, and the deposition of layers of such compounds have been achieved through a variety of techniques, both physical and chemical, such as PVD/CVD [5], layer-by-layer electrostatic adsorption [6] , and self-assembling monolayer [7] to name a few. Lately, a non-conventional approach consisting in an UV-light induced deposition of these molecules has been demonstrated on various surfaces, leading to the growth of discrete crystals or uniform thin films [8, 9].

Recent results have shown that porphyrin derivatives are well suited for integration with optical fiber technology, critical for remote sensing within hazardous environments. For instance, fluorescence quenching was investigated for different

porphyrins in combination with complex bifurcated optical fiber probes to detect berberine, mercury ions and picric acid [10-12]. Alternative fiber optic sensing configurations were based on the observation of signature bands in the absorbance spectra of properly selected porphyrins, and an acid-sensor based on the protonation of a porphyrin solution within a single-hole structured optical fiber has been recently reported in the literature [13]. In this case, the critical issue remains the geometrical complexity of the experimental setup: two different fibers need to be perfectly aligned to measure transmitted spectra, while a gap in between is requested to allow the diffusion of acid. As well, a gas sensor able to detect ammonia emitted from human skin has been obtained through coating an unclad fiber with a multilayered porphyrin film [14]. However, while cladding removal permits light interaction with the active multilayer, the final device would exhibit poor mechanical robustness.

We proposed in the previous chapter integration of different molecules on the optical fiber exploiting a UV induced technique. Employing some materials for instance tetrakis (4-sulfonatophenyl) porphyrin (TPPS) in the form of thin film can lead to open possibilities for optical sensing [15, 22, and 23]. Regarding to the results of the previous chapter a self-aligned thin film on the core region is presented as schematically presented in figure3.1. (a) [1]. Figure 3.1 (a) through a self-aligning UV-light induced procedure, as technological platform to realize novel in-fiber devices. This porphyrin has been selected for its capability to form uniform films rather than isolated aggregates with the chosen deposition method [13]. Also, TPPS is able to switch between different aggregation forms in response to the presence of acidic or basic vapors, namely J- and H-type (a cartoon representation is shown in figure.3.1 (b) [16], exhibiting distinctive spectral features [17].

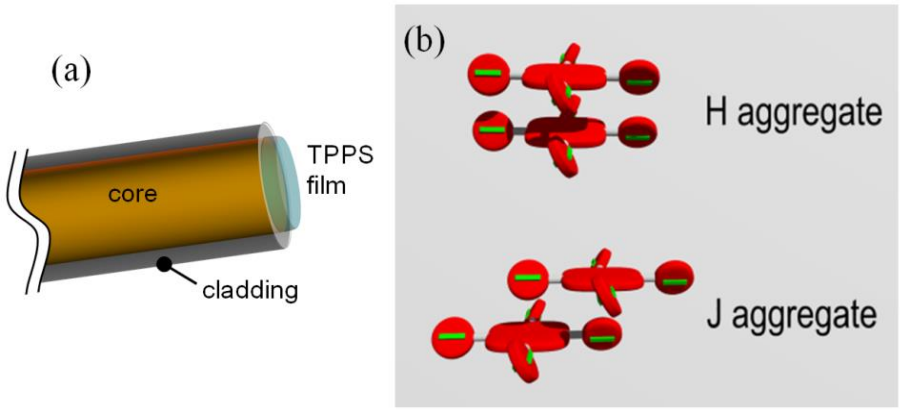

Figure 3. 1: (a) deposited optical fiber, as optical fiber sensor (b) the cartoon presentation of H- and J aggregation of TPPS molecule

3.2 Deposition process: TPPS film deposition

The deposition of TPPS film is achieved by dipping the tip of a multimodal fiber in a TPPS solution in dichloromethane (CH_2Cl_2) and by the subsequent irradiation with UV light coupled to the fiber optics as presented in figure 2.2

The mechanism of film formation on the optical fiber with UV-induced technique, better illustrated elsewhere, [8, and 15] consists in:

(i) The slow decomposition of the halogenated solvent by UV photons, with the localized formation of hydrochloric acid (HCl) near the fiber end;

(ii) The consequent protonation of the dye molecules by the tip with a reduction in their solubility;

(iii) The deposition of the protonated dyes as self-assembled thin film right at the surface of the fiber tip.

The major improvement in the presented experimental setup lies in the versatility of the fiber optics which plays a multiple role:

(i) it permits to guide the UV radiation up to the fiber tip surface triggering the film deposition only on the core region (due to the UV light emission);

(ii) The tip surface acts as support for the sensing material;

(iii) In the characterization step (see below), the optical fiber behaves as waveguide both for the incident (interrogation) radiation and for the backscattered (response) signal in the VIS range.

TPPS film was deposited onto non-standard optical fibers (Ocean Optics) with 200 μm core diameter and 20 μm cladding thickness, for their capability to propagate in UV-VIS range. Fiber tips were prepared by appropriate fiber cleaver and a He-Cd laser (λ = 325 nm; 9.5 mW) was employed as UV source to irradiate a dilute TPPS solution in CH_2Cl_2 (5×10^{-5} mol L^{-1}). It is worth noting that even if the laser wavelength falls outside the strongest absorption region for the solvent (below 240 nm), with a reduced yield of its photochemical decomposition reaction, it still allows a satisfactory deposition. Figure 3.2 (a) and (b) compare microscope images of pristine and deposited

fiber tips, respectively, in the former being clearly distinguishable core and cladding regions, and the crack at the bottom right being a cleaving defect.

Due to our discussion in the chapter two, and the time of deposition, our experiments finally represents that a UV irradiation time around 2 hours leads us in a proper spectral results. The TPPS deposition that is achieved after 2 hours of irradiation, due to the intensity profile of the UV radiation at the fiber tip, the self-assembled film forms mainly at the fiber core in a sort of self-aligning process as we have reported this issue in the chapter two.

Referring the previous chapter analysis, the simplicity of the deposition approach of TPPS film could be easily extended to different molecules (especially porphyrin derivatives) and to different fiber optic configuration providing a new class of devices to be efficiently used in high sensitive environment monitoring. Besides, this intrinsically self-limiting process triggered by the UV radiation could be useful to deposit porphyrin based sensing material with appropriate shape or pattern [8] to enhance light-matter interaction.

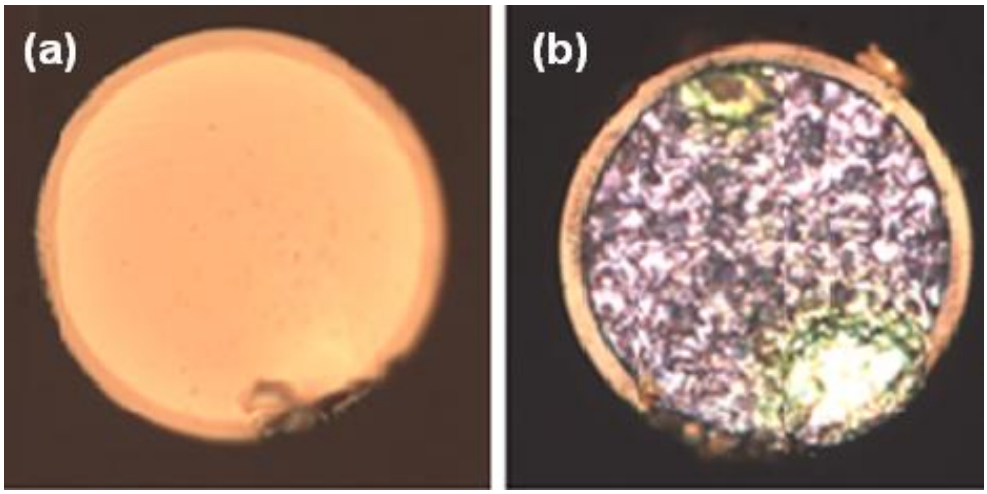

Figure 3. 2: (a) bare fiber (b) the deposited optical fiber tip.

3.3 Reflectance Spectra analysis

Spectroscopic measurements of the reflected signal by the fiber tip have been performed as it is depicted in figure 3.3, by coupling the fiber to a broadband light source emitting in the visible range and to an optical spectrometer (Avantes AvaSpec

mod. 2048) through a 2×1 coupler (50% power splitting in both arms) which allows to split the incident and reflected light.

The reflectance spectra have been obtained by normalization of all signals to the bare fiber spectrum (just after end cleaving), in order to remove the effects of non-flat light source and detector sensitivity across the entire visible range. As we have mentioned in the chapter one it is an important aspect to improve the performance of the optical fiber sensors.

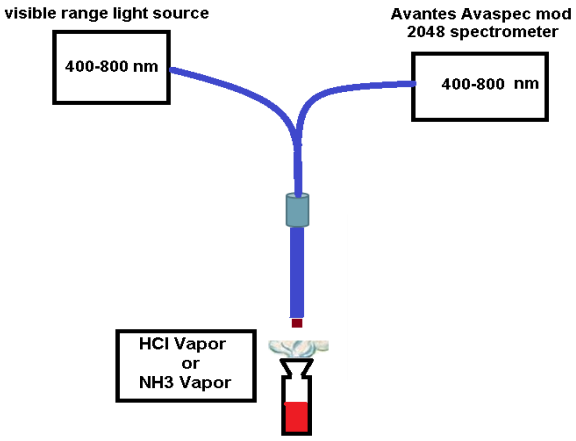

Figure 3. 3: Spectroscopy setup for reflectance analysis of acid and base exposure with sensing aim

Figure 3.4 plots the reflectance spectra of the TPPS coated fiber (dotted black line), where the presence of the self-assembled film causes a decrease in reflectance intensity of about 40% as compared with the 100% reference value. At a difference with the deposition obtained onto quartz in a planar arrangement [15], which allows for a spectroscopic analysis of the light transmitted through the film, the TPPS-coated fiber tip does not exhibit clear spectral features in its reflected spectrum right after film deposition.

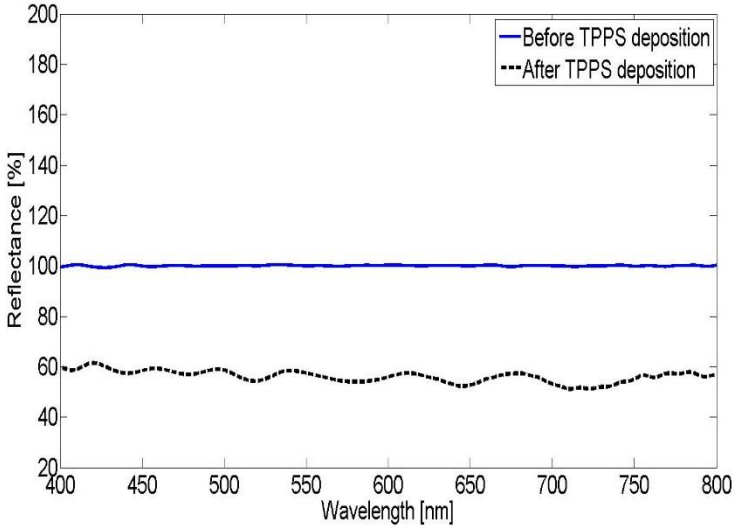

Figure 3. 4: the normalized bare fiber dotted blue curve and TPPS coated film on fiber end (dashed black curve).

To achieve the expected spectral feature we proposed a post deposition process in order to achieve J-aggregate. It is worth noting this process is under a complete control in sense of spectral analysis, steps are the following and in figure 3.5:

1. exposing the thin film with ammonia two minutes
2. Placing the deposited fiber in the air in 5 minutes
3. Controlling the spectral graphs
4. Exposing the film with Hydrochloric acid
5. Remove the fiber to air in 5 minutes
6. Controlling the spectral feature
7. Repeating the steps 1 to 6 since a peak at 490 nm appears after acid.

We should now answer to this question, why the treatment works? The answer is related to the interaction of acid vapor and base vapor, actually when the TPPS film is treated to the base and remains small amount of basic molecules on the optical fiber end, in the second step with exposing in the acid medium acid medium, the film will be protonated and small amount of acid molecule remains on the surface of the thin film. On the other step when the film is treated to the base vapors the remaining acid and base is forming salt and accordingly to the amount of remaining acid and base

,water forms (let's consider this as a formation of water in a controllable manner). This process must be controlled in sense of water amount because the TPPS molecule is water soluble and if the water increases it can wash literally the thin film fiber, so the five minutes between the acid or base is designed for controlling the amount of water formation on the thin film and the cycling steps is in order to increase the formed water amount in a controlled regime.

The presence of controlled water on the thin film is favoring the formation of J-aggregate on the solution form of the TPPS and Silica deposited form. On the other hand the protonation of the film with the water assistance leads to a well arranged J-aggregate.

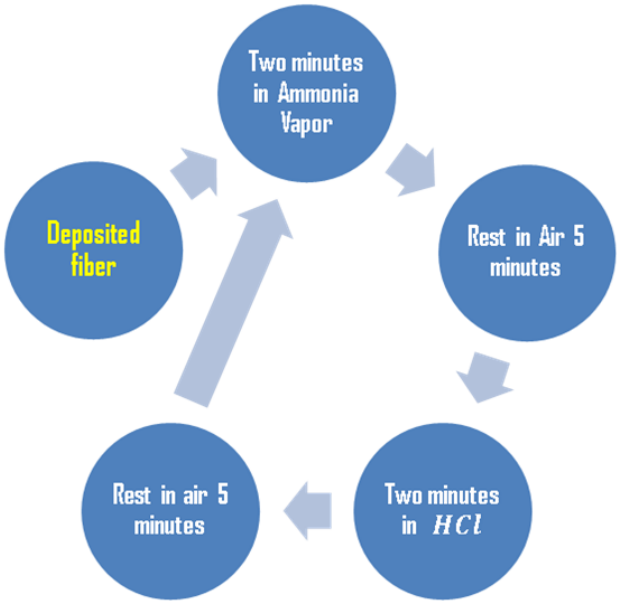

Figure 3. 5: the post deposition treatment on the fiber tip.

3.4 Sensing capability to detect acid vapor

The sensing capability of the TPPS-coated fiber tip was explored aiming to detect the presence of aggressive vapors by monitoring the changes in its reflected spectra.

To this aim, the fiber tip covered by the functional organic layer is put in contact first with ammonia (NH_3) vapors, given that the as-deposited film is acidic in nature. As a consequence, four wells appear in the reflectance spectrum of the film between 500 and 700 nm (Figure 3.6 solid red line), in agreement with the presence of four Q-bands which characterize the typical absorption spectrum of TPPS H-aggregates [15, 17].

When the coated fiber is exposed to acid vapors, the reflected signal exhibits a significant attenuation (between 550 and 750 nm) probably due to the absorption from the acidified TPPS molecules [15,19], with the growth of a resonant light scattering (RLS) signal around 490 nm (approximately +14% from the baseline). The RLS peak amplitude significantly grows upon further cyclic exposures to HCl and NH_3 vapors, while the spectral response to the presence of basic vapors is quasi unchanged. After four cycles, the RLS peak displayed by the film in the presence of acid is very sharp, with a bandwidth of about ~29 nm, and it reaches a reflectance value which is almost twice that of the reference (Figure 3.6, dashed green line).

This particular feature indicate the presence of very ordered J-aggregates [20,21,22] whose growth is favored by water which forms in situ after cycling between ammonia and hydrochloric acid vapors. After this signal is obtained, the functional film will respond to the contact with acid or base vapors by switching between J- or H-type aggregates, respectively, the reflected spectra switching between those reported in Figure 3.6 as solid red and dashed-dot green lines, respectively. Such behavior exhibits a good reproducibility over several cycles

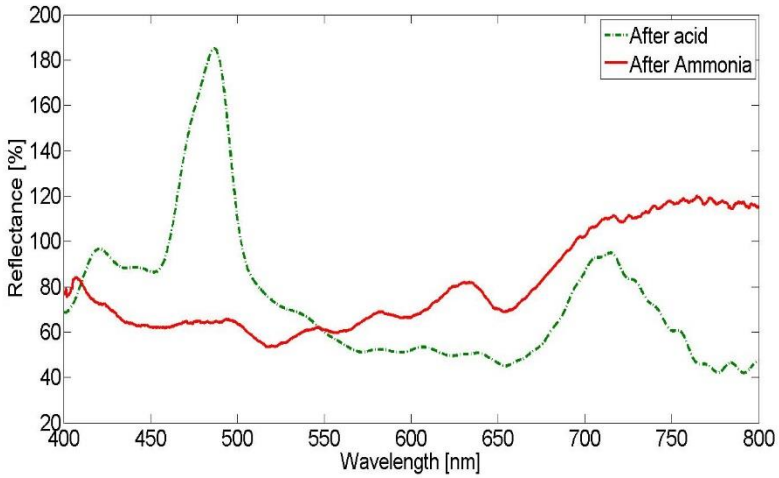

Figure 3. 6: Comparison of the reflectance spectra of the fiber tip in different statuses.

The figure 3.7 reports the amplitude of the reflected signal at λ=490 nm vs. the number of cyclic exposures to HCl and NH_3 vapors. The stability of the signals is remarkable, with changes in the observable value of less than 13%.

However, a higher number of cycles induce a decrease in the RLS peak amplitude probably due to TPPS film damage/poisoning. Several aspects can be the reason to

name, formation of so much water on the optical fiber surface, or mechanical damage due to removing from a medium to another.

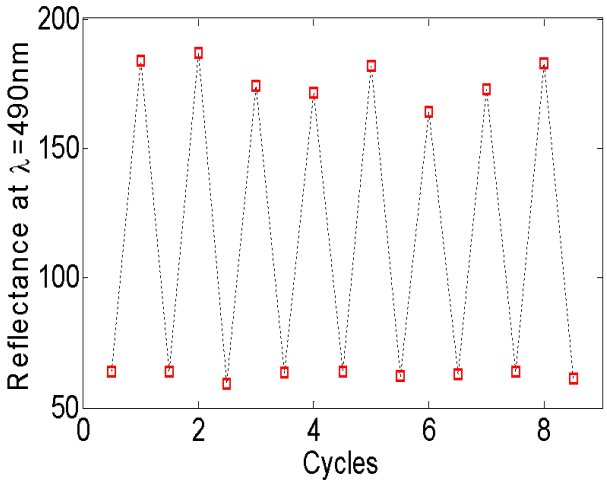

Figure 3. 7: The amplitude of the reflected signal at 490 nm vs. exposure cycles.

The repeatability and reversibility of material in the chemical sensors is one of the most important aspects to control, as we have concluded in the current section current sensor is illustrating a good stability versus the exposure cycles.

3.5 Dynamic response of the sensor

As in past we have shown there are several peaks in the spectral analysis of the TPPS thin film, to choose the best wavelength for dynamic analysis respecting figure 3.8 we consider the wave length with maximum variation in acid (figure 3.8 green curve)and base (red curve) form. Different wavelengths is shown in the graph by vertical lines such as 407nm, 420 nm, 490nm, and 700 nm. Clearly for this investigation the wavelength around 550 nm is not a good candidate due to unchangeable in different environments.

On the other hand the wavelength range between 550 nm -600nm even if the presences of Q-bands are clear but the change between them is not considerable.

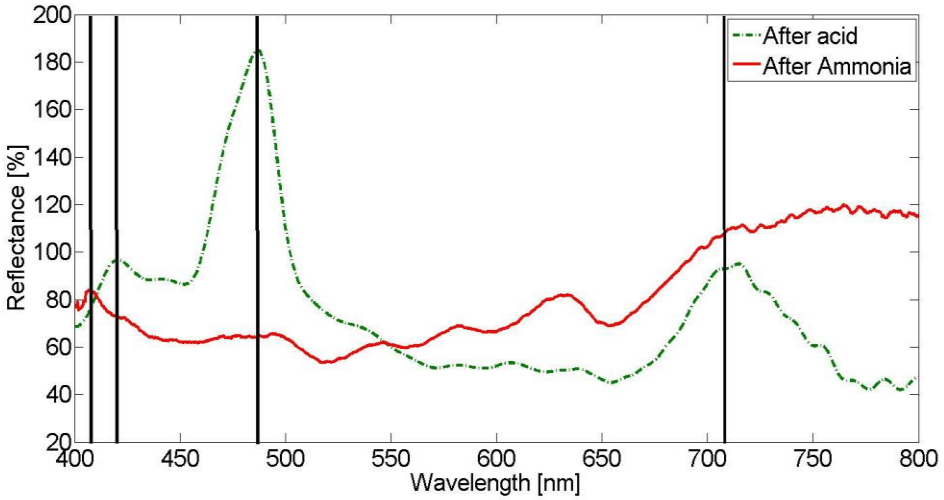

Figure 3. 8: The green curve presenting the acid form and the base form is presented in red curve the important wavelengths are shown by vertical lines.

Hence the time response of the sensor is studied by observing the signal amplitude of the main resonant peak vs. time after exposure to base or acid vapors (Figure3.9 (a) and 3.9 (b), respectively; λ = 490 nm). The observed dynamic response is fast as compared with previous work involving porphyrin species and optical fiber technology [13].

Especially when considering the decrease in signal intensity occurring after exposure to base vapor which is of the order of very few seconds, less than 10 seconds in all our experiments. We can interpret this in sense of aggregation switching; it can be evident of a turn from J-Aggregate to H-Aggregate or instability of J-form of aggregation in presence of Base.

In the case of exposure to acid, the change in reflectance at 490nm initially shows a slow induction period where the signal amplitude displays approximately a 10% increase in about 50 seconds and, then, a fast increase at least 180% reflectance is observed in about 10-12 seconds.in all of our experiments we got the same level of increase which can be interpreted for the repeatability of our experimental results and opening a promising field for a new class of pH sensors on the optical fiber technology.

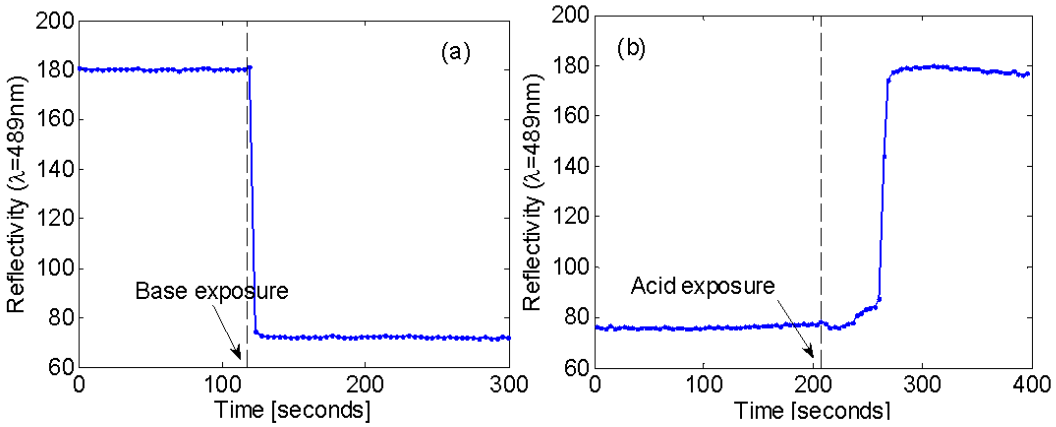

Figure 3. 9: Amplitude of the reflected signal at fixed wavelength 489nm versus time during (a) base exposure and (b) acid exposure.

As we have shown the fast response is achievable with our arrangement of TPPS molecules deposited on the optical fiber end. These studies present a very simple arrangement of TPPS integrated to optical fiber is potentially good insitu optical fiber.

3.6 Fluorescence Spectroscopy

In this section finally our studies on the TPPS film deposited on the optical fiber end promoted us to investigate the possibility to use TPPS-coated fiber tips as sensors for aggressive vapors also by monitoring the fluorescence spectra from the functional organic layer. The optical setup of the fluorescence investigation as shown in figure 3.10 is consist of an spectrometer a visible range light source and deposited optical fiber and another optical fiber for delivering visible light to the fiber tip.

the fiber tip covered by the TPPS layer was directly connected with the optical spectrometer (avaspec 2048 mod) to analyze the fluorescence emission in the visible range which couples with fiber optic (optical fiber ocean optics with 200 μm core diameter) working on the UV-Visible range, and that has been excited by lateral illumination of the tip with a white light source.

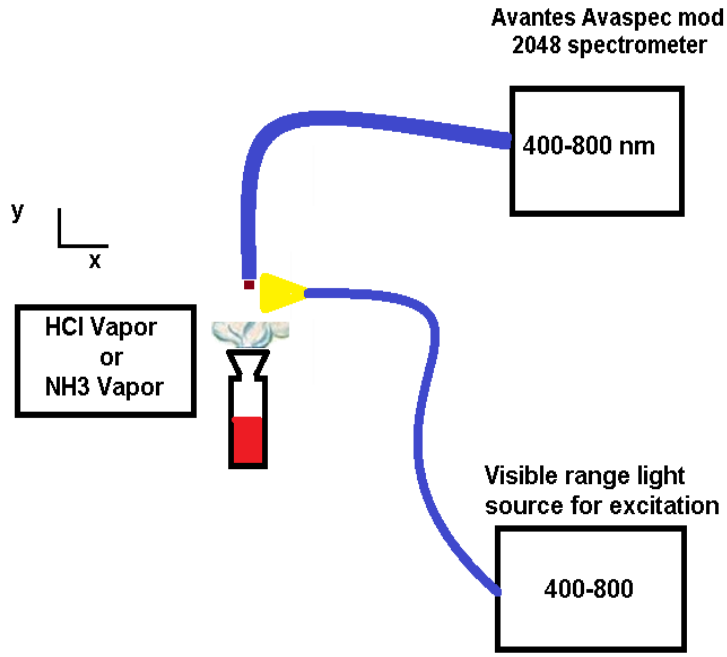

Figure 3. 10: Presenting the optical setup to achieve fluorescence spectrum of acid vapor or alkaline sensor.

The orthogonal illumination let us to excite the film avoiding to couple the exciting emission to the fiber, it assure us the observed light on the fiber is florescence emission from the TPPS coated film in presence of acid vapor or alkaline.

The spectrum obtained through the described experimental setup right after film deposition exhibits a quasi-constant zero value (figure 3.11 black line), which is almost in dark state. That means the deposited film itself does not present any fluorescence feature in the neutral form (neither acidic nor basic) or better to say the deposited film on the fiber end itself does have sort of aggregation leads to florescence spectrum, it is an important point while for selectivity of the sensor in presence of acid or base vapor. whereas after a few cyclic exposures to HCl and NH3 vapors, both the acidic and basic forms of the TPPS thin film starts presenting clear spectral features. The spectrum collected in the presence of acid exhibits an apparent maximum in the green region (λ about 560 nm the figure 3.11 blue curves) which is feasibly due to resonant scattering from the film. In its turn, the second strong feature observed at longer wavelengths (λ > 700 nm) is compatible with fluorescence emitted by the deposited organic layer [15] that successfully couples with the multimodal fiber optics.

In its basic form, the signal recorded for the TPPS film is heavily modulated by absorption, showing four wells which correspond to the four Q-bands characterizing

the spectrum of the basic porphyrin. Also in this case, the signal collected at longer wavelengths ($\lambda > 650$ nm figure 3.11 red curve) can be attributed to the thin film fluorescence, in good agreement with the spectra recorded with a standard setup [15]. All this evidence support the possibility to exploit the strong differences in the spectral features recorded with the just-described optical setup, yielding other observables that can be used to detect the presence of harsh vapors.

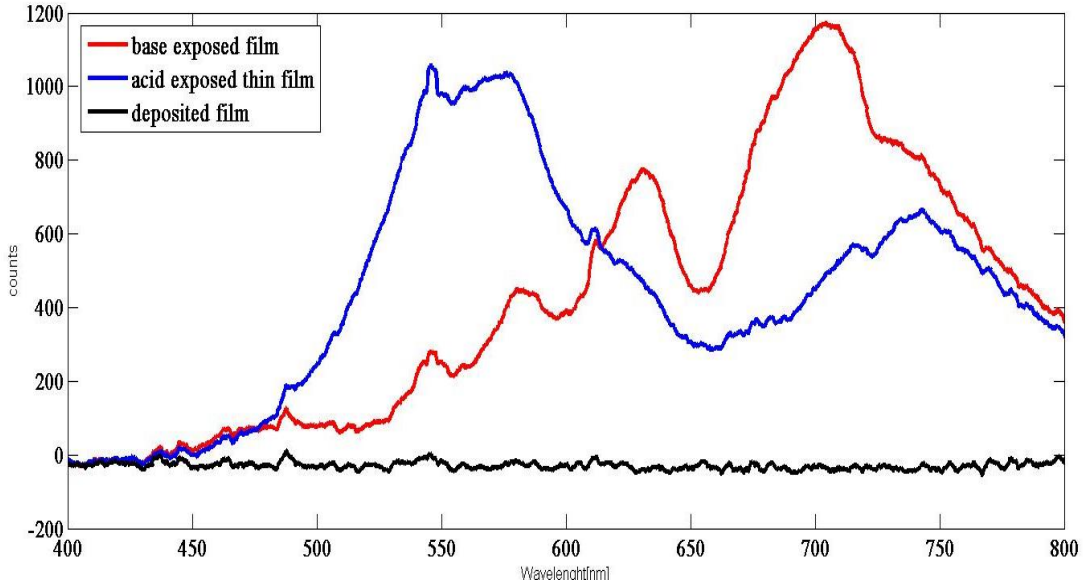

Figure 3. 11: The deposited film without any treatment black line, the TPPS coated film treated by acid (blue curve) and base exposed TPPS coated film (red curve).

3.7 Microscopic results for Acid and Base vapor exposed films

The different spectroscopic features exhibited by the self-assembled TPPS film are evident also when the samples are analyzed through optical microscopy, where blue-green and red-brown colors are displayed by the organic layer in the presence of acid or basic vapors (Figure 3.12 a (a)and (b), respectively).

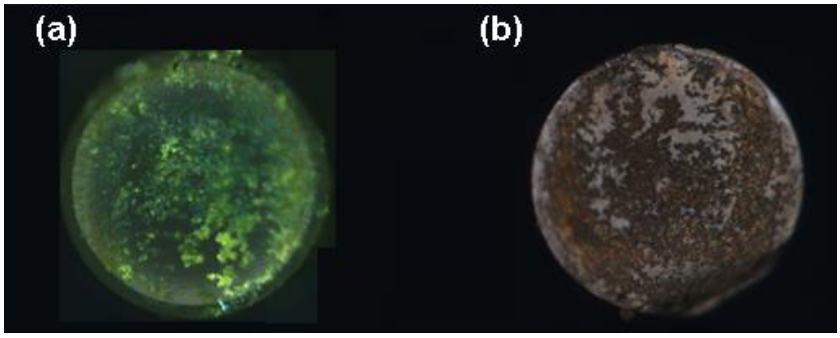

Figure 3. 12: (a) Acid exposed film deposited on the optical fiber (b) base exposed thin film on the optical fiber.

The microscopic images also reveal that the TPPS film is actually damaged by the cyclic exposure to HCl and NH_3 vapors. But one of the reasons can be the amount of water formed during several cyclic exposures and more over the salt crystallization on the fiber tip. For a better understanding of this phenomenon some more work is currently under further investigation in our group.

In another sample with longer deposition time around 3 hours of UV irradiation the cyclic acid and base exposure presents similar aspects in agreement to the color of thin film similar with figure 3.12 the red-brown surface related to figure 3.13 (b) and green surface related to figure 3.13 (a) are presenting the exposed film with base and acid respectively.

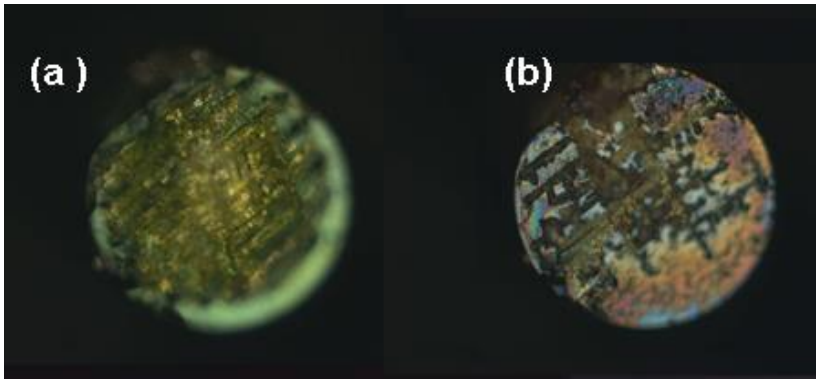

Figure 3. 13: (a) acid exposed thin film (b) base exposed thin film.

Another microscopic analysis with exposing the film on the sample of figure 3.13 (b) with acid for 5 minutes is acid medium, is also presenting the green film with more damage respecting to figure 3.13 (a) as depicted in figures 3.14.

About self-alignment referring to figure 3.13 (a) the thin film shows the border for core and cladding while in the base form in figure 3.13 (b) the effect also is removed and accordingly in figure 3.14 the self-alignment is also a destroyed phenomenon. Maybe one of the possible explanations in this issue is expanding the film on the surface due to formation of water in different cycles, thus consequently decreasing the thickness of the TPPS film has happened.

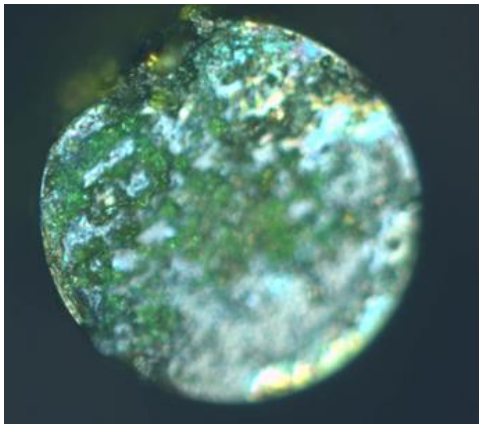

Figure 3. 14: The film treated by acid just after base and second round with base.

3.8 Summary

In conclusion, in this chapter we demonstrated the possibility to use the UV-light induced deposition technique to integrate a porphyrin layer with optical fiber technology, providing novel optoelectronic devices. This technique with a very simple process very stable film on the optical fiber thus presents a very stable integrated device on optical fiber.

This configuration already allows to obtain an early warning of the presence of hazardous gases in the environment by monitoring spectral features of the TPPS films through the back scattered resonant signal and/or the fluorescence components. The backscattered signals clearly presenting the presence of J- form of aggregation and H-form of aggregation in presence of acid gases (protonated TPPS film) and base gas (deprotonated TPPS film) respectively.

Bibliography

1. M. Giordano, M. Russo, A. Cusano, A. Cutolo, G. Mensitieri, and L. Nicolais, "Optical sensor based on ultrathin films of δ-form syndiotactic polystyrene for fast and high resolution detection of chloroform," Appl. Phys. Lett 85, 5349 (2004).
2. Cusano, P. Pilla, L. Contessa, A. Iadicicco, S. Campopiano, A. Cutolo, and M. Giordano, "High-sensitivity optical chemosensor based on coated long-period gratings for sub-ppm chemical detection in water," Appl. Phys. Lett 87, 234105(2005).
3. S. H. Lim, L. Feng,J. W. Kemling, C.J. Musto,K. S. Suslick, "An Optoelectronic Nose for Detection of Toxic Gases," Nature Chemistry, 1, 562-567 (2009)
4. K. M. Kadish, K. M. Smith, R. Guilard, R., Eds. *The Porphyrin Handbook*, (Academic Press, New York, 2000), Vol. 6
5. S. Stelitano, G. De Luca, S. Savasta, and S. Patanè, "Polarized emission from high quality microcavity based on active organic layered domains," Appl. Phys. Lett 93, 193302 (2008).
6. K. Araki, M. J. Wagner, and M. S. Wrighton, "Layer-by-layer growth of electrostatically assembled multilayer porphyrin films," Langmuir 12, 5393–5398 (1996).
7. Z. J. Zhang, S. F. Hou, Z. H. Zhu, and Z. F. Liu, "Preparation and characterization of a porphyrin self-assembled monolayer with a controlled orientation on gold," Langmuir 16, 537-540 (2000).
8. L. Monsù Scolaro, A. Romeo, M. Castriciano, G. De Luca, S. Patanè, and N. Micali, "Porphyrin Deposition Induced by UV Irradiation," J. Am. Chem. Soc. 125, 2040-2041 (2003).
9. G. De Luca, G. Pollicino, A. Romeo, S. Patane, and L. Monsù Scolaro, "Control Over the Optical and Morphological Properties of UV-Deposited Porphyrins Structures," Chem. Mater 18, 5429-5436 (2006).
10. X. B. Zhang, Z. Z. Lib, C. C. Guoa, S. H. Chena, G. L. Shena, R. Q. Yua , "Porphyrin–metalloporphyrin composite based optical fiber sensor for the determination of berberine," Analytica Chimica Acta 439, 65-71 (2001).

11. X. B. Zhang, C. C. Guo, Z. Z. Li, G. L. Shen, and R. Q. Yu , "An optical fiber chemical sensor for mercury ions based on a porphyrin dimer," Analytical Chemistry 74, 821-825 (2002).
12. R. Ni, R. B. Tong, C. C. Guo, G. L. Shen, and R. Q. Yu, "An anthracene/porphyrin dimer fluorescence energy transfer sensing system for picric acid," Talanta 63, 251-257 (2004).
13. G. Huyang, J. Canning, M. L. Åslund, D. Stocks, T. Khoury, and M. J. Crossley , "Evaluation of optical fiber microcell reactor for use in remote acid sensing," Optics Letters 35, 817-819 (2010).
14. S. Roman, K. Sergiy, Y. Wataru, and L. Seung-Woo, "A Preliminary Test for Skin Gas Assessment Using a Porphyrin Based Evanescent Wave Optical Fiber Sensor," Sensors & Transducers 125, 54-67 (2011).
15. G. De Luca, G. Pollicino, A. Romeo, and L. Monsù Scolaro, "Sensing Behavior of Tetrakis (4-sulfonatophenyl) porphyrin Thin Films,"Chem. Mater 18, 2005-2007 (2006).
16. M. Kasha, H. R. Rawls, and M. A. El-Bayoumi, "The exciton model in molecular spectroscopy," Pure Appl. Chem 11, 371-392 (1965).
17. G. De Luca, A. Romeo, V. Villari, N. Micali, I. Foltran, E. Foresti, I. G. Lesci, N. Roveri, T. Zuccheri, and L. Monsù Scolaro, "Self-Organizing Functional Materials via Ionic Self Assembly: Porphyrins H- and J-Aggregates on Synthetic Chrysotile Nanotubes," J. Am. Chem. Soc 131, 6920-6921 (2009).
18. R. F. Pasternack and P. J. Collings, "Resonance light scattering: a new technique for studying chromophore aggregation," science 269, 935-939 (1995).
19. G. De Luca, A. Romeo, and L. Monsù Scolaro, "Counteranion Dependent Protonation and Aggregation of Tetrakis (4-sulfonatophenyl) porphyrin in Organic Solvents," J. Phys. Chem. B 110, 7309-7315 (2006).
20. O. Ohno, Y. Kaizu, and H. Kobayashi, "J-aggregate formation of a water-soluble porphyrin in acidic aqueous media." J. Chem. Phys 99, 4128-4140 (1993).
21. P. J. Collings, E. J. Gibbs, T. E. Starr, O. Vafek, C. Yee, L. A. Pomerance, and R. F. Pasternack, "Resonance Light Scattering and Its Application in

Determining the Size, Shape, and Aggregation Number for Supramolecular Assemblies of Chromophores," J. Phys. Chem. B 103, 8474-8481 (1999).

22. Bahrampour A, et al. Optics and Laser Technology (2013), http://dx.doi.org/10.1016/j.optlastec.2013.01.019i.
23. Bahrampour, A. Iadicicco, G. De Luca, M. Giordano, A. Cutolo, L. Monsù Scolaro, and A. Cusano, "Sensing Characteristics to Acid Vapors of a TPPS Coated Fiber Optic: a Preliminary Analysis" proceeding World Academy of Science, Engineering and Technology Venice,November 2012, https://www.waset.org/journals/waset/v71/v71-2.pdf

Section II

Chapter 4

Introduction to Photonic crystal fibers

4.1 Introduction

Optical fibers were known as a composite of two different transparent material in a cylindrical form famous as core and cladding.

A revolutionized idea came out in 70s first by Yeh et al. [1], they proposed an air guiding optical fiber using concentric cylinders. Latter in 1995 a brilliant work presents a 2-D photonic crystal (PC) lattice can be employed to fabricate optical fiber [2]. The idea was to use a silica with a lattice of periodic holes which run along the fiber. This new idea open possibilities to have a new index guiding and Photonic bandgap (PBG) guidance.

Photonic crystal fiber (PCF) with solid core is more similar to conventional fibers with almost similar properties. Light is confined to core because of presence of holes around the core induced a reduction in refractive index average [3], the resulting index difference permits light propagation similarly to conventional optical fibers. It is nice to mention about these fibers which, guidance is based on the change of the refractive index as function of wavelength considerably. Therefore they call it modified total internal reflection (MTIR). The mentioned mechanism, as well as high refractive index contrast provides wide range of new interesting features like, high birefringence[4], enhanced Raman scattering[5].

Other mechanism rely on possibility of light propagation in the region or core with refractive index less than cladding. Basically it is not possible with Total internal reflection (TIR) [6]. Therefore we should look for another idea to trap light in the core of the fiber instead of TIR. The idea come from mirror formation phenomena, professor Yeh 1978 represented this possibility with concentric layers of different glasses [1]. Latter in a private communication and conference professor Philip Russell spoke about the possibility of air guiding (core with lower refractive index) via employing a PBG

phenomenon (PBG). PBG is a wavelength region which light cannot propagate through the crystal. The air holes and refractive index contrast of air-silica cause a PBG.

Introducing a defect in a PC structure, like a hole can induce the light propagation in defect because the PBG stops light propagation in the microstructured cladding. This guiding mechanism, represented vast field of potentiality in front of scientists. The air guiding opens a completely new series of application for optical fibers resulting to high impact enhancement in different applications of optical fibers.

In particular light which is confined in air, opens the hope to break ceiling of the loss with reducing Rayleigh scattering, and reduced nonlinearities and also high power light delivery without the risk of fiber damage [7].

Hollow core Photonic crystal fiber(HC-PCFs) present extreme dispersion properties and more over as discussed in literature, once the holes are filled with gases and are effected by some physical properties can lead to physical and chemical sensors [8]. In reality the HC-PCF has improved the science of optical fiber sensing with its outstanding properties, reduced luminescence and long length interaction with gap medium. Which leads to find high nonlinearities of gases [9].

This research line due to opening many engineering and scientific interests become so intriguing and many people are working on different aspects of PCFs.

The geometrical tuning of PCFs can control the modes, field profile, and guiding properties. For example PCF endlessly single mode fiber can be achieve by a careful control of triangular lattice [10]. low air filling and large pitch can lead to high-power propagation [11] a significant asymmetry can induce birefringence (which is practically possible also based on the different fabrication abilities) [4]. Therefor dispersion properties are completely tailored with the geometry.

In this chapter the aim is accurately studying and understanding of PCF and PBG of the hole-silica PCs. The bandgap study and gap map representations will be well depicted in this chapter and beside all a hollow core PCF will be studied. Air guiding fundamental mode of the HC-PCF will be analyzed by a finite element method (FEM). It is very intriguing to know how far we can go from the well-defined PCF and how the geometry properties are entangled with guiding properties. In the next chapters we will devote our work on the geometrical study of the PBG fibers. We will study the effect of different geometries in aperiodic class on the guiding properties.

4.2 The Light confinement mechanism

Photonic crystal fiber (PCF) also famous as microstructured optical fibers, due to microstructure geometry, can be divided to 1-D or 2-D PCFs.

These fibers can be divided to few category of guiding mechanism as well. PCFs guiding mechanism is divided to index guiding, or the light is confined in core using a band gap phenomena. It is important to repeat, which the 2-D PCFs with a solid core figure 4.1 (a), can be presented when the holes are used to provide a lower effective (average of refractive) index of cladding region. These fibers are famous as index guiding PCF or solid core PCF. There is no band gap mechanism associated to this fibers. This class of fiber represents very good nonlinearities, or unusual dispersion due to high dielectric contrast which generally is not possible with standard fibers.

Photonic bandgap fibers is studied in two different structural fashions:

1. 1-D microstructure: This structure is made of concentric layers and is well studied by Yeh et al in 1978 [1], figure 4.1(b) represents the schematic of this structure. This structures are famous as Bragg fiber or omnidirectional optical fibers.
2. 2-D microstructure: The most commonly used and studied PCF of this category is holey fiber, in which 2-D periodic array of holes running along the whole fiber.in figure 4.1. (c).

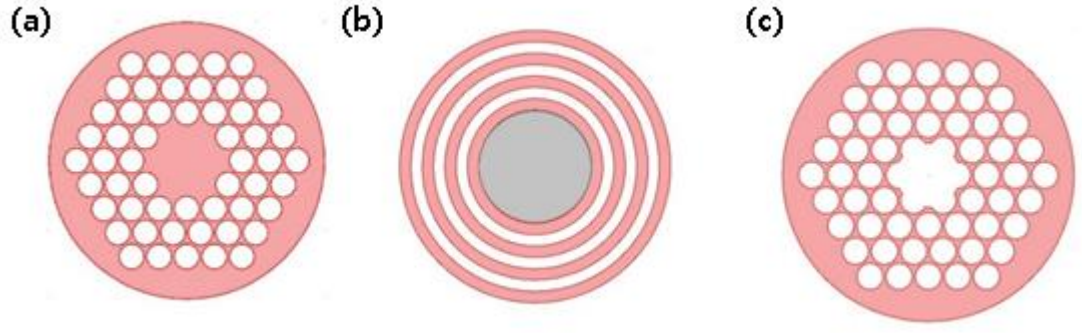

Figure 4. 1 (a) Solid core PCF, (b) Bragg fiber schematic, (c) Hollow core PCF.

In this chapter we focalized our attention on the 2-D periodicity in transverse direction of optical fiber and we will study a hollow core PCF with presenting the band gap structure, modal study of the optical fiber with light confinement in air core. In this thesis all the calculation is provided with finite element method, for finding and

analyzing the fiber modes an eigenmode problem is solved with respect to find effective index as eigenvalue.

4.2.1 Modified total internal reflection

The possibility of using PC instead of cladding is approved in several works [1-7] considering a solid glass core surrounded by PC Figure 4.1 (c) is an example of solid core fiber with a cladding of a triangular lattice of air holes. This fibers as we mentioned are famous as "index guiding PCF" and "solid core PCF". These fibers have presented several properties in compare with standard TIR fibers. From these optical fibers phenomena of endlessly single-mode fiber appeared [10]. Considering a fiber with a triangular lattice as cladding and with hole radius of r=150 nm and hole to hole spacing Λ of 2.3 nm experimentally it proof the possibility of presence of only one mode and even in short wavelengths, no more modes appear. In reality the confined modes in core always have a single strong central lobe filling the core which means the fundamental mode can be excited with any other mode so even if there are more modes they excite the fundamental mode [6].

Let's explain a bit of physics of MTIR mechanism, light in air holes are in form of evanescent waves and air holes are playing the role of barriers to stop light propagating in crystal. Let us assume the fiber as a sieve and the lattice of holes like the wire lattice of sieve as fundamental mode in the fiber is only made of a single lobe that with considering the diameter of it is almost 2 Λ and its size define the size of seeds cannot go out of the fiber. So just considering we increase the hole diameter it means the smaller lobe size also can trap in the core, so with increasing *r* the number of modes which can trap in core increases [6].

Taking the advantages of single mode properties, it is potentially possible to design very large-mode surface fibers. It can be used to deliver high power light, for medical use. Non linearity's in this fibers are enhanced and mentioned in literature [5].

4.2.2 Photonic bandgap guidance

HC-PCF, fibers with hollow core as presented in figure 4.2, are new design of optical fiber based on the propagation mechanism. It is due to the PBG of the crystal. Considering PC cladding where the modal index is supporting the modal index

of β/k_0 , while it is not possible to find propagation mode in the crystal. This situation which is called photonic crystal band gap don't let light propagation and penetration in the crystal.

These modes are similar to the modes propagating in the 2-D photonic crystal with a difference in the incident wave. The incident wave contain also a non-zero value of out of plane wave vector.

Considering why we employ PBG mechanism to propagate light in air, because using Total internal can provide light propagation in air if it is possible to find an appropriate material to fabricate cladding, with refractive index less than air, which to this moment there is no evident to open this possibility[12].

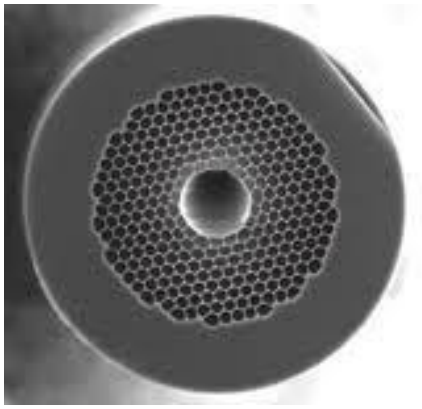

Figure 4. 2: Is presenting the triangular lattice. And its fabrication. The microscopic photography is kindly provided by Optoelectronic group university of Naples "Parthenope".

We would like to provide a more detail for the PBG guidance in hollow fiber. As aforesaid the PBG let the light to be confined in the waveguide in lower refractive index.

Let's assume a 2-D PC structure which is running along the length of optical fiber, two consideration will be taken in to account, first of all a discrete translational symmetry related to x-y plane, and a continues translation symmetry along z-direction. The fiber due to the z-axis symmetry cannot have complete band gap in any wave vector k_z and actually it is not necessary to have a complete band gap for the optical fiber. Resulting from continuity of translational symmetry the wave vector would be conserved along the optical fiber, therefore a band gap in 2-D with considering non-zero k_z is enough and useful.

Let's consider the cladding with periodic structure without core defect, considering that in any k_Z the bands of the structure are the usual Bloch modes and forming a band

structure in a two dimensional Brillion zone (B-zone). Our aim is to find a range for wave vector of k_Z which will be existed a gap between 2 consequent bands.

In spite of having a 2-D periodic structure we cannot consider our problem as planar x-y PC and the band gap in 2-D PC does not provide enough sense. The reason is due to the presence of third dimension as optical fiber length and the fiber problem itself requires another propagation component in z-direction ask_Z. Therefore considering a two dimensional problem is not enough, so the problem will be in two dimension taking care of $k_Z \neq 0$ as it is depicted in figure 4.3.

On the other hand for the planar structure at $k_Z = 0$ the low refractive index contrast is not letting to appear band gap.

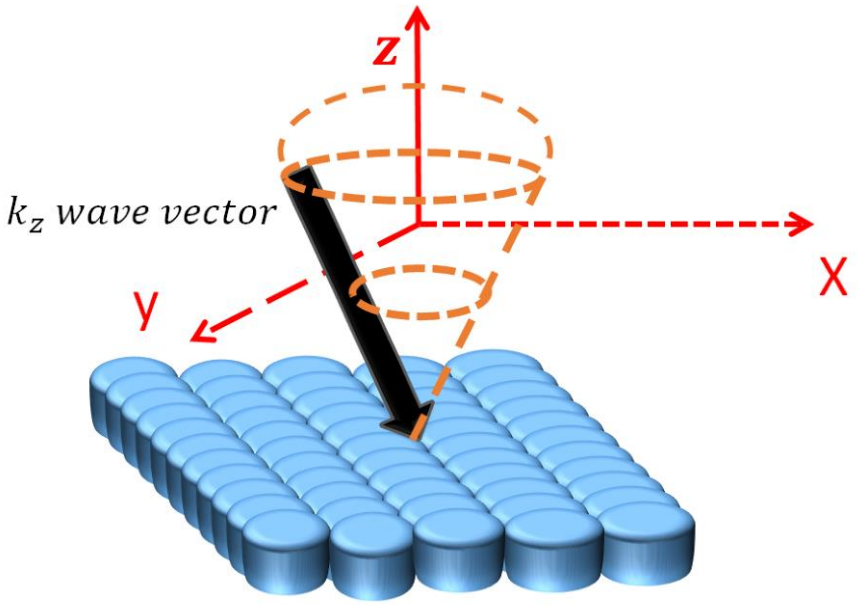

Figure 4. 3: The schematic presentation of the HC-PCF problem.

If we would have a band gap in $k_z = 0$ for sure it will be a range $k_z \neq 0$ which the band gap existed, but unfortunately the silica-air refractive index contrast is an important matter of unfortunate [13,14].

It became clear $k_z = 0$ is not advantageous to solve our problem so we will explain gap formation behavior where $k_z \neq 0$.

It is important to notice assuming the $k_z \neq 0$ the distinction between TE modes and TM modes disappear, hence we may look for the hybrid modes HE/EH modes in solving the PCF. To explain better the physics of the problem we considered a

structure with a triangular lattice and we tried to calculate PBG and modes of the fiber using finite element method.

4.2.2.1 Triangular lattice as photonic crystal fiber

Triangular lattice as periodic lattice is a good candidate to study PBG of the HC-PCF and the study of the mechanism of light confinement. There are several works studied this structure [15]. As it is shown in figure 4.4 (a) a triangular lattice is made of a periodic array of holes on silica where $\frac{r}{\Lambda} = 0.45$, r is representing the radius of the holes and Λ is the pitch (hole-to-hole distance) the mentioned ratio induce a surface air filling of the PC:

$$S_{AFF} = \frac{surface\ of\ air}{all\ the\ surface} = 0.75$$

In figure 4.4 (b) a unitcell of the structure is depicted, and with defining vectors $a_1 = \Lambda(1,0), a_2 = \Lambda\left(\frac{1}{2}, \frac{\sqrt{3}}{2}\right)$, $and\ R = l_1 a_1 + l_2 a_2$, where $l_1\ and\ l_2$ are integer numbers we can define all the lattice geometrically.

We chose the refractive index of glass considered as $n_{glass} = 1.46$ and the refractive index of air is considered as $n_{air} = 1$.

To calculate the band diagram we solve an eigenfrequency problem to find the band with changing the plane wave vectors around the irreducible B-zone. Band gap as a matter of interest is found when two preceding bands are considered and the lower band's maximum is lower than the upper band's minimum, this situation a frequency gap will be defined and presented as a function of in plane wave vector. The result of band diagram as a function of in plane wave vector in the irreducible B-zone (figure 4.5 (inset)) is calculated using finite element method, at different out-of-plane wave vector figure 4.5 is representation of band diagram when $k_z \Lambda / 2\pi = 0.05$. As it is well presented there are no band gap in this diagram and it is due to disappearing (better to say mixing) pure TE and TM modes and low refractive index contrast.

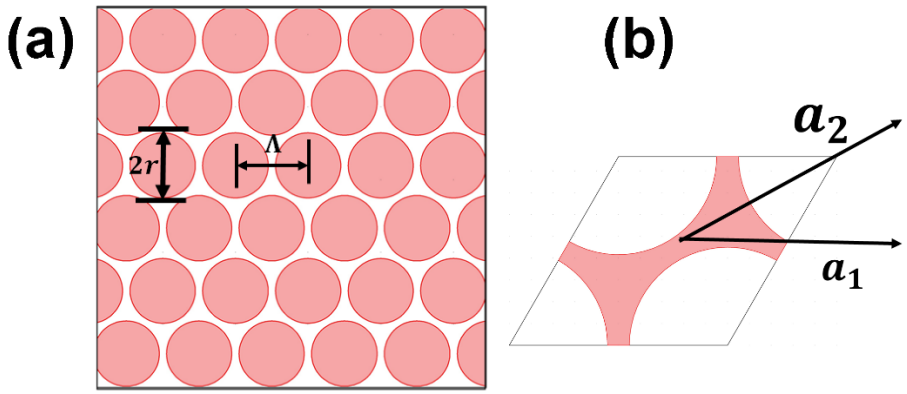

Figure 4. 4: (a) The triangular lattice (b) unitcell to define lattice.

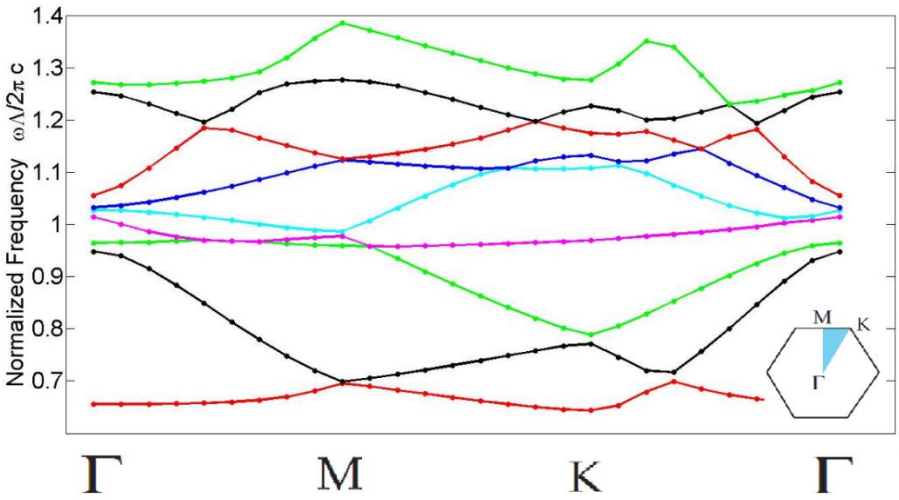

Figure 4. 5: The band diagram versus in-plane wave vector in the irreducible B-zone (inset) at the out of plane$kz\ \Lambda/2\pi\ = 0.05$.

We are aimed to increase k_z and observe dependence of wave vector controlling on the band structure. With an increase of $k_z\Lambda/2\pi$ to $k_z\Lambda/2\pi = 0.5$ the band diagram of triangular lattice as function of in-plane wave vector representing band gaps as it is depicted in figure 4.6.

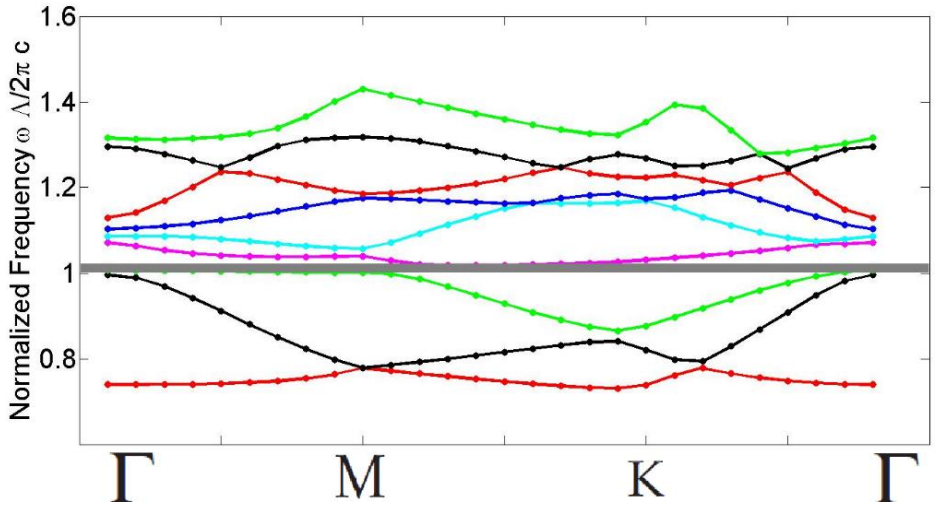

Figure 4. 6: Is representing the band diagram versus in plan wave vector in the Irreducible B-zone at kz Λ/2π =0.5.

The tiny shaded region representing the band gap at mentioned wave vector and it is intriguing to have band gap in this level of index contrast. Notice: the other hand the gap is calculated in the same irreducible B-zone.

The same analysis is implemented for calculating band diagram when $k_z\Lambda/2\pi = 1.6$ representing the appearing a wide band gap as shaded region in figure 4.7.

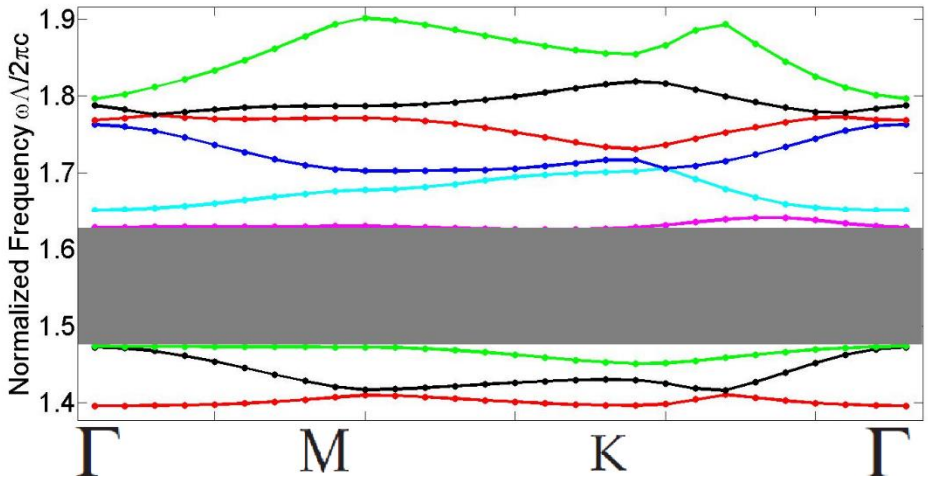

Figure 4. 7: Band diagram versus in plane wave vector at kz Λ/2π =0.5.

The band gap appearance in increasing the wave vector is depicted in figure 4.6 and 4.7 but actually, air guiding is our limit to increase the k_z, when we can have the guiding in the air which the gap open-up is not belong to a high wave vector. Therefore the limit is when the band gap is above the line of air $\omega = ckz$, which if we denote

normalized frequency (ω_n) and normalized wave vector (k_n) then the light line is($\omega_n = k_n$).

To represent our calculation for the band gap diagram, we need to calculate the band diagram as a function of out of plane wave vector k_z, the mentioned graph called projected band diagram and as it is shown in figure 4.8 representing the path way which light can propagate inside the hollow core. In our calculation the core defect is not considered and all calculation of band gap is based on the microstructured cladding of the fiber. As it is represented in figure 4.8 with increasing the wave vector the band gap the width of blue error bars increases, and at a certain frequency it passes the air-line which is important turn point for fiber calculation.

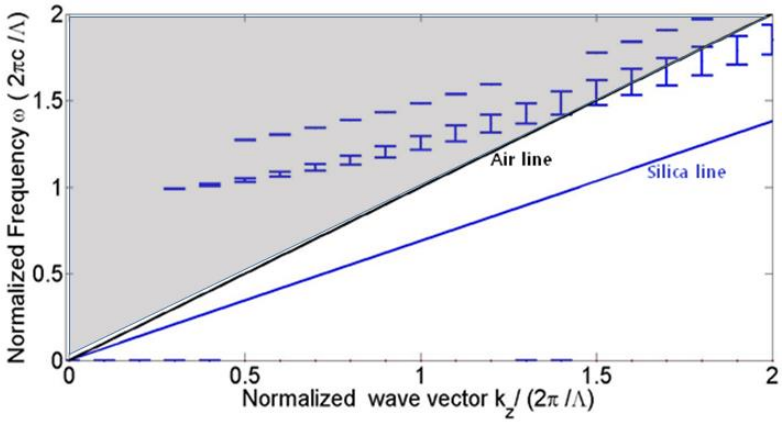

Figure 4. 8: The projected band gap as function of out of plane wave vector.

For band gap map presentation we prefer (due to our modal study of HC-PCF) the representation of effective index versus normalized wavelength. Referring to figure 4.9 the shaded grey region is where the band gap fall and a blue curve representing the light cone. We already stated the limitation of the wave vector is where the bandgap is above the light cone (grey region) in figure 4.8 but in the figure 4.9 due to different bandgap presentation, "the intersection of bandgap with region $n_{eff} < 1$" is the region which light can propagate in hollow core and remain completely confined in the core of the fiber. That means we must look for the effective index which are less than one in our modal analysis.

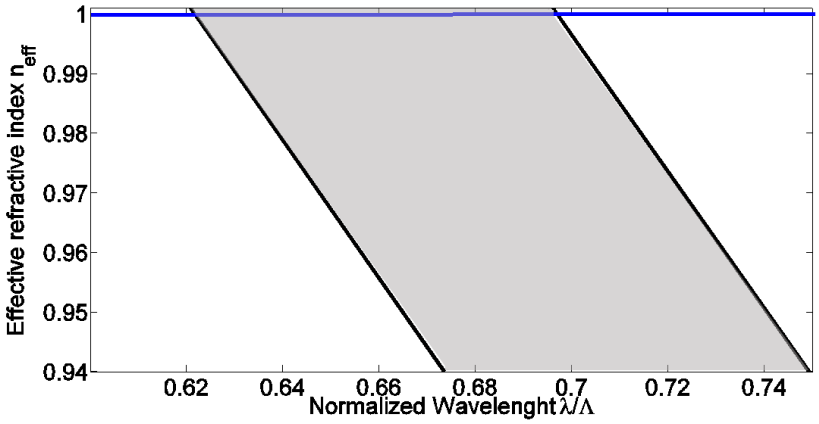

Figure 4. 9: Representation of the band gap a function of effective index vs. normalized wavelength.

4.2.2.2 Guided modes in hollow core

Regarding to aforesaid structure of band gap now we consider the presence of defect core, famous as hollow core to realize the fiber. The figure 4.10 depicting the optical fiber structure with a hollow core which we are studying. The hollow core is covering the area of seven holes and the core radius of $R = 1.202\ \Lambda$. The fiber is made of 4 layers of holes and completely periodic.

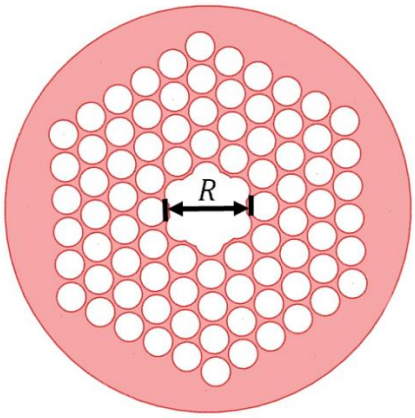

Figure 4. 10: The optical fiber with a hollow core of diameter of R formed by triangular periodic structure

Respecting to previous section the first bandgap is considered. The fundamental mode of fiber is studied and found with solving an eigenvalue problem, the results for effective index of the fiber structure (figure 4.10) is depicted in figure 4.11. Figure 4.11

representing the dispersion of the fundamental mode in hollow core. Actually they are two degenerate modes.

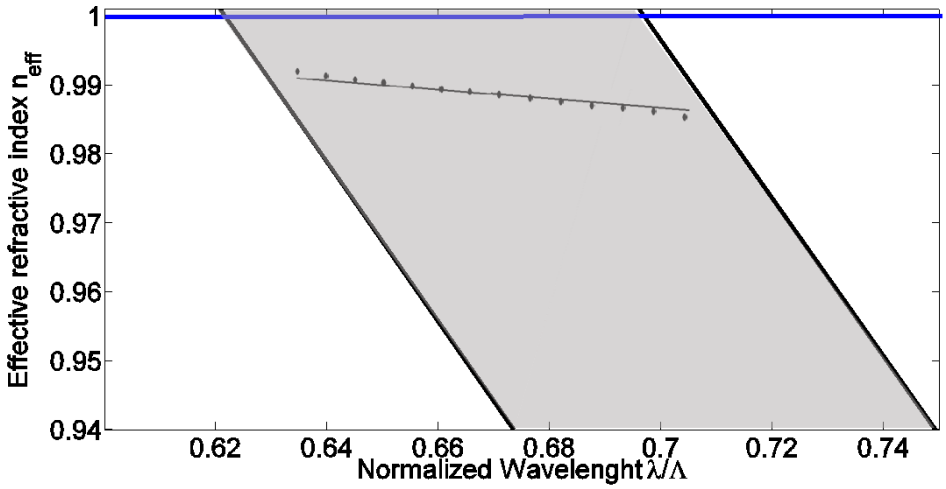

Figure 4. 11: The representation of dispersion relation for the fundamental mode of the hollow core.

To categorize the modes the best idea is to take in consideration two aspects either based on the core modes or surface mode. Our attention is relying on the modes of core and non-surface modes. The fundamental mode is represented as a degenerated mode this aspect is in agreement with [2, 14].

Figure 4.12 is corresponding to z-component of poynting vector for $\frac{\lambda}{\Lambda} = 0.63$, $\frac{\lambda}{\Lambda} = 0.67$ *and* $\frac{\lambda}{\Lambda} = 0.71$ in figure 4.12 (a), (b) and (c) respectively. Intensity light profile reveal Striking difference between the different point along the band gap.as in figure 4.12 (a) the EM wave is at the shorter wavelength edge of band gap the light is not well confined to the core and it get focalized with increasing the wavelength so in figure 4.12 (b) we have well localized light in the core of the fiber and with going to the other border of the gap again the mode will be deform and lose the localization in figure 4.12 (c). It is noticeable, which we have two different modes with orthogonal electric field to each other.

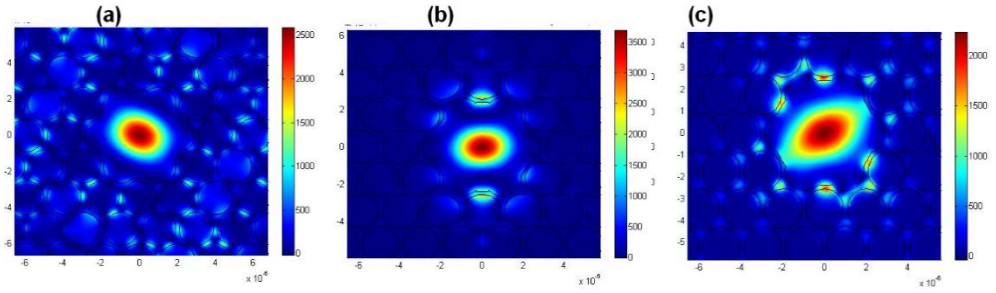

Figure 4. 12: The Intensity patterns ($e_z \bullet Re[E^{\wedge} * \times H]$) of the Hollow-core fiber, corresponding to (a) λ/Λ=0.63 (b) λ/Λ=0.67(c) λ/Λ=0.71

The figure 4.13 representing the two degenerate modes of the fiber at certain normalized wavelengths vector of electric field.

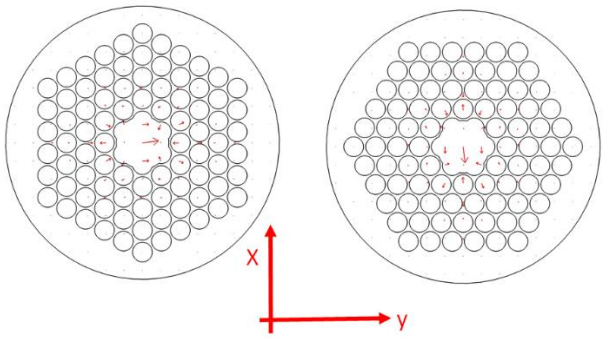

Figure 4. 13: The electric field representation of the fundamental mod at λ/Λ=067.

If we were to make the core bigger with increasing the surface of the core the number of surface modes increases consequently.

4.3 Properties and applications

Air holes and the ability to tune the optical properties of fiber with tuning the geometry of holes opens a very wide range of possibilities. The control of refractive index contrast between core and clad simply with the control of air filling or change the distribution of the index in cladding can be mentioned.

As this chapter is strongly dedicated to HC-PCF so our aim is to study and represent the optical properties of the mentioned class of PCFs. Actually it is a good choice since

HC-PCFs have great potential, due to the light confinement in hollow core exhibit a low level nonlinearity and high damage threshold [16-19].

Since they exhibit low nonlinearity, and air guiding increase the potentiality to use in future communications and transmission systems. Another application of the HC-PCFs is high power continues wave nanosecond and picosecond laser beam propagation. This application takes place in laser surgery, marking, laser fusion [19].

More over many applications due to their air guiding and low luminesce effect, lead to measurement for fluorescence and luminescence of other material, and it is proposed as sensing capabilities [20].

Moreover, air-guiding PCFs are suitable for nonlinear optical processes in gases, which require high intensities at low power, long interaction lengths and good-quality transverse beam profiles [9].

A range of sensing possibilities using hollow core PCF has been discussed in literature in different arrangement for different transducers and sensing wide range of material.

On the other hand highly Birefringence fibers [4], high level of nonlinearities and control on the dispersion [14] has been well reported about solid core PCF in literature.

4.4 Loss mechanisms

4.4.1 Intrinsic loss of solid core PCF

As optical fiber started to be part of telecommunication and science, a very important factor of the optical fibers introduced loss level. The technological achievement from glass research to optical fiber design decreases the loss to slightly less than 0.2 dB/km at 1550 nm. Further improvement is seems unachievable in conventional optical fibers since this fiber achieved to highest potentialities in this sense, thanks to 30 years of scientific efforts in this aim. Now a days one of the solutions to recover the loss is using Erbium doped fiber amplifiers and it is a major cost of the optical fiber in long-haul. Several researches are going on with the aim to design amplifiers [21, 22].

A technological perspective of loss for PCF are presented in details. Optical loss of the optical fibers are measured with in unit of $\frac{dB}{km}$, loss in PCFs generally can be described as formula 4.1:

$$\alpha dB = \frac{A}{\lambda^4} + B + \alpha_{OH} + \alpha_{IR} + \alpha_{co} + \alpha_{Be}, \qquad (4.1)$$

Where A is Rayleigh scattering coefficient, B is the loss induced by imperfection in fabrication process, α_{OH} , α_{IR} are the losses due to OH-absorption and the absorption associated to infrared wavelength and finally $\alpha_{co} and\, \alpha_{Be}$ are respecting the confinement loss and bend loss. We consider $\alpha dB - \alpha_{co} - \alpha_{Be}$ as intrinsic loss of the fiber and we would like to stress on the effect of OH-absorption and imperfection loss of the fiber. These two contributions of the loss are dominating the intrinsic loss [23].

Very serious loss in the PCFs caused by the imperfection of fabricated optical fiber. To make it clear, we are speaking about the surface roughness on the internal surface silica capillaries, if any sort of imperfection's dimension (like scratched), can be found comparable to wavelength range, then it effects on the optical fiber loss. This loss can be very high and it is a serious scattering loss, especially in HC-PCFs. It is suggested to improve fabrication process in order to remove such sort of imperfection. On the other hand it remained another imperfection due to surface waves inside of the holes during drawing process. Usually this effect also practically effects pitch and core size consequently band gap of optical attenuation, to clarify this effect it is important to note ,which due to fluctuation of air holes along the fiber the bandgap and attenuation play not a well-defined behavior [23].

Some words about Rayleigh scattering, lead us to the material which light is travelling in. considering the HC-PCF, luckily does not interact with glass or other material with high Rayleigh scattering coefficient, hence this loss in the HC-PCFs are negligible[23]. On the other hand PCFs with MTIRmechanism have the same Rayleigh scattering influence of conventional optical fibers.

Regarding to aforesaid we don't expect a lower loss from a solid core PCF and several reports of different works with an approach to fabrication improvement, geometrical improvement, and materials employing shows this drawback which this fibers cannot go more than conventional ones for long range transmission.[23-27].

4.4.2 Intrinsic loss for Hollow-core fibers

Air guiding as the most important advantages of Hollow Core –PCF and it is effecting the losses fiber. Generally in a HC-PCF the losses are:

1. Bend loss,
2. Confinement loss,
3. Rayleigh scattering,
4. Absorption,
5. Fabrication imperfection and variation along the optical fiber.

Due to air-guiding mechanism of HC-PCF the level of most of losses which is based on the interaction of light with material decreases. However due to light propagation medium it seems an open room to reduce the loss bellow conventional fibers. Scatterings and absorptions are low, as it is theoretically indicated and experimentally investigated the mode coupling and scattering loss at the internal air–silica interfaces is scaled by the wavelength with this relation$\propto \frac{1}{\lambda^3}$.[28] . Several works also represent the effect of increasing core size to decrease the loss level, it can be explained due to decreasing the overlap of guided mode with the interface of capillaries, therefore less involvement with the glass and consequently less imperfection loss and less scattering loss [29]. But we may notice that with increasing the core size the surface of cylinder of core will increase, hence number of modes and surface modes increases and dispersion curve goes closer to air-line [30].

Concerning HC-PCFs loss, the contribution of Rayleigh scattering is negligible with a good design of the structure. Instead the effect of surface roughness, fabrication imperfections, structural fluctuation, and variation along the fiber due to drawing process remains always less studied. Since this loss is playing an important rule, a careful fabrication process in order to reduce no uniformity can be effective in some level, but it is not able to remove surface capillary waves which are frozen into the core and capillaries. Capillary waves cannot be completely removed and it is nature of glass [23]. This roughness scatters light from fundamental mode to PC modes and it is reported which this surface roughness losses eventually will stop the reduction of loss in a certain level [25, 26] as we have mentioned in case of increasing the surface of core here also we would like to mentioned the same approach can be useful for removing this loss [26]. On the other hand we know that the PCF can tune the

propagated mode with tuning the geometrical structure. Therefore designing a fiber with a smaller surface for the fundamental mode together with smaller core can have good advantages [24-27].

With a proper deign of PCF and controlling the operating wavelength in infrared it is reported which the attenuation decreases with behavior of $\frac{1}{\lambda^3}$ as aforesaid. A loss about 0.13 dB/km is reported and it is suggested to improve the geometrical and material of fiber structure. There is another loss in hollow core fibers in wavelength ranges of band gap which coupling between fundamental mode and confined surface modes of the fiber can occur. Surface modes their selves overlap extensively with glass and core walls, and resulting to a high loss. Presence of surface modes strongly effects the guiding spectral windows, so by influence to reducing the width of their transmission range losses consequently increases [31]. The loss mechanism related to surface modes is complete by considering that they are highly overlapped and coupled with the continuum of the extended modes in the cladding [32].

4.4.3 Confinement loss of PCFs

Confinement loss is a new class loss belong to new class of fiber, actually this loss would not be existed if the number of holes in the PC was infinite. This loss is due to the non-perfect bandgap since it is not possible to have an infinite periodic structure which permit the electromagnetic wave leaks out of waveguide. That is why this loss is famous as “leak loss”. This contribution in both solid core and hollow core PCFs is necessary to be considered. Consequently all the PCF guided modes are leaky. For example in solid core PCF the confinement is very dependent to the core hole sizes and pitch so for reducing the leak loss the lattice structure should stop light propagation in transversal direction. This can be achieved with an appropriate design of holes. It is reported which with a proper design of single mode fiber the confinement loss can be negligible [33-34].

It is reported as well with increasing the holes number and layers the leakage loss decreases drastically [35] and in literature it is mentioned which the effect of ring number in HC-PCF is lower than solid core PCF [34].

In order to give the view of the leakage loss in hollow core regarding to different lattices, the study a calculation of imaginary part of fundamental mode is leading to confinement loss [35].

4.5 Fabrication process of photonic crystal fibers

Fabrication of optical fiber is a challenging problem from the very beginning of this technology. One of the most important questions for the design of optical fiber rely on the ability of fabrication of designed structure. Several works are devoted to this technology. PCF from solid core to hollow core fibers requesting methods to introduce holes on the silica. The air holes have some technological advantages like, air is thermally compatible to most of materials, transparent over a broadband spectral range, low refractive index in most of frequencies, and low non linearity, to name.

Due to high rate of development and huge amount of production the production of optical fibers now a days is very cost effective.

The typical strategy of production is based on the fabrication of a preform and drawing it with a high temperature furnace [37]. Fiber fabricated with air hole studied vastly because silica viscosity in high temperature don’t change dramatically and it is a good material to work.

Different Vapor deposition techniques has been employed to manufacture the preform, for instance, modified chemical vapor deposition (MCVD), the vapor axial deposition (VAD), and the outside vapor deposition (OVD), are all employed to this aim.

The conventional single mode optical fibers are produced with employing one of these techniques with taking in consideration refractive index different of 1%. While for the PCF a refractive index contrast differing from 50-100% [30]. As a result we can claim that, the mentioned techniques are not applicable directly for microstructures fibers. One of the reasons is the previous techniques are taking the advantages of continues circular symmetry of the conventional fiber, while in microstructures fibers the symmetry is discretized.

In the conventional drawing procedure, the viscosity is the only material properties to deal with, while in the PCF fabrication several forces take role in the manufacturing process to name, viscosity, gravity, and surface tension.

The larger surface area in microstructure geometry and especially near the core site is the reason of adding new aspects in the fabrication process. Thus the choice of base material strongly effects the technological issues in fabrication process.

4.5.1 Stack-and-draw technique

Micro structures fiber fabrication, initiate with producing a preform. A preform is a macroscopic scale of interested structure. To introduce the air-holes to silica, one of the approaches is to drill some tenths of holes on a silica structure, another approach has been developed by Birk in university of bath represents facile and simple process to fabricate the preform. It is called stack-and-draw technique. [38]. the preform is realized by hand stacking interested number of capillaries and rods made by silica to obtain desired structure. This technique provides a fast, clean, accurate, low-cost preform with taking in consideration the flexibility and high degree of freedom to fabricate desired structure as depicted figure 4.14.

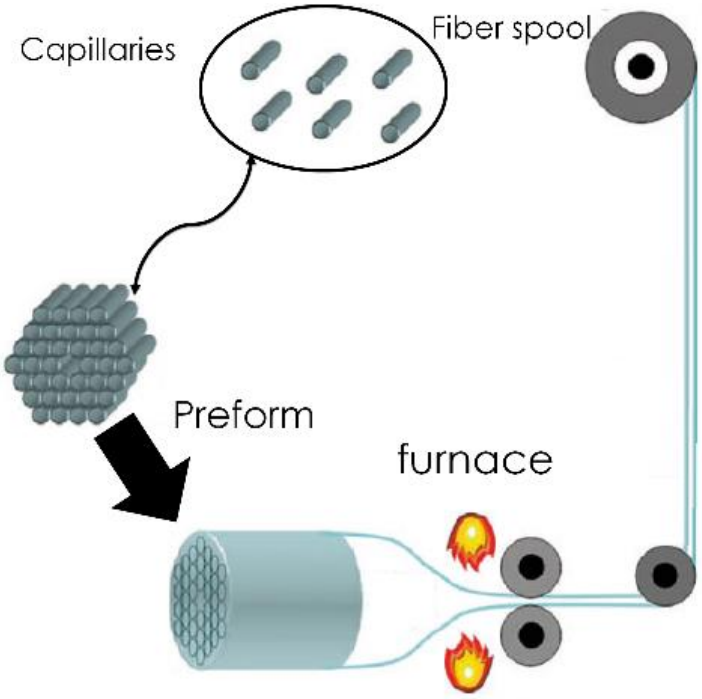

Figure 4. 14: The drawing and stack process

This flexibility to design the preform permit to design the desired index profile with designing the cladding region. After stacking, the capillaries and rods held together using thiny wires, an intermediate drawing process permits the preform, to fused

capillaries and rods to each other. This intermediate drawing is necessary, where the preform is drawn into preform canes. In order to develop and optimize the drawing process numerous preform cane will be necessary, to obtain the final dimension of PCF [37]. The preform usually has a diameter around 20 mm and in the drawing process its cross section diameter decrease to ~100 μm. It is worth noting that the drawing process is almost similar one with the conventional method with a different on temperature of furnace. The surface tension due to high temperature increases and the possibility of collapsing the air holes is so high. Therefore in the drawing process the temperature of the furnace is kept 1900◦C instead of 2200◦C. In order to carefully control the air-hole size during the drawing process, usually a slight over pressure is applied (from inside) [37].

To conclude the mentioned optical fiber structures are presenting a wide possibility to design and manufacture. High level of freedom to design the structure. The manufactured fiber with a polymer coating provides the same mechanical robustness like the conventional one, and easy handling is in results. The other open possibility rely on the similarities to the conventional fiber in order to use the conventional optical fiber tools.

As we have mentioned before these fiber's dispersion, birefringent and loss is controllable with controlling the geometrical and physical properties of capillaries. So the high degree of freedom by using this technique let to tune the optical fiber which we are interested.

In 1999 this method has been used to create the world's largest hole [6]

By the way stacking method requires a very careful handling, and the control of air-hole dimensions, positions, and shapes in PCFs makes the drawing significantly more complex [37]. Finally, it is important to underline that the fabrication process of PCFs with a hollow core, realized by removing some elements from the stack center, at the beginning it was much more difficult than that of standard optical fibers, even if at present fibers with low loss and practical lengths have been obtained [39].

4.5.2 Extrusion fabrication process

Extrusion technique, has been applied for the materials which are not existed in the rod form and of course presenting new and intriguing optical properties. In case of modified index guiding fibers they can provide wider wavelength range of transmission

or higher nonlinearities of the material. The extrusion technique is a suitable platform to create preform of different materials. [37] These materials usually have lower softening and consequently lower melting temperature. In extrusion technique a molten glass or transparent material will be forced through a suitable design pattern of holes die. Extrusion permit to direct drawing from the bulk glass. Most of structures can be suitable for this technique. The calcogenide, polymer, and compound glass are from the list.

But a drawback in this method is to define the structure freely as we could in the previous method therefore doping material in some part, or changing the refractive index in different point of the fiber is a difficult work.

4.6 Summary and some considerations

In the current chapter we have spent time to introduce new structures of PC as optical fiber. We introduce PC with different guiding mechanism. We study numerically and theoretically of FEM the band analysis and modal analysis of a triangular lattice. When the PCFs are showing very good ability to guide the light in the air core, surface states degrade the performance of optical fiber. The practically increase the loss with scattering due to surface roughness and it is a big unfortunate.

On the other hand PCFs are potentially great structures, but they are not able to take advantages of several different rotational symmetries. PCFs are limited to 5 different symmetry class and this is as unfortunate, deprives PCF from geometrical richness of higher order of symmetry of fiber.

In the next chapters we will take part to study quasicrystals with higher order of symmetry and introducing optical fibers with the aim to check the possibility of air guiding and band diagram analysis.

Bobliography

1. Pochi Yeh, Amnon Yariv, and Emanuel Marom ,"Theory of Bragg fiber", 68, 9, 1, 1196–1201,(1978).

2. J. C. Knight, T. A. Birks, P. S. J. Russell, and D. M. Atkin, “All-silica single-mode optical fiber with photonic crystal cladding: errata,” Opt. Lett. 22, 484–485 (1997)

3. P. J. Bennett, T. M. Monro, and D. J. Richardson, “Toward practical holey fiber technology: fabrication, splicing, modeling, and characterization,” Optics Letters, vol. 24, pp. 1203–1205, (1999).

4. F. Poletti, N. G. R. Broderick, D. J. Richardson, and T. M.Monro, “The effect of core asymmetries on the polarization properties of hollow core photonic bandgap fibers,” Optics Express, 13, pp. 9115–9124, (2005).

5. A. Apolonski, B. Povazay, A. Unterhuber, W. Drexler, W. J. Wadsworth, J. C. Knight, and P. St. J. Russell, “Spectral shaping of supercontinuum in a cobweb photonic-crystal fiber with sub-20-fs pulses,” Journal of Optical Society of America B, vol. 19, pp. 2165–2170, (2002).

6. P. St. J. Russell, “Photonic crystal fibers,” Science, vol. 299, pp. 358–362, (2003).

7. John D. Joannopoulos, Steven G. Johnson, Joshua N. Winn, and Robert D. Meade, “Photonic Crystals: Molding the Flow of Light second edition", Princeton University Press, [BOOK] (2008)

8. Ana M. R. Pinto and Manuel Lopez-Ammo,"Review Article, Photonic Crystal Fibers for Sensing Applications", Journal of Sensors, (2012), Article ID 598178, doi:10.1155/2012/598178, (2012).

9. F. Benabid, F. Couny, J. C. Knight, T. A. Birks, and P. S. Russell, "Compact, stable and efficient all-fibre gas cells using hollow-core photonic crystal fibres," Nature, 434 (7032), pp. 488-491, (2005)

10. T. A. Birks, J. C. Knight and P. S. J. Russell "Endlessly single-mode phototonic crystal fiber" Optics Letters, 22 (13), pp. 961-963, (1997).

11. B. Temelkuran, S. D. Hart, G. Benoit, J. D. Joannopoulos, and Y. Fink, “Wavelength-scalable hollow optical fibres with large photonic bandgaps for CO2 laser transmission,” Nature, vol. 420, pp. 650–653,(2002).

12. J. C. Knight, “Photonic crystal Fibres,” Nature, vol. 424, pp. 847–851, (2003)

13.J. Limpert, T. Schreiber, S. Nolte, H. Zellmer, and A. T¨unnermann, “Allfiber chirped-pulse amplification system based on compression in airguidingphotonic bandgap fiber,” Optics Express, vol. 11, pp. 3332–3337, (2003)

14. D. N. Schimpf, R. A. Barankov, and S. Ramachandran,"Cross-correlated (C2) imaging of fiber and waveguide modes",19,14 / OPTICS EXPRESS 13008,(2011)

15. Jes Broeng, Stig E. Barkou, Thomas Søndergaard, and Anders Bjarklev, "Analysis of air-guiding photonic bandgap fibers", OPTICS LETTERS, 25, 2, (2000)

16. D. G. Ouzounov, F. R. Ahmad, D. M¨uller, N. Venkataraman, M. T.Gallagher, M. G. Thomas, J. Silcox, K. W. Koch, and A. L. Gaeta,"Generation of megawatt optical solitons in hollow-core photonic bandgapfibers," Science, vol. 301, pp. 1702–1704,(2003).

17. C. J. S. de Matos, J. R. Taylor, T. P. Hansen, K. P. Hansen, and. Broeng, "All-fiber chirped pulse amplification using highly-dispersiveair-core photonic bandgap fiber," Optics Express, vol. 11, pp. 2832–2837, (2003).

18.C. J. S. de Matos and J. R. Taylor, "Chirped pulse Raman amplification with compression in air-core photonic bandgap fiber, "Optics Express, vol. 13, pp. 2828–2834,(2005).

19. G. Humbert, J. C. Knight, G. Bouwmans, P. St. J. Russell, D. P. Williams, P. J. Roberts, and B. J. Mangan, "Hollow core photonic crystal fibers for beam delivery," Optics Express, vol. 12, pp. 1477–1484, (2004).

20. P. Ghenuche, H. Rigneault,J. Wenger, "Hollow-core photonic crystal fiber probe for remote fluorescence sensing with single molecule sensitivity",Opt Express. ; 20(27), (2012).

21. A.R.Bahrampour, Sh.Keyvaninia, M.Karvar,"An inhomogeneous theory for the analysis of an all-optical gain-stabilized multichannel erbium-doped fiber amplifier in the presence of ion pairs", Optical Fiber technology (2007).

22. J. C. Knight, "Photonic crystal fibres," Nature, vol. 424, pp. 847–851, (2003).

23.K. Kurokawa, K. Tajima, K. Tsujikawa, and K. Nakajima, "Reducingthe losses in photonic crystal fibres," in Proc. European Conference onOptical Communication ECOC 2005, Glasgow, Scotland, Sept. 25–29,(2005).

24.K. Tajima, K. Nakajima, K. Kurokawa, N. Yoshizawa, and M. Ohashi,"Low-loss photonic crystal fibers," in Proc. Optical Fiber CommunicationsConference OFC 2002, Anaheim, California, USA, Mar. 17–22,523–524,(2002).

25. L. Farr, J. C. Knight, B. J. Mangan, and P. J. Roberts, "Low loss photoniccrystal fiber," in Proc. European Conference on Optical CommunicationECOC 2002, Copenhagen, Denmark, Sept. 8–12, (2002).

26. K. Tajima, J. Zhou, K. Nakajima, and K. Sato, "Ultra low loss and long length photonic crystal fiber," in Proc. Optical Fiber CommunicationsConference OFC 2003, Atlanta, Georgia, USA, Mar. 23–28, (2003).

27. K. Tajima, J. Zhou, K. Kurokawa, and K. Nakajima, “Low water peak photonic crystal fibers,” in Proc. European Conference on Optical Communication ECOC 2003, Rimini, Italy, Sept. 21–25, (2003).

28.P. J. Roberts, F. Couny, H. Sabert, B. J. Mangan, D. Williams,L. Farr, M. Mason, A. Tomlinson, T. A. Birks, J. C. Knight, and. St. J. Russell, “Ultimate low loss of hollow-core photonic crystal Fibres,” Optics Express, vol. 13, pp. 236–244, (2005).

29. B. J. Mangan, L. Farr, A. Langford, P. J. Roberts, D. P. Williams, F. Couny, M. Lawman, M. Mason, S. Coupland, R. Flea, H. Sabert,T. A. Birks, J. C. Knight, and P. St. J. Russell, “Low loss (1.7 dB/km) hollow core photonic bandgap fiber,” in Proc. Optical Fiber CommunicationsConference OFC 2004, Anaheim, California, USA, Feb. 23–27, (2004).

30.J. C. Knight, “Optical fibres using microstructured optical materials,” in Proc. European Conference on Optical Communication ECOC 2005, Glasgow, Scotland, Sept. 25–29, (2005).

31. R. Amezcua-Correa, N. G. Broderick, M. N. Petrovich, F. Poletti,and D. J. Richardson, “Optimizing the usable bandwidth and loss through core design in realistic hollow-core photonic bandgap fibers,” Optics Express, vol. 14, pp. 7974–7985, (2006).

32. J. A. West, C. M. Smith, N. F. Borrelli, D. C. Allan, and K. W. Koch, “Surface modes in air-core photonic band-gap fibers,” Optics Express, vol. 12, pp. 1485–1496, (2004).

33. D. Ferrarini, L. Vincetti, M. Zoboli, A. Cucinotta, and S. Selleri, “Leakage properties of photonic crystal fibers,” Optics Express, vol. 10, pp. 1314–1319, (2002).

34. L. Vincetti, D. Ferrarini, M. Zoboli, A. Cucinotta, F. Poli, and S. Selleri, “Leakage losses in photonic band gap fibers,” in Proc. European Conference on Optical Communication ECOC 2003, Rimini, Italy, Sept. 21–25, (2003).

35. D. Ferrarini, L. Vincetti, M. Zoboli, A. Cucinotta, F. Poli, and S. Selleri, “Leakage Losses in Photonic Crystal Fibers,” in Proc. Optical Fiber Communications Conference OFC 2003, Atlanta, Georgia, USA, Mar. 23–28, (2003).

36. Xiwen Sun and Dora Juan Juan Hu,"Air Guiding With Photonic Quasi-Crystal Fiber", IEEE PHOTONICS TECHNOLOGY LETTERS, 22, 9,607-611, (2010).

37. J. Lægsgaard and A. Bjarklev, “Microstructured optical fibers – fundamentals and applications,” Journal of the American Ceramic Society, vol. 89, pp. 1–12, Jan. (2006).

38. T. A. Birks, D. M. Atkin, G. Wylangowski, P. St. J. Russell, and P. J. Roberts, "2D photonic band gap structures in fibre form," in Photonic Band Gap Materials, C. M. Soukoulis (ed.) Dordrecht: Kluwer, 437–444. (1996).

39.D. J. Richardson, F. Poletti, J. Y. Y. Leong, X. Feng, H. Ebendorff- Heidepriem, V. Finazzi, K. E. Frampton, S. Asimakis, R. C. Moore,J. C. Baggett, J. R. Hayes, M. N. Petrovich, M. L. Tse, R. Amezcua, J. H. V. Price, N. G. R. Broderick, P. Petropoulos, and T. M. Monro, "Advances in microstructured fiber technology," in Proc. IEEE/LEOS Workshop on Fibres and Optical Passive Components WFOPC 2005, Palermo, Italy, June 22–24, (2005).

Chapter 5

Introduction to Photonic Quasicrystals

5.1 Introduction

Revolutionized discovery of quasicrystals in solid state physics induced same impact in the field of optics. The idea of quasicrystal as an aperiodic structure with perfect long-range spatial symmetry was introduced in solid-state physics by Levine and Steinhardt (Nobel laureates in chemistry 2011) [1]. Recently it has become obvious which in addition of crystalline structure and completely random structure (Amorphous), another arrangement of structure between the two well-defined condensed matter states existed. Likewise, this intermediary class called aperiodic deterministic structures in solid state physics.

The practice of optical interference to boost optical devices performance is one of the most important tools in modern optics. Some of the intriguing examples are photonic crystals [2–4], and Anderson localization of light [5, 6].

Overwhelmingly, periodic optical structures as photonic crystals are used for applications based on optical interference such as HC-PCFs [7]. On the other hand some phenomena like Anderson localization [5, 8] in random structures has been introduced. These two phenomena invite many scientist to study structures in transient from periodic to random arrangement. Predicted structures are known as quasicrystals or aperiodic structures. Principally it has not been widely that aperiodic structures, can meet and enhance optical properties and functionalities of photonic crystals. The least opportunity which aperiodic structures offer us is their geometrical flexibility in compare with periodic structures.

An array of 1D dielectric multilayers photonic quasi crystal has been studied in the field of optics. the structure hold a long range order to form a Fibonacci sequence,

which induces efficiently constructive interference [10] and represents optical localization in the structure. Successively, a wide range of photonic quasicrystals as deterministic aperiodic structures with long-range order have been engineered and analyzed by optical means [11-12]. In all of these studies, interference has played a crucial role in the optical properties of each structure. Transferring to 2-Diensional quasicrystal (2-D QC) structures it is reported which 2-D QCs can possess higher degree of rotational symmetry than photonic crystals. As a consequence, photonic quasi crystals are demonstrated to be more advantageous to present novel photonic bandgap features. One of the most important of these features is, complete photonic bandgaps under lower dielectric contrast [13].

In this chapter we initiate with some historical issues and algorithm to quasicrystal and then with presenting some optical properties of photonic Quasicrystals (QCs) we continue this chapter. Consequently with design of Amnan-Beenker (an 8-fold symmetry) and 12-fold structure we calculate Bloch modes of QC, with taking the advantages of a supercell approach.

5.2 Mathematics and generation Algorithms of Quasicrystal patterns

5.2.1 Periodicity to Aperiodicity: historical remarks

Long time before the age of quantum mechanics and solid state physics and the discovery of present materials, Architectures and Mathematician were excited with aperiodic structures. The reason was beauty and richness of mentioned geometry due to rotational and long term translational symmetry.

In 17^{th} century Kepler proposed, that the visible symmetries of crystals in macroscopic scale is influenced by microscopic crystals scale.

Bravias introduced a theory for crystalline structures presented by some symmetry groups. All he spoke about, was about crystals are built up by a microscopic unit which periodically fill the space. His theory predicts, with considering 14 Bravias lattices and the 32 crystallographic point group, 239 space group can be derived.

In 1912 all the mathematical model of Bravias lattice have been approved by X-ray diffraction method by Max von Laue.

The brilliant idea was when all the "crystals acquire their order via periodicity". As a result periodicity become a useful tool to study and understand physics of materials in solid-state physics.

Here we would like to mention some lines about tilling and periodic structures. Definition says tilling is a sort of algorithm or method which allows to cover surfaces with specific tile size and geometries. A theorem in tilling theory helps us to understand limits of periodicity.

Theorem 5.1: Any tilling with n-fold rotational symmetry, where n > 6 or n=5, are incompatible with periodicity.

This theorem confirm as higher rotational symmetry we would like to exploit, we lose the possibility of study based on periodicity.

5.2.2Algorithms to generate quasicrystal structures

Quasicrystals can be formed in 1-D, 2-D and 3-D. since our activity relies of the study of fiber so we charge most of our attention on the 2-D Quasicrystals. In the following we present some methods to build up quasicrystals of 2-D.

5.2.2.1 8-fold symmetry

One of the most commonly studied QC patterns is 8-fold symmetric. Ammann-Beenker tiling is a famous tilling associating with an octagonal symmetry, which can be decorated with an algorithm called canonical substitution [19]. Starting with an original tile of two rhombi with acute angle of $\frac{2\pi}{8}$ radian and a square, all the lengths of edges are equal to Λ and cylinder radius of r on each point, and as it is presented in figure 5.1(a).

For decorating all to be done is:

1. First expanding the tilling with mentioned tile as the solid lines in figure 5.1(b)

2. Rescale the original tile generator with the rate equal to $\frac{1}{\sqrt{2}+1}$.

3. Decorate resulting structure tiles in step 1 with the rescaled tile in step 2 as mentioned in figure 5.1 (b).

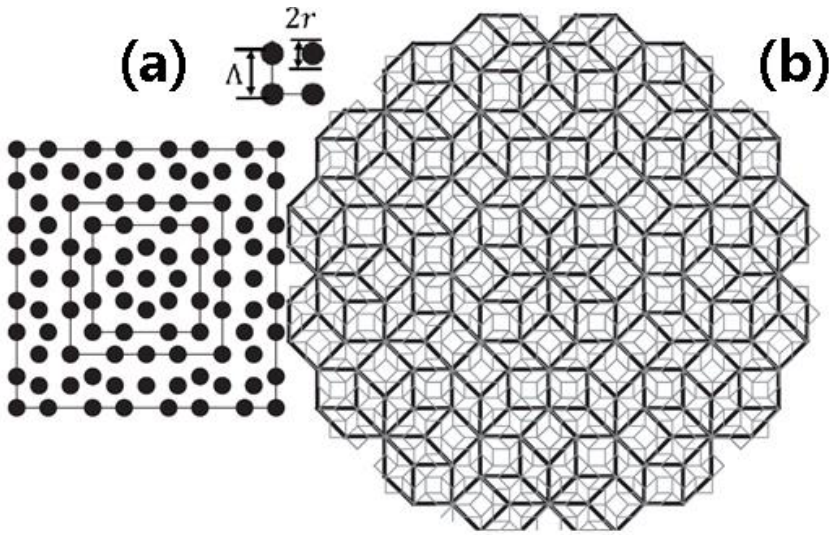

Figure 5. 1: 2-D Ammann-Beenker tiling with 8-fold symmetry, (a) the sizes and geometrical specification, and (b) decorating process by canonical substitution.

5.2.2.2 10-fold symmetry

The most famous non periodic tilling is Penrose tilling on the name of Sir Roger Penrose, who have played important role to develop tilling theory [20].

5-fold and 10 fold symmetry is referring to Penrose structures. The importance of these tilling is due to symmetry level of tilling which is less than 6-fold and cannot provide periodicity based on theorem5.1.

Decagonal tilling as it is shown in figure 5.2 is a well-known pattern between Penrose structures. Following method can be used to generate the Penrose lattice:

A dual multi-grid technique, a regular star formed by the set of five basic vectors constructed as the starting point. These vectors are defined here:

$$v_i = cos\left(\frac{2\pi}{i}\right)x + \sin\left(\frac{2\pi}{i}\right)y) \;\; for \;\; i = 0{:}4$$

Then a grid is decorated with fivefold rotational symmetry whose dual transformation will give the desired Penrose lattice.

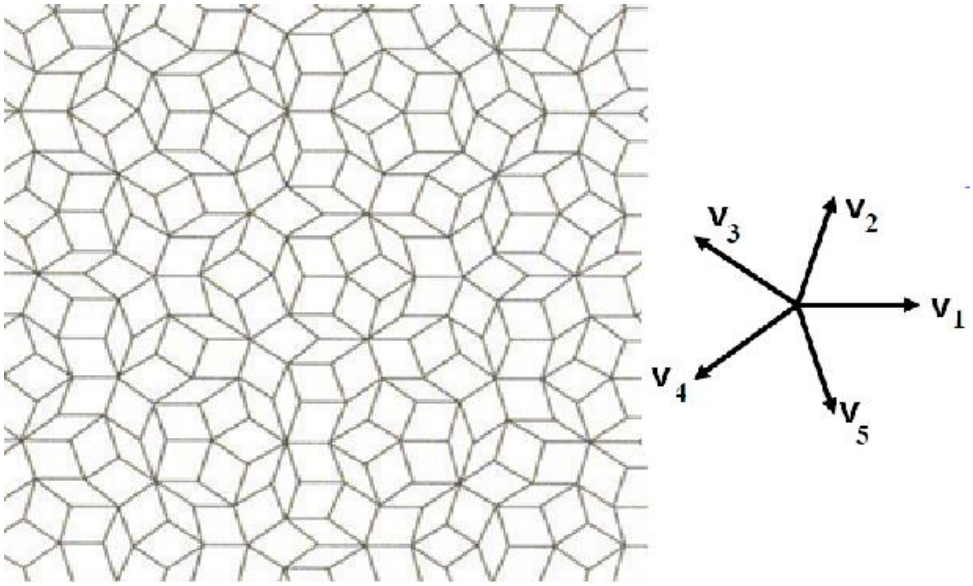

Figure 5. 2: 10-fold geometry structure.

5.2.2.3 12-fold symmetry

Several 12-fold structures are known but the most famous one of them is stampifli or dodecagonal tiling an algorithm to regenerate a 12-fold is reported here.

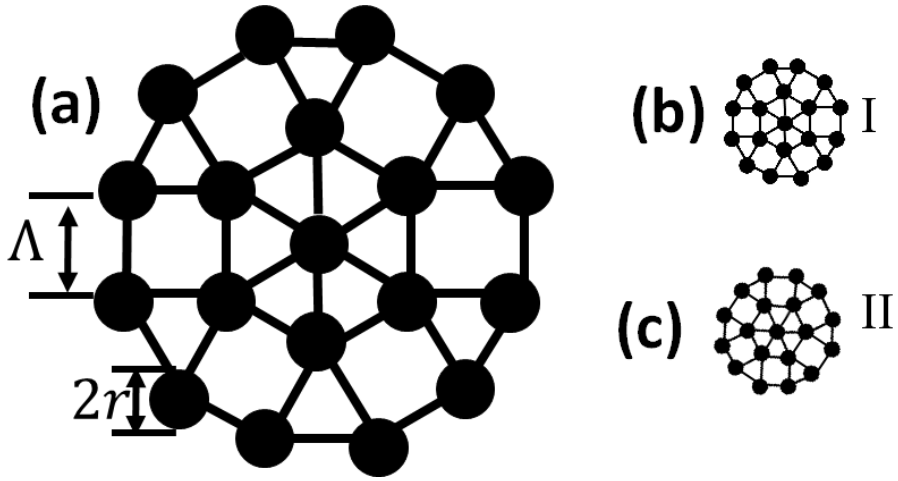

Figure 5. 3: (a) the generator (b), (c) off-spring dodecagon type I, II respectively.

First step is decorating a dodecagonal structure with squares and triangles (square-triangular tilling) all the edges size equal to Λ. As shown in figure 5.3 (a). We consider this structure as first generator. In the second step by a factor of $\frac{1}{2+\sqrt{3}}$ rescale generator to the off-spring dodecagon we name it, off-Spring dodecagon type I (figure 5.3(b)) and with rotating it by $\frac{\pi}{3}$ radian generate off-spring dodecagon type II figure5.3 (c).

Step three, place off-spring dodecagons on each vertex of the parent. Last step, repeat second and third step.

5.3 Photonic properties of quasicrystals

5.3.1 Light propagation in 2D photonic quasicrystals and localization

It is useful to observe the role of disarray in localization of photon in 2D QCs. Introducing disorder into a photonic crystal, adjust the nature of light propagation through the material changes from constructive to a sort of diffusive behavior. With increasing uncertainty of structure geometry to a higher level of randomness, the interference between separate scattering events ultimately causes spatial localization of light, this is, what called "Anderson localization" [5-6]. In contrary with this performance, it is proposed that defected periodicity or quasiperiodicity in photonic quasicrystals can actually improve transport instead of localization. To understand this apparently counter property, a 2D Penrose quasicrystal has been employed in a refractive index crystal [21], quasicrystal pattern confined light only in the *x*–*y* plane, therefore permitting a free propagation along the *z*-axis [21].

5.3.2 Plasmonics in metallic photonic quasicrystals

Whereas most of the optical techniques discussing on dielectric photonic quasicrystals (both insulators and semiconductors), recently there has been interest in applying collective charge oscillations along metal–dielectric interfaces as surface plasmon–resonance (SPRs), for the subwavelength control of light [22]. By using stationary localized surface plasmon in metal nanoparticles, or propagating SPRs at metal-dielectric interfaces, extraordinary control over light–matter interactions has been achieved [23-25]. Such interactions have led to significant advances in the ability to obtain large field enhancements, as well as the localization and modification of the local density of states [26]. The plasmon mediated in- and out-coupling of incident light, which governs both the near- and far-field optical properties of these structures, strongly depends on the shape and size of individual features, as well as the geometrical

and physical structure of underlying array. In contrast with periodic cases, even though aperiodic arrays exhibit meaningfully richer optical spectra [26].Therefore light–matter interactions in such structures are not easy to understand, and require more development of sophisticated measurements and numerical tools [26].

5.3.3 Laser action in aperiodic structures

Laser act needs a setup including an optical pump, an active medium and a feedback mechanism. The feedback mechanism can be either provided by mirrors that form a well-defined Fabry–Pérot cavity, or a 'mirrorless' which does not require a well-engineered cavity [27]. Mirrorless lasing can be introduced by two categories:

1. Coherent emission
2. Incoherent Emission

Lasing in photonic crystals is of the coherent emission category [28]. While according to aperiodic structures laser action can be divided into two different class of obtained modes, localized and delocalized lasers.

Delocalized photonic crystal lasers are aged almost 10 years [28]. Latter it has been predicted which the concept of photonic crystal lasers can be directly transferred to photonic quasicrystals. In a pioneer work of reference [29], a photonic quasicrystal in which a 2-D Penrose structure for lasing action was demonstrated, a decagonal Penrose, hole-silica pattern was fabricated and overlaid by a laser dye (DCM) surrounded in an organic gain medium. If the photonic bandgap of quasicrystal stay within the optical gain spectrum of the lasing medium, then lasing action is obtained. The researchers found that the laser mode wavelength scaled with the size of pitch of Penrose pattern. Amazing discovery was, belong to the relation of the modes and symmetries of the structure. Vast research activity on lasing in quasiperiodic structures is implementing and results represents enhancement in the lasing action [30-32].

5.3.4 Negative refraction

Negative refractive index in periodic photonic structures has been reported in last decade [33, 34]. In the previous works majority attentions were focused on the periodic structures. Zhang et al represent a theoretical model and experimental evident to proof negative refraction can appear in some transparent quasicrystaline photonic patterns. PQCs based on their model can have effective index close to -1 in a certain frequency band. Intriguingly, a superlens based on the 2D PQCs can form as non-near-field subwavelength image whose position varies with the source distance. These properties represents the richness of optical properties of photonic crystals in matter of taking advantages of higher order of symmetry [33].

5.4 Quasicrystal band analysis

To calculate band structure of photonic crystals we introduced a unitcell which, with introducing proper boundary conditions and Bravias vector, we could analysis band structure of PCs. While as we have mentioned in this chapter a quasicrystal pattern, by definition is not associated to a short range of spatial symmetry. In order to analysis the band structure of QCs few approaches are found in literature.

A general idea of cut and projection which comes from a mathematical approach to QCs has been employed to determine periodic structure in higher order dimension [35]. Consequently it is proposed a computational method to solve for the spectra and eigenstates of quasicrystalline electromagnetic structures by directly solving a periodic eigenvalue problem in a higher-dimensional lattice.

Johnson et al. presented a numerical approach to solve Maxwell's equations extended to a periodic unitcell of higher dimensions. This allow to solve the problem to employ Bloch's Theorem. The answers for 1-D Fibonacci photonic QC are in agreement with experimental works. This work represent the possibility of extending in higher dimension of QCs [35]. The mentioned method is presenting a brilliant idea of band calculation but more development is needed for higher dimensions to realize 2- and 3-

D quasi periodic structures. However it shows huge difficulties, to apply this method for calculations related to fiber structure

In other approach study of QC band structure have been implemented with employing Bloch theorem for 2-D 12 and 8-Fold structure, and then with employing perturbation theory the band structure as an eigenfrequency case obtained. This method meets the results of theoretical investigations about 12-fold and 8-fold regarding bandstructure and isotropic level. Bandgap in a lower index contrast is forming due to rotational symmetry and higher isotropic structure [36] but this method cannot present trustable results under a certain level of refractive index contrast, which for sure cannot be useful for optical fiber question.

Regarding to previous methods it was on hand which, for calculating eigenstates of a quasicrystal we should find a leeway to a periodic structure. The previous methods look very complicated and still not well-built. With right selection of a portion of quasicrystal pattern and choosing compatible Bravias vectors we can generate the quasicrystalline structure with a reasonable size of portion (based on our numerical sources). For example 12-fold pattern as depicted in figure5.4 is such way.

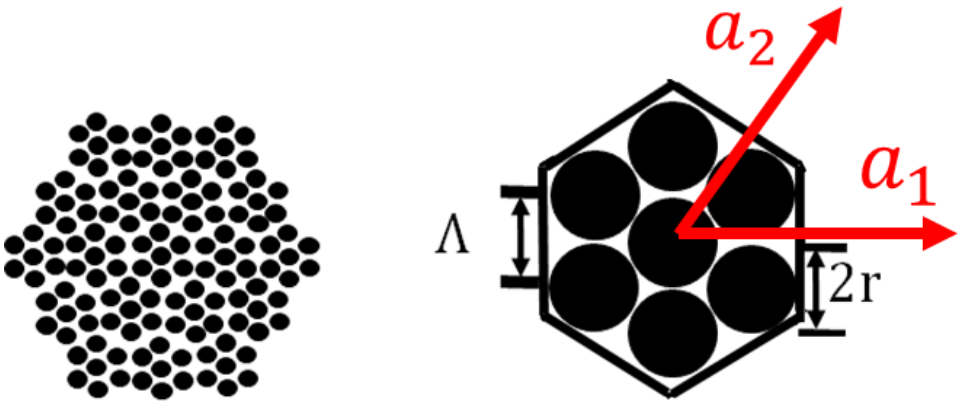

Figure 5. 4: 12-fold structure and approximant for band calculation

But if we consider a Penrose tile (5-, 10-fold) or Ammann-Beenker (8-fold) structure as it is shown in figure 5.5 (a) and (b) respectively, the repeating portion in translational symmetry cannot be found in a number of holes comparing with the size of 12-fold chosen cell. Therefor a portion of 8-fold or Penrose with taking in consideration of two parameters can be chosen:

1. Enough similarity to the original tilling

2. Compatible with our computational resources

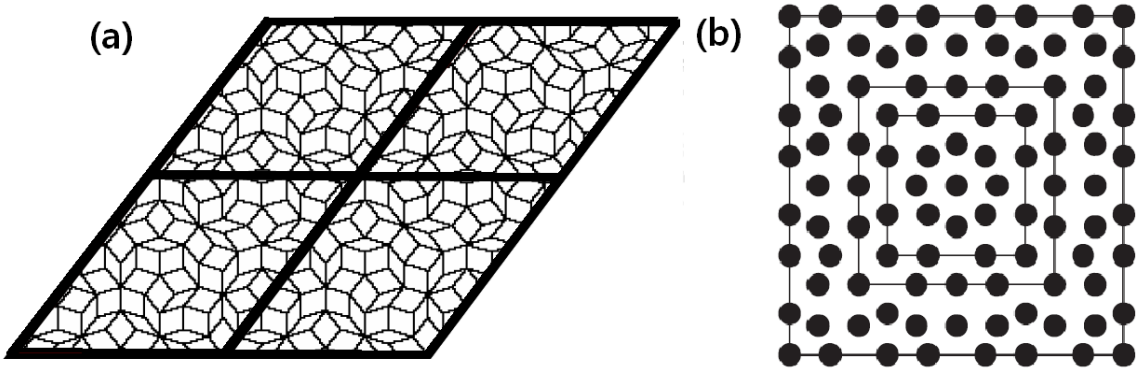

Figure 5. 5: (a) decagonal repeating portion, (b) 8-fold different portion

We know as we choose the bigger approximant will result to higher precision numerical output, while as aforesaid the size of supercell or approximant is limited to our computational source [35, 36]. Since we are interested on the PBG of the structure it is worth highlighting, that there is indication that a least approximant size is required for the formation of a true PBG where light intensity decays exponentially with increase of system size [37].

In this section, we report studies of the band structures of 2D photonic quasi crystals with an approximant for a 12-fold and an octagonal quasicrystal with the aim of finding the bandgap and band gap dependent to out of plane wave vector. 2D photonic Quasicrystal shaped of air cylinders of radius r into a silica plane for which the refractive index taken to be $n_{glass} = 1.46$ and a constant of quasi crystal as hole-to-hole spacing of Λ are the physical and geometrical parameters for our calculation method.

5.4.1 Band analysis of 12-fold

Here we present the band analysis of a dodecagonal (12-fold) lattice. The geometry is presented in figure 5.4, and the structure can be characterized by a constant length of Λ as shown in figure 5.4, which is the distance of holes next to each other and Radius of cylinders which indicated by r. In what follows, the band structure calculation for the 12-fold QC is revealing. The primitive cell which contains 7 cylinders with a certain cylinder radius of $r = 0.49\Lambda$, the primitive cell is a hexagonal as shown in figure 5.4.

Therefore the band structure is investigated for a large air filling. The mentioned rate of r/Λ=0.49 can interpret as a surface air filling equal to:

$$s_{AFF} = \frac{sum\ of\ cylindars\ surfaces}{total\ surface} \times 100 = 82\%$$

The photonic bandstructure of a crystal based on such primitive cell is calculated by applying periodic boundary condition at the sides of hexagonal approximant. The periodicity is defined by $R = l_1 a_1 + l_2 a_2$ where k_1 and k_2 are integers and $a_1 = \left(1+\sqrt{3}\right)(\Lambda, 0), a_2 = (1+\sqrt{3})(\frac{\Lambda}{2}, \frac{\Lambda\sqrt{3}}{2})$ are translational vectors.

Bravias vectors are depicted in figure 5.4. The photonic bandstructure of 12-fold crystal based on mentioned approximant is calculated by applying periodic boundary conditions at the edges of the primitive cell and using FEM. The same work has been reported recently regarding to calculation of band structure for 12-fold with a rectangular unitcell using Plane wave expansion method [38] we believe that the rectangular unitcell is not a right choice for 12-fold since with hexagonal we can get higher similarity.

It should be highlighting that the primitive cell has 3 pair of boundary conditions, and therefor with a careful defining of boundary condition a more precise band structure is expected. Which is due to higher level of similarity with the considered 12-fold structure.

Regarding to the mentioned issues in chapter 4, our intention is to calculate band structure of a 2-D quasicrystal with present of out of plane wave vector which is well discussed elsewhere [39]. The band structure solved by FEM and resulting band structures is presented in figure 5.6.

Our calculations show that significant band-gaps only occur in the band structure when the out of plane wave vector increase. Starting from figure 5.6 (a) to (c) with $\frac{k_z\Lambda}{2\pi} = 0.4$, $\frac{k_z\Lambda}{2\pi}$ =0.6 and $\frac{k_z\Lambda}{2\pi}$ =1 respectively. We can observe the direct increase of band gap while in the 2D problem with $k_z \leq 0.4$ we cannot observe any kind of gap due to non-enough refractive index contrast 1:1.46.

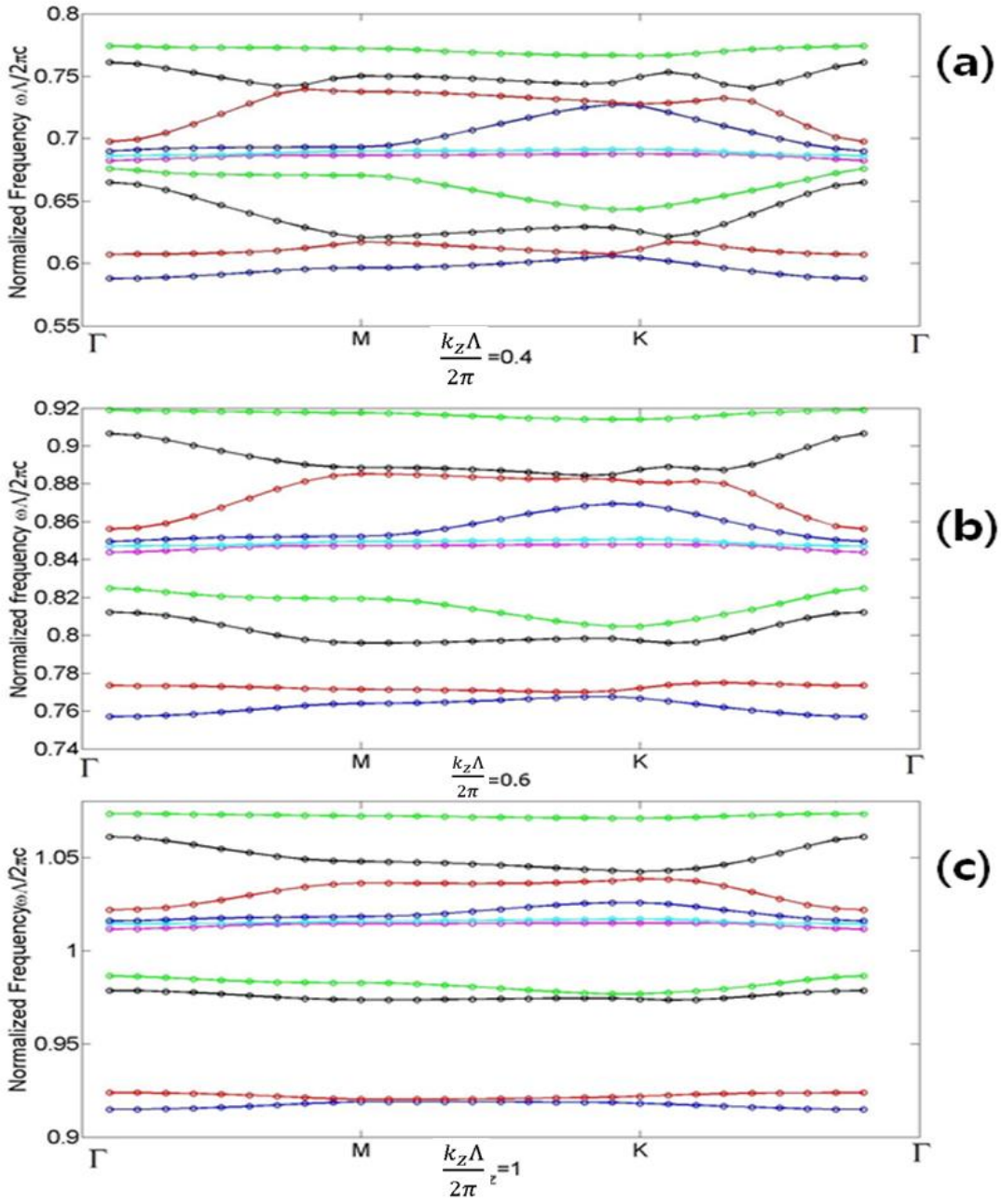

Figure 5. 6: Band structure of 12-fold quasi crystal calculated by FEM in presence of (a) $k_z \Lambda/2\pi = 0.4$, (b) $k_z\Lambda/2\pi = 0.6$ and $(c) k_z \Lambda/2\pi = 1$.

The FEM method used in the calculation of the band structures in figure 5.6 permits the calculation of the electromagnetic field profiles of individual eigenfrequency. Figure5.7 shows an example of such a profiles.

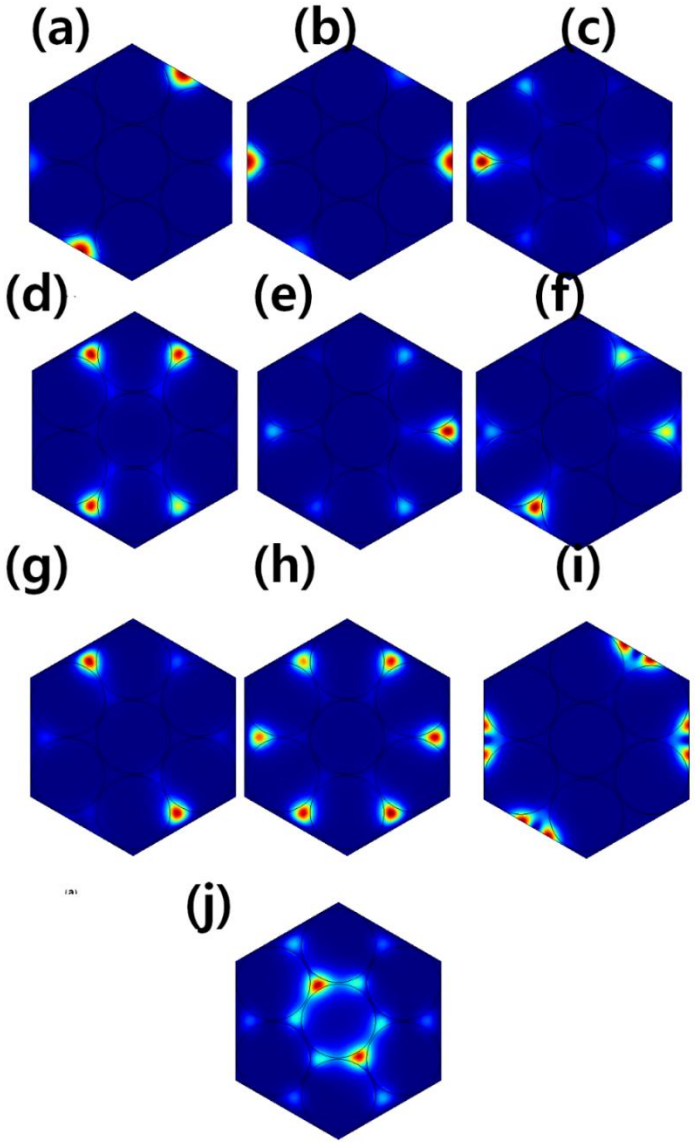

Figure 5. 7: Electromagnetic field profile calculated for a structure with 7 cylinders of r/Λ=0.49 as approximant. The fields are corresponding to eigenfrequency of (a) ωΛ/2πc=0.6, (b) ωΛ/2πc=0.61, (c) ωΛ/2πc=0.6105, (d) ωΛ/2πc=0.64, (e) ωΛ/2πc=0.68, (f) ωΛ/2πc=0.68

In figure 5.7, the electromagnetic field profile is shown for the unitcell of containing 7 cylinders with $\frac{r}{\Lambda} = 0.49$. The particular state shown are at the $k_x = 0.5, k_y = 0.5$ and $k_z = 0.4$ point in reciprocal space, and corresponds to eigenfrequency of $\frac{\omega\Lambda}{2\pi c} = 0.6$, $\frac{\omega\Lambda}{2\pi c} = 0.61$, $\frac{\omega\Lambda}{2\pi c} = 0.6105$, $\frac{\omega\Lambda}{2\pi c} = 0.64$, $\frac{\omega\Lambda}{2\pi c} = 0.68$, $\frac{\omega\Lambda}{2\pi c} = 0.6805$, $\frac{\omega\Lambda}{2\pi c} = 0.72$, $\frac{\omega\Lambda}{2\pi c} = 0.73$, $\frac{\omega\Lambda}{2\pi c} = 0.74$, $\frac{\omega\Lambda}{2\pi c} = 0.76$ at figure5.7 (a), (b), (c), (d), (e), (f), (g), (h), (i), (j) Respectively. As different eigenfrequencies proof field profile displays the strict 6-fold symmetry and while most of the frequency states represent the majority of electromagnetic energy on the edges.

5.4.2 Band analysis of 8-fold Ammann-Beenker

In the current section we present the band analysis of an octagonal lattice as shown in figure 5.1, the geometry of the structure can be defined by a constant length of Λ , which is the length of the sides of the square tiles in the structure (depicted in figure 5.1) and radius of cylinders which indicated by r . In what follows, the band structure will study for the 8-fold structure with an approximant which contains 14 cylinders with a certain cylinder radius of r=0.37Λ. The approximant size is a square with the edge size of $L = 2 + \sqrt{2}$ as shown in figure 5.8. The cylinder radius considered is r=0.37Λ while for r>0.37 Λ cylinders start overlapping. Therefore the band structure is investigated for the largest air filling for the range. The mentioned rate of $\frac{r}{\Lambda} = 0.37$ induces a surface air filling equal to:

$$s_{AFF} = 51\%$$

The photonic band structure of a crystal based on such approximant is calculated by applying periodic boundary condition at the sides of square approximant. The periodicity is defined by $R = l_1 a_1 + l_2 a_2$ where $l_1 and\, l_2$ are integers and $a_1 = (L, 0), a_2 = (0, L)$ are translational vectors.

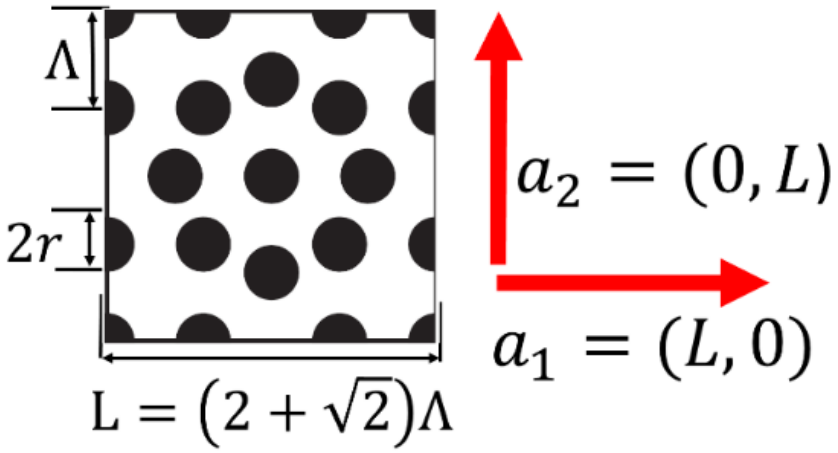

Figure 5. 8: approximant for 8-fold and Bravias vectors.

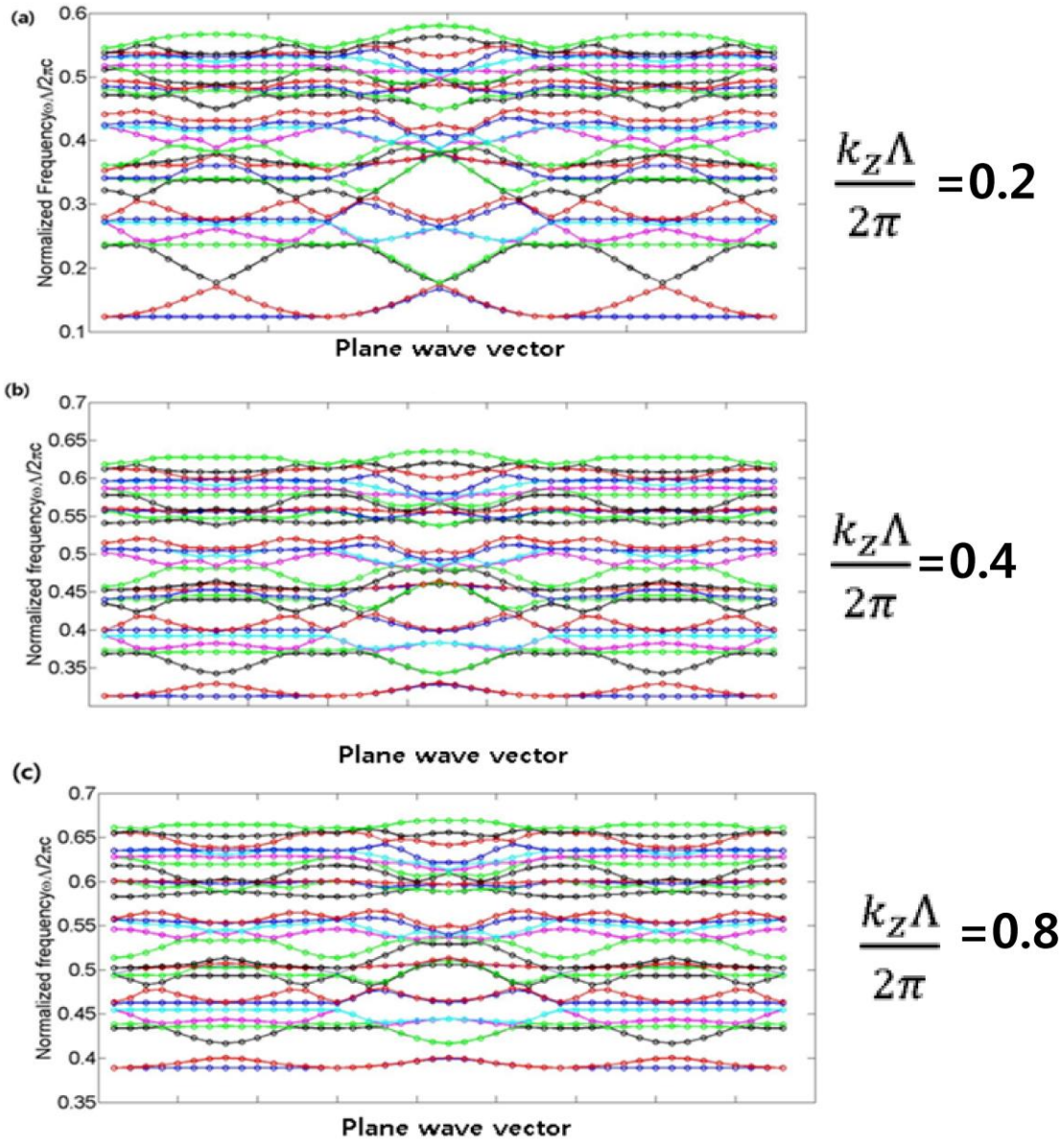

Figure 5. 9: Band structure of a 2-D, 8-fold symmetry with employing a square approximant for different out of plane wave vector, (a)$\frac{k_z\Lambda}{2\pi} = 0.2 (b)\ (k_z\Lambda)/2\pi = 0.4, (c)\ (k_z\Lambda)/2\pi = 0.8$.

The photonic bandstructure of a crystal based on mentioned approximant in figure 5.8 has been calculated by applying periodic boundary conditions at the edges of the square unit cell and using Bloch theorem [38]. It should be mentioned that the resulting structure is not pure quasicrystalline, but rather pure periodic one, actually a short-range eight-fold rotational symmetry within the approximant is reflected.

As far as our intention is to calculate band structure of a 2-D quasicrystal with present of out of plane wave vector which is well discussed in chapter 4 and previous section

and related works [39]. The 8-fold case has been analyzed via FEM and resulting band structures is presented in figure 5.9 (a), (b) and(c).

Our calculations show that band-gaps only occur in the band structure while increasing the out of plane wave vector. No gap is detectable in figure 5.9 (a) with $\frac{k_z\Lambda}{2\pi} = 0.2$ and we can observe the presence of band gap while increasing the out of plane wave vectork_z, as shown in figure 5.9 (b) and (c) corresponding to $\frac{k_z\Lambda}{2\pi} = 0.4\ and\ \frac{k_z\Lambda}{2\pi} = 0.8$. The band gaps are represented clearly. Actually the 2-D problem with $\frac{k_z\Lambda}{2\pi} \leq 0.2$ we cannot see any kind of gap due to non-enough refractive index contrast 1:1.46 and calculation in hybrid mode not in TE mode which is reported in some works for 8-fold [36].

The FEM method used in the calculation of the bandstructure of figure 5.9 permits to calculate of the electromagnetic field profiles of individual eigenfrequencies. Figure 5.10 shows an example of such a profiles. In figure 5.10, the electromagnetic field profile is shown for the approximant of containing 14 cylinders of radius $r = 0.37\Lambda$. The particular state shown is at the $k_x = 0.5,\ k_y = 0.5\ and\ \frac{k_z\Lambda}{2\pi} = 0.2$ point in reciprocal space, and have frequencies of $\frac{\omega\Lambda}{2\pi c}$ =0.52055, $\frac{\omega\Lambda}{2\pi c}$ =0.5205, $\frac{\omega\Lambda}{2\pi c}$ =0.5202, $\frac{\omega\Lambda}{2\pi c}$ =0.5201, $\frac{\omega\Lambda}{2\pi c}$ =0.5106, $\frac{\omega\Lambda}{2\pi c}$ =0.5103, $\frac{\omega\Lambda}{2\pi c}$ =0.4507, $\frac{\omega\Lambda}{2\pi c}$ =0.441, $\frac{\omega\Lambda}{2\pi c}$ =0.4306 and $\frac{\omega\Lambda}{2\pi c}$ =0.4303 at figure 5.10 (a), (b), (c), (d), (e), (f), (g), (h), (i) and (j) respectively. Different eigenfrequencies proof field profile displays the strict 4-fold symmetry. Most of modes represent the majority of electromagnetic energy on the edges, which means the electromagnetic waves consider edges of structure as defects of quasicrystal and it is represented which most of the states is localized around defect. If we step inside of the quasicrystal and closer to center local 8-fold symmetry can be seen as well.

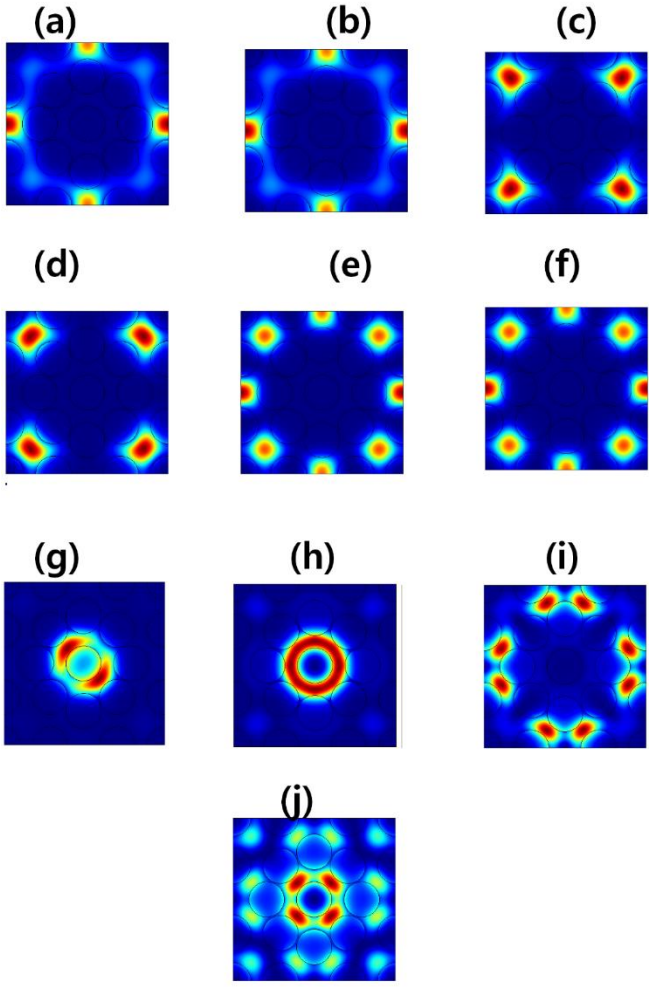

Figure 5. 10: Electromagnetic field profile calculated for a structure with 14 cylinders of r/Λ=0.37 in the approximant. The field profiles is belong to eigenfrequencies of (a) ωΛ/2πc=0.52055, (b) ωΛ/2πc=0.5205, (c) ωΛ/2πc=0.5202, (d) ωΛ/2πc=0.5201, (e) ωΛ/2πc=0

5.5 Summary

In this chapter with introducing quasi crystal structures and their application in photonic we started and we represent different algorithms to build up quasicrystals with different rotational symmetry levels. We represent a suitable mathematical method to calculate band structures and field profile caalculating different eigenfrequencies. The mentioned method is applied for 8-fold and 12-fold symmetry quasicrystals and represented results in agreement the works in related field. Behind the output of band structures evident of presenting good band map for 12-fold is clear while about 8-fold no sufficient results is shown and it shows that band gaps cannot satisfy conditions for

PBG guiding for fibers. More studying is represented in chapter 6 about modification and employing these structures as optical fiber.

Bibliography

1.D. Levine and P. J. Steinhardt, “Quasicrystals: A new class of ordered structures,” Phys. Rev. Lett. 53, 2477–2480 (1984).

2. John, S. Strong localization of photons in certain dielectric superlattices. Phys. Rev. Lett. 58, 2486–2489 (1987).

3. Yablonovitch, E. Inhibited spontaneous emission in solid state physics and electronics. Phys. Rev. Lett. 58, 2059–2062 (1987).

4. Joannopoulos, J. D., Meade, and R. & Winn, J. Photonic Crystals: Molding the Glow of Light (Princeton Univ., 1995).

5. Anderson, P. W. Absence of diffusion in certain random lattices. Phys. Rev. 109, 1492–1505 (1958).

6. John, S. Electromagnetic absorption in a disordered medium near a photon mobility edge. Phys. Rev. Lett. 53, 2169–2172 (1984).

7. Philip St.J. Russell,"Photonic-Crystal Fibers", Vol. 24, Iss. 12 — Dec. 1, 2006 pp: 4729–4749, (2006)

8. M. Golshan, A. R. Bahrampour, and A. Langari, A. Szameit ,"Transverse localization in nonlinear photonic lattices with second-order coupling", arXiv:1302.3124v1

9. Carter, W. H. & Wolf, E. Coherence properties of lambertian and non-lambertian sources. J. Opt. Soc. Am. 65, 1067–1071 (1975).

10.Kohmoto, M., Sutherland, B. & Iguchi, K. Localization of optics: Quasiperiodic media. Phys. Rev. Lett. 58, 2436–2438 (1987).

11. Steurer, W. & Sutter-Widmer, D. Photonic and phononic quasicrystals. J. Phys. D 40, R229–R247 (2007).

12. Albuquerque, E. L. & Cottam, M. G. Theory of elementary excitations in quasiperiodic structures. Phys. Rep. 376, 225–337 (2003).

13. M. E. Zoorob, M. D. B. Charlton, G. J. Parker, J. J. Baumberg, M. C. Netti,"Complete photonic bandgaps in 12-fold symmetric quasicrystals", NATURE, 404, 13, (2000)

14. E. Yablonovitch, "Inhibited Spontaneous Emission in Solid state Physics and Electronics", Phy. Rev. Lett., 58, 2059, (1987).

15. Cheng, Z., Savit, R. & Merlin, R. Structure and electronic properties of Thue–Morse lattices. Phys. Rev. B 37, 4375–4382 (1988).

16. Liu, N. Propagation of light waves in Thue–Morse dielectric multilayers. Phys. Rev. B 55, 3543–3547 (1997).

17. Dulea, M., Johansson, M. & Riklund, R. Localization of electrons and electromagnetic waves in a deterministic aperiodic system. Phys. Rev. B 45, 105–114 (1992).

18. Steurer, W. & Sutter-Widmer, D. Photonic and phononic quasicrystals. J. Phys. D 40, R229–R247 (2007).

19. E.O. Harriss, J.S.W. Lamb,"Canonical substitutions tilings of Ammann–Beenker type", 319, 1–3, 241-279 (2004).

20. Brando, G. C, Grünbaum, Shephard, "Tilings and Patterns", New York: W. H. Freeman, ISBN 0-7167-1193-1, (1987).

21. Levi, L. et al, "Disorder-enhanced transport in photonic quasicrystals", Science 332, 1541–1544 (2011).

22. Maier, S. A. Plasmonics: Fundamentals and Applications (Springer, 2007).

23. Ozbay, E. Plasmonics: Merging photonics and electronics at nanoscale dimensions. Science 311, 189–193 (2006).

24. Gramotnev, D. K. & Bozhevolnyi, S. I. Plasmonics beyond the diffraction limit. Nature Photon. 4, 83–91 (2010).

25. Schuller, J. A. et al. Plasmonics for extreme light concentration and manipulation. Nature Mater. 9, 193–204 (2010).

26. Z. Valy Vardeny, Ajay Nahata and Amit Agrawal,"Optics of photonic quasicrystals", Nature photonics, (2013)

27. Siegman, A. E. Lasers (Univ. Science Books, 1986).

28. Noda S. et al. Polarization mode control of two-dimensional photonic crystal laser by unit cell structure design. Science 293, 1123–1125 (2001).

29.Notomi, M., Suzuki, H., Tamamura, T. & Edagawa, K. Lasing action due to the two-dimensional quasiperiodicity of photonic quasicrystals with a Penrose lattice. Phys. Rev. Lett. 92, 123906 (2004).

30. Nozaki, K. & Baba, T. Quasiperiodic photonic crystal microcavity lasers. Appl. Phys. Lett. 84, 4875–4877 (2004).

31. Kim, S.-K. et al. Photonic quasicrystal single-cell cavity mode. Appl. Phys. Lett. 86, 031101 (2005).

32. Nozaki, K. & Baba, T. Lasing characteristics of 12-fold symmetric quasi-periodic photonic crystal slab nanolasers. Jpn J. Appl. Phys. 45,
6087–6090 (2006).

33.Xiangdong Zhang, Zhifang Feng, Yiquan Wang, Zhi-Yuan Li, Bingying Cheng, Dao-Zhong Zhang,"Negative Refraction and Imaging with Quasicrystals",Springer Series in Materials Science, 98,167-182,(2007).

34.Xiwen Wang, Z. Ren, and K. Kempa, "Unrestricted superlensing in a triangular two dimensional photonic crystal,", 12, 13, 2919–2924,(2004).

35.Alejandro W. Rodriguez, Alexander P. McCauley, Yehuda Avnie and Steven G. Johnson, "Computation and visualization of photonic quasicrystal spectra via Bloch's theorem",arXiv:0711.2052v2 [physics.optics] 7 Mar 2008

36.Marian Florescu, Salvatore Torquato, and Paul J. Steinhardt,"Complete band gaps in two-dimensional photonic quasicrystals",PHYSICAL REVIEW B 80, 155112 (2009).

37. M. A. Kaliteevski, V. V. Nikolaev, R. A. Abram, S. Brand, "Bandgap structures of optical Fibonacci lattices after light diffraction," Opt. Spectrosc. 91, 109-118 (2001).

38. Xiwen Sun; Hu, D.J.J., "Air Guiding With Photonic Quasi-Crystal Fiber," Photonics Technology Letters, IEEE , vol.22, no.9, pp.607,609, May1, (2010).

39.Jes Broeng, Stig E. Barkou, Thomas Søndergaard, and Anders Bjarklev,"Analysis of air-guiding photonic bandgap fibers",OPTICS LETTERS,25, 2 ,15,(2000).

Chapter 6

Hollow core photonic quasicrystal fiber

6.1 Introduction

Photonic crystal fibers (PCFs) refer to a new class of optical fibers that have wavelength-scale morphological microstructure running down their length [1-3]. They, according to their guiding mechanisms, are divided into index-guiding PCFs (IG-PCFs) and photonic band-gap fibers (PBFs). In light of their composite nature, PCFs enable a plenty of possibilities and functionalities hitherto not possible. In the last decade, particular attention has been focused on PBFs due to the lattice assisted light propagation within the hollow core (HC) [3]. This particular feature, indeed, has a number of advantages such as lower Rayleigh scattering, reduced nonlinearity, novel dispersion characteristics, and potentially lower loss compared to conventional optical fibers [4]. In addition, the hollow core PCFs (HC-PCFs) also enable enhanced light/material interaction, thus providing a valuable technological platform for ultra-sensitive and distributed biochemical sensors [5]. To further enhance the potential of HC fibers, in-fiber components such as wavelength selective gratings are proposed [6]. The geometrical structure of the micro-structured cladding is playing an important rule acting on the bandgap regime. However, all HC-PCF fiber are focused on periodic structures and thus are limited to few geometry such as a triangular, square, honeycomb, or Kagome periodic arrays lattice.

In this work the idea is to explore new functionalities and increase the freedom degrees of HC-PCFs by studying new kinds of fibers based on quasi-crystals (PQs). As already mentioned in chapter 5, PQs are aperiodic crystal (1D, 2D or 3D) which have the lack of translational symmetry. The quasicrystal structure presented intriguing achievements in optics as well as crystallography. Optical properties such as complete photonic bandgap, laser microcavity and guided resonance in different aperiodic

structures are investigated and reported elsewhere [7-10]. Moreover these photonic quasi crystals can provide higher rotational symmetry and potentially open the ability to have band gap in lower refractive index contrast [7]. Recently PQs have been investigated principally for IG-PCFs [11] while Sun et al. [12] for the first time proposed a hollow core quasi crystal fiber based on 12-fold symmetric structure. They demonstrated that 12-fold fibers exhibit a double photonic bandgaps.

In the present work we numerically study the propagation properties of hollow core photonic quasi crystal fibers (HC-PQFs). In particular we propose different structures such as the 12-fold (accordingly to the ref. [12]) and a modified 8-fold. In this chapter we will attain bandgap maps and propagating modes of two HC-PQFs via finite element method. The dispersion curves of the fundamental modes for the two proposed HC-PQFs will be investigated and compared. The presence of two photonic bandgap at $\lambda/\Lambda<1$ is demonstrated for both fiber geometries.

6.2 Band and modal study of 12-fold air hollow core quasi crystal fiber

Dodecagonal symmetry, is one of very first geometries which its optical properties has been studied. Several works about this structure admits the formation of bandgap in lower refractive index contrast. On the other hand we already present a method to calculate band gap of 12-fold structure using a supercell technique.

In the current section we consider a 12-fold portion which obtained by aforesaid algorithm in chapter 5 to generate stampifli 12-fold, and we obtain geometry which is depicted in figure 6.1. It is well shown the structure is decorated by squares and triangles. The edges Λ_1 andΛ_2, are considered and geometry of 12-fold induces $\Lambda_1 = \Lambda_2 = \Lambda$ as constants of QC lattice. Generally in quasicrystals always existed such length for determining the lattice.

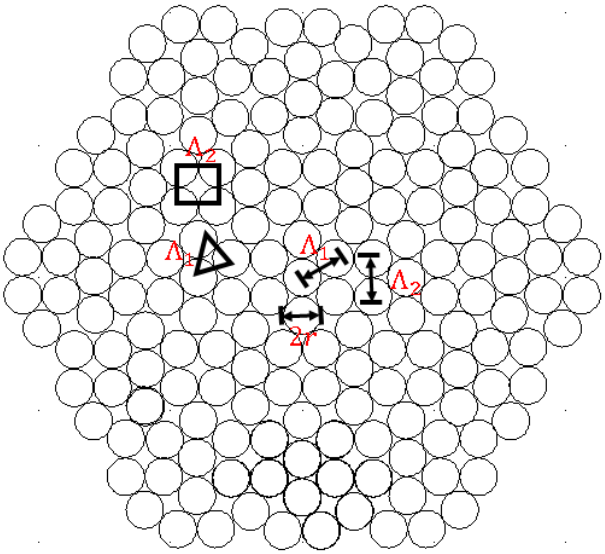

Figure 6. 1: A big portion of 12-fold generated by stampifli algorithm.

We define the geometrical properties of 12-fold QC with r and Λ where r is the radius of capillaries all over the lattice and Λ is a characteristic of lattice famous as hole-to-hole spacing or Pitch. In following the ratio of r/Λ is kept fixed at 0.49 permitting a good air filling factor. Consequently the surface filling factor as S_{AFF} for the considered structure is:

$S_{AFF} = 82\%$ (1)

We construct fiber with exploiting the 12-fold structure defined in figure 6.1 as transversal section of HC-PQF and holes which represents capillaries travelling along fiber length. To introduce the core of fiber we integrate 7 capillaries and an air core with radius of R=1.38Λ is obtained as shown in figure 6.2 (a) and another fiber with a core made of 19 integrated holes with radius of R=2.05Λ as depicted in figure 6.2 (b) is obtained.

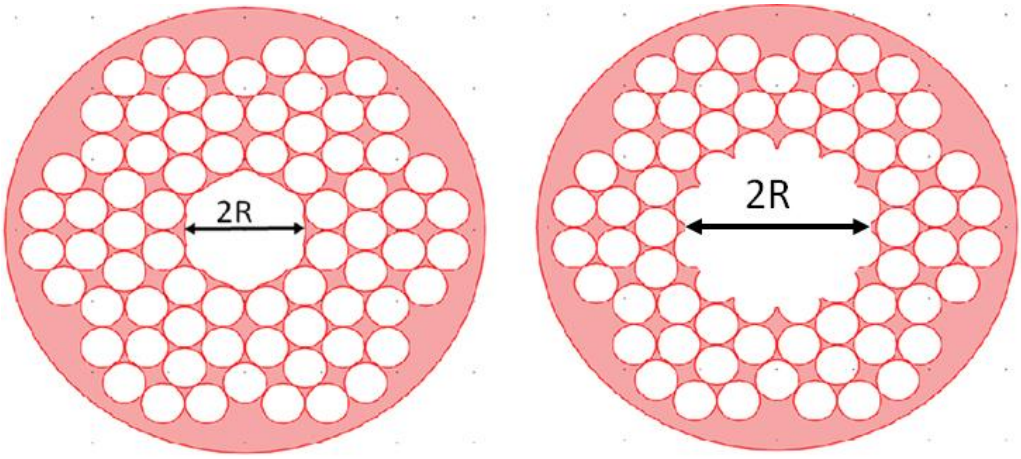

Figure 6. 2: the 12-fold HC-PQF cross section with a core of (a) 7 holes integrated (b) 19 holes integrated.

The refractive index of the structure in our calculation is $n_{glass} = 1.46$ for the glass region and air refractive index is considered $n_{air} = 1$, the wavelength dependence of refractive index is negligible.

6.2.1 Primitive cell and bandgap calculation of 12-fold

As we have mentioned in chapter 4 light propagation in the core with refractive index less than cladding needs PBG phenomena, so to study the light propagation in HC-PQF it is necessary to study band structure of the plane lattice in presence of out of wave vector. The same as we already analysis in chapter 4 for triangular lattice.

Regarding to our studies in chapter 5 several band gap calculation method is presented in literature but a supercell method represents the possibility of band analysis, with choosing an enough big portion of the geometry with taking in mind which a minimum size of supercell is obligatory. On the other hand the same study of band gap calculation (chapter 5) with considering an approximant of 7 holes has been implemented.

To rebuild the lattice with the mentioned primitive cell, we introduce two translational vectors to span all the lattice $a_1 = \left(1+\sqrt{3}\right)\Lambda(1,0), a_2 = \left(1+\sqrt{3}\right)\Lambda\left(\frac{1}{2},\frac{\sqrt{3}}{2}\right)$ and $R_B = l_1\, a_1 + l_2\, a_2$, where R_B can span all the lattice while l_1 and l_2 are integers.

The band calculation should be done by specifying a longitudinal part of the wave vector, the plane PBGs of the HC-PQFs can be calculated exactly as a function of out of plane wave vector. Therefor the same method as previously discussed in chapter 5 for 12-fold will be presented. The bandgap map as a function of plane wave vector has been calculated as it is illustrated in figure 6.3.it is important to highlight the number of bands in this calculation where 10 therefore, the gap map is not satisfying the conditions for light propagation in the fiber. More over the gaps which are presented in figure 6.3 are not presenting significant bandgaps.

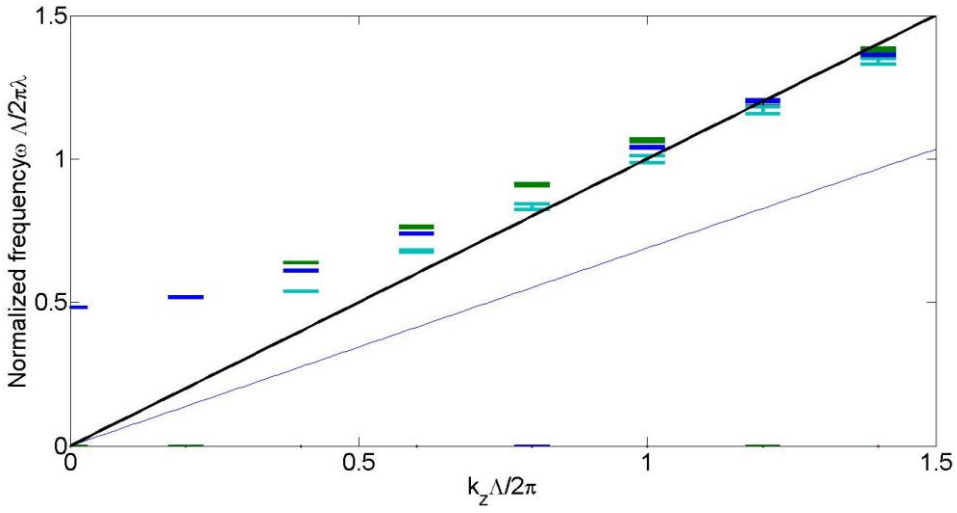

Figure 6. 3: Bandgap map of the 12-fold structure as a function of out of plane wave vector, investigation between 10 bands.

The conditions listed below guarantee a fiber works in PBG mechanism:

1. Band gap stay in a region for $\frac{\lambda}{\Lambda} \leq 1$
2. The band gap fall above the air line, $\omega = ck_z$.

To overcome the conditions, we run the same method of calculation but with higher number of eigenfrequencies (bands) in compare to eigenfrequency number of chapter 5 (10 bands) for the same problem structure.

Therefore the out of plane band gap map is calculated with a FEM method with finding 20 bands. Figure 6.4 (a) and (b) represents the band structure of 12-fold lattice for

$\frac{k_z\Lambda}{2\pi} = 1.6$, $\frac{k_z\Lambda}{2\pi} = 1.7$ shaded areas presented in figure 6.4 (b) is bigger than the wave number comparing to figure 6.4 (a)

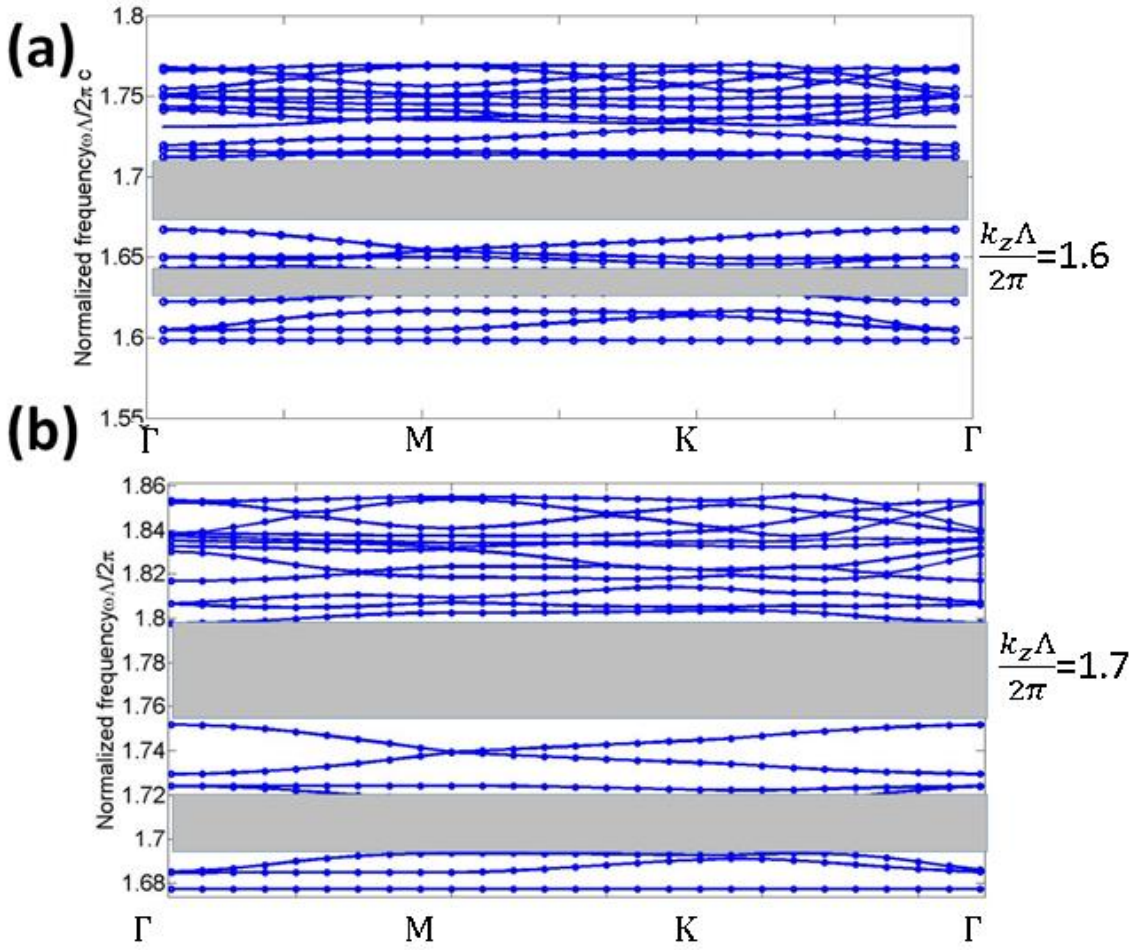

Figure 6. 4: Band diagram calculated for 12-fold considering 20 bands where (a) $(k_z\,\Lambda)/2\pi = 1.6$, $(b)(k_z\,\Lambda)/2\pi = 1.7$.

Since objective of this session is calculating the gap map as function of $\frac{k_z\Lambda}{2\pi}$ for light propagation in HC-PQF. Figure 6.5 shows the bandgap map of 12-fold structure with shaded regions as effective refractive index vs. normalized wavelength. The equivalent graph as frequency versus out of plane wave vector also depicted in figure 6.5 (inset). It is worth noting that there are two PBGs opening in the $\lambda/\Lambda<1$ region in the structure. Respect to 2 photonic bandgap, new possible applications in sensing and communication fields, accordingly to the ref [12] is supposed. We would like to stress the advantages of the double PBG with PQC structure as compared with double photonic bandgap in periodic lattice structure proposed by Light et al. [13] where a

careful control of the strut thickness and apex size is required, and there exists unwanted surface mode. In comparison, PQF does not have such problems.

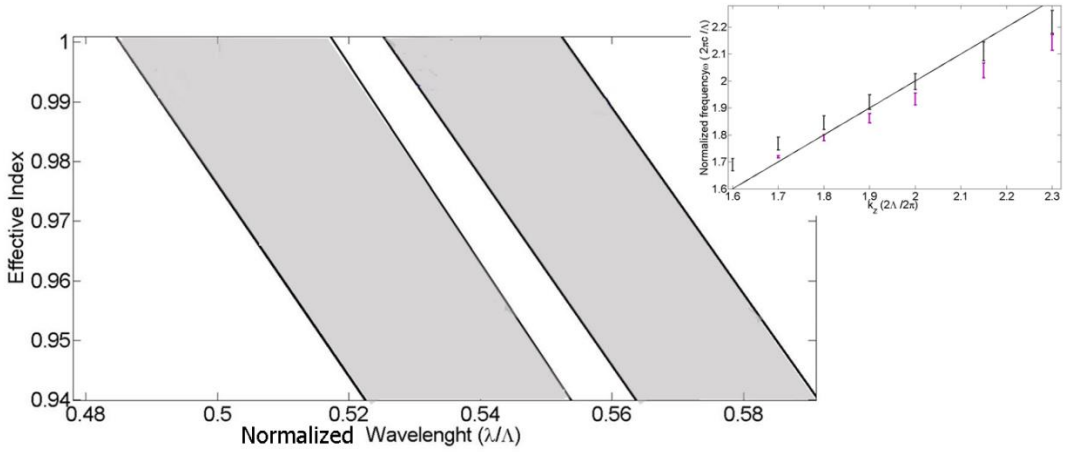

Figure 6. 5: Band diagram of 12-fold structure as effective index vs. normalized wavelength, (inset) band gap as function of out of plane wave vector(two gaps is shown by violet and black error bars).

6.2.2 Modal analysis and results of 12-fold HC-PQF

In the present work two different 12-fold HC-PQFs are designed and investigated. Schematic cross section for both are illustrated in figure 6.2(a) and 2(b). The former is constructed with a local part of the 12-fold symmetric PQs as in with a radius of R=1.38Λ with jointing 7 central holes to each other[12] while the second one is realized with a radius R= 2.05Λ obtained as removing 19 capillaries so we achieve a quite big core respect to total structure of fiber.

Fundamental mode for both fiber with different core size has obtained throw FEM method. Figure 6.5 depicting effective index of fundamental mode for bigger core (black line) and small core (blue line). The results representing better confinement due to bigger size of core, as its effective index is closer to one, which is the line cone. Both of modes are behaving very nearly linear, but bigger size of core usually have a drawback and that is the bigger number of surface modes due to higher interaction surface will appear.

It is necessary to note that, even if the core size increase but in the band gap with longer wavelength a phenomena is seen, which the propagated range is not covering all the

gap range. The reason is due to less layer of air holes around the core and as it is mentioned in literature the number of layers around core effects confinement loss drastically, therefore the mode can be disappeared [12].

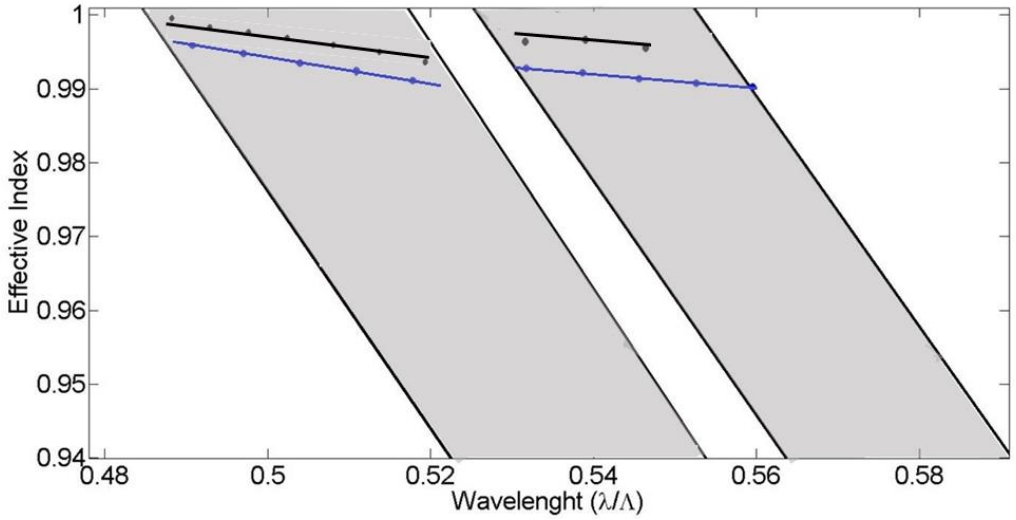

Figure 6. 6: Effective index of fundamental mode of fiber with core of R=2.05Λ black line and fiber with core R=1.38Λ blue solid line.

6.2.3 Electromagnetic field profile for 12-fold

The intensity of electromagnetic profile of the fundamental mode for 12-fold HC-PQF in both photonic bandgaps, is defined as the measure of poynting vector, $|s| = |Re(E^* \times H).e_z|$. We exploit again the same analysis approach of FEM for calculation of electromagnetic field profile intensity. Figure 6.7 (a) is depicting field profiles of HC-PQF with R=2.05Λ corresponding to normalized wavelengths of λ/Λ=0.5 in figure6.7 (a) and λ/Λ=0.55 in figure 6.7 (b).

As it is well presented both of electromagnetic field profiles are confined in the core. Both of them are modes of different gaps and representing circular symmetry regarding to symmetry of 12-fold HC-PQF.

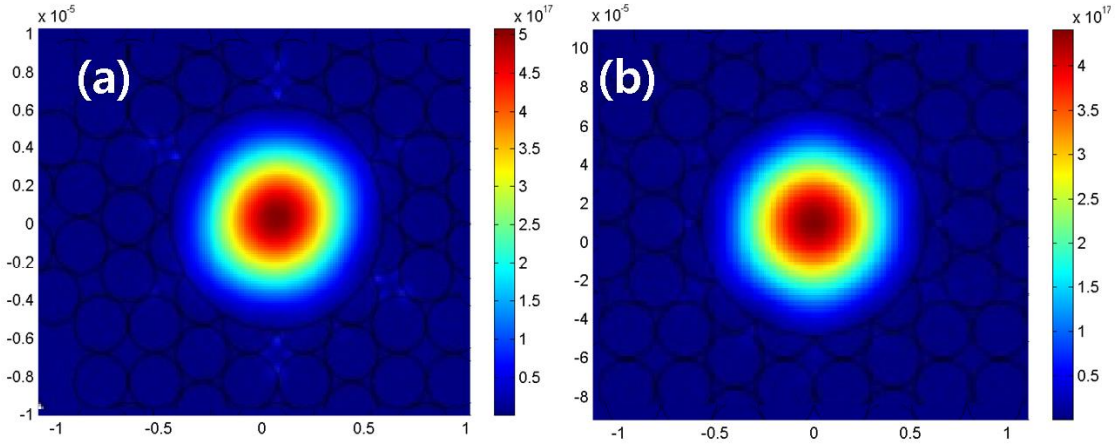

Figure 6. 7: The electromagnetic field profile of 12-fold HC-PQF in case where R=2.05Λ at (a) λ/Λ=0.5, (b) λ/Λ=0.55.

The field profile analyses has been done for 12-fold HC-PQF where core size is R=1.38Λ and Figure 6.8 (a) is representing field profiles corresponding to normalized wavelengths of λ/Λ=0.51 in figure (a) λ/Λ=0.55 in figure 6.8 (b)

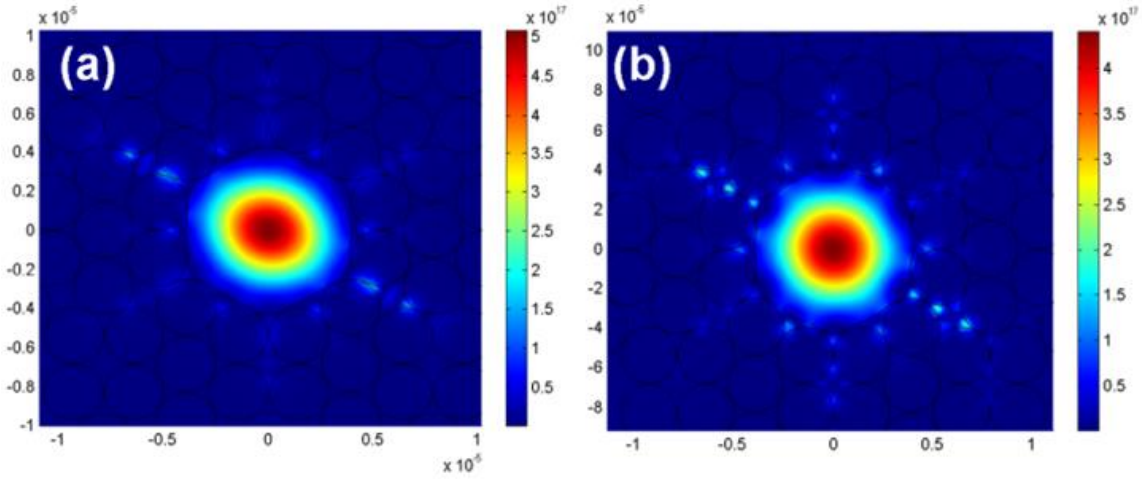

Figure 6. 8: The electromagnetic field profile of 12-fold HC-PQF in case where R=1.38Λ at (a) λ/Λ=0.51, (b) λ/Λ=0.55.

As it is presented the fields are well confined in the air core and, the field profile surface is not approaching the edge of the core-cladding interface. In both 12-fold fibers there is no surface mode observable and the circularity of the fundamental modes is remarkable.

6.2.4 Confinement loss for 12-fold HC-PQF

The confinement loss of fundamental mode fir HC-PQF in both PBG are calculated by the full-vector finite- element method (FEM) with considering a circular perfectly matched layer (PML) [12]. Due to finite numbers of air holes in the cladding, modes always suffering from some leakage loss. Figure 6.9 illustrating the leakage loss of the fundamental mode versus variation of normalized wavelength for HC-PQF with core size of R=1.38Λ. The confinement loss behavior clearly is in agreement with bandgap. Increasing the number of layers are so important to heal this unfortunate. Since the loss decreases almost linearly on a logarithmic scale with respect to cladding ring number [4], we suggest that ten rings are necessary to reduce the loss below 1 dB/km. We can see that there are two lowest central frequencies in the PBG region. Therefore, we can obtain simultaneous guidance of two span wavelengths with low loss in a single fiber.

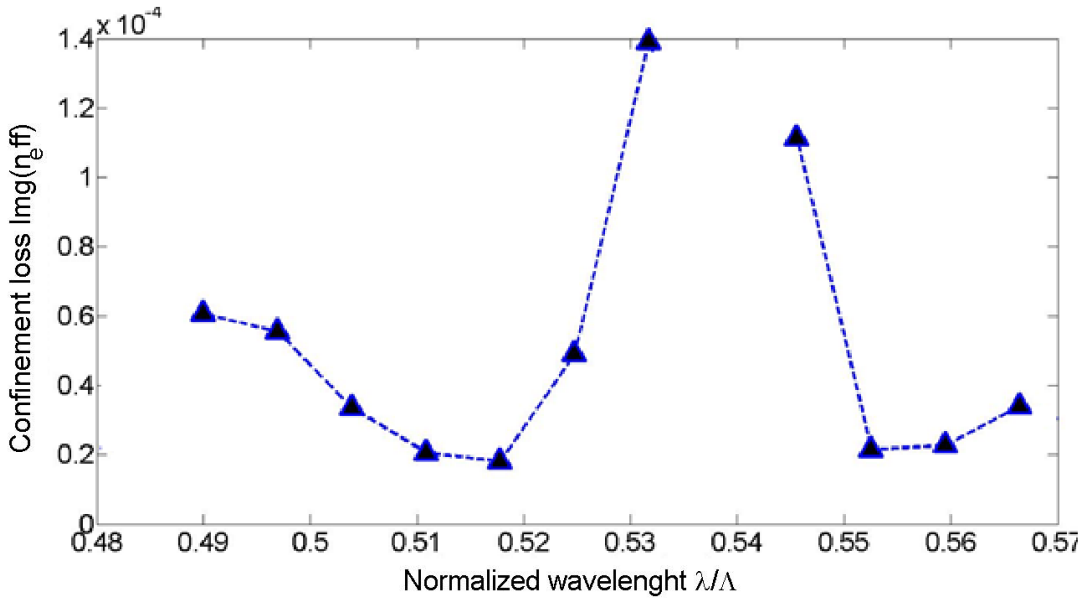

Figure 6. 9: Represents confinement loss for 12-fold HC-PQF for R=1.38Λ.

6.3 8-fold challenges and solution

8-fold QC is one of the most studied structure in photonics, several optical properties such as microcavity, guided resonance in QC slab[10], and most important of all of them formation of bandgap has been reported for this structure. We already study 8-

fold bandstructure in quite low refractive index contrast of 1:1.46. In the previous chapter we came to conclusion which bandgap can appear in the sort of hybrid modes (neither pure TE and nor pure TM due to non-zero out of plane wave vector) when normalized k_z increases as an outcome, the bandgaps appear and accordingly increase.

This study at the beginning represents promises in order to find band gap, for a PBG mechanism of propagation in the fiber. Unfortunately our results based on the photonic bandgap map are not presenting an eligible gap in appropriate range of normalized wavelength λ/Λ<1 and gap do not fall above the air line ($\omega = ck_z$), as it is shown in figure 6.10.

But for the 12-fold structure, we already discussed equal phenomena, it might be possible to find gap for higher number of eigenfrequency. In case of 8-fold we already chose 35 bands which is a big number. On the other hand this result was expected for a photonic crystal with the same filling factor of$S_{AFF} = 52\%$ ($\frac{r}{\Lambda} = 0.37$).

Unfortunately the filling factor for studied Amnan-Beenker structure has taken its maximum level, therefor with increasing radius of holes, capillaries start overlapping. So the Amnan-Beenker structure itself is not an appropriate case of study for fiber, hence in following section we will provide an approach to solve the problem.

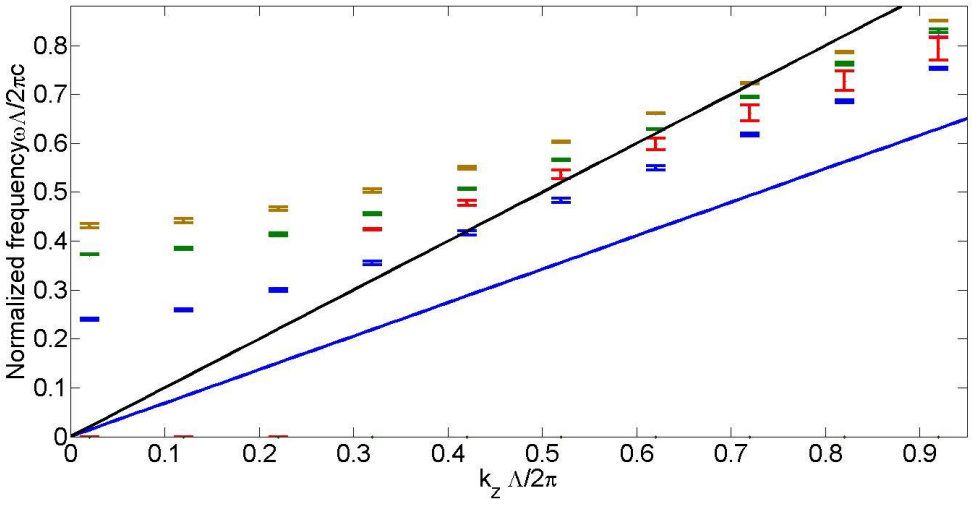

Figure 6. 10: Representing the bandgap map of 8-fold.

6.3.1 Geometry for a Modified 8-fold structure

The employment of symmetry is one of the reason which take us to quasicrystal structures. Our aim is to take advantages of higher order of symmetry in the fiber structure instantaneously with aperiodic structure. We can claim if we present an octagonal symmetry in any case we have a quasicrystal structure as an upshot of theorem 5.1.

Let have a flash back to geometry of 8-fold in previous chapter as we already speak about its geometry where it is made of rhombi of acute angle of π/4 and squares as shown in figure 6.11(a).

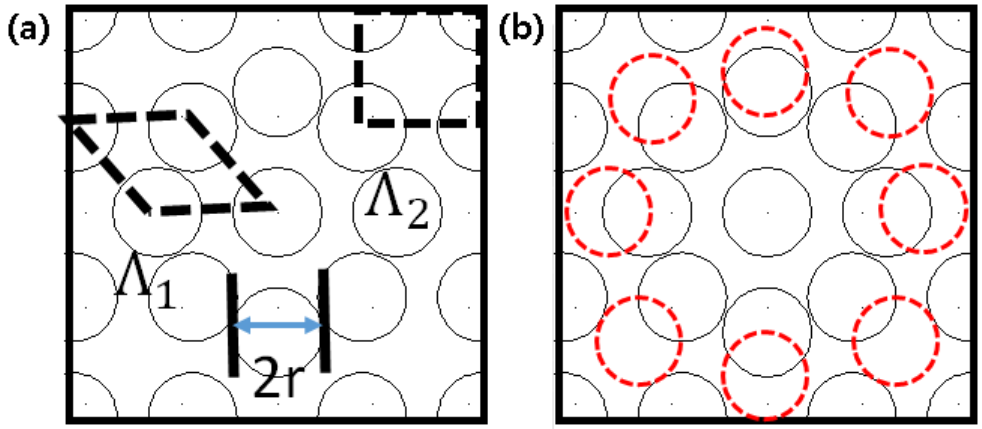

Figure 6. 11: (a) Ammann–Beenker structure and (b) a modification approach as dotted red circles.

As it is well seen in figure 6.11 (a), whole rhombi and squares are composing the 8-fold structure, and since rhombi and squares have intersected edges therefore $\Lambda_1 = \Lambda_2 = \Lambda$, that is why it is called pitch or quasicrystal constant.

An idea of modification for 8-fold structure has been presented for study of cavities phenomena elsewhere [9], in their work a modification of 8-fold have been suggested. Modifications is depicted as red dotted circles in figure 6.11(b). Actually it is generally a good idea since this because this changes don't break symmetry but increase the freedom for choosing hole size of bigger with staying in the same surface .the red dotted circles as modified part is reported elsewhere [9].

But the mentioned changes in figure 6.11 (b) cannot increase air filling solely, therefor two sort of changes, including the replacement of holes and changing radii of holes simultaneously is needed. Regarding to complication of mentioned changes, Different

attention is required to work with the modified 8-fold. First of all our proposal is depicted in figure 6.12 (a) the red dotted line represent pristine octagonal lattice and solid black circles are depicting new structure with higher air filling.

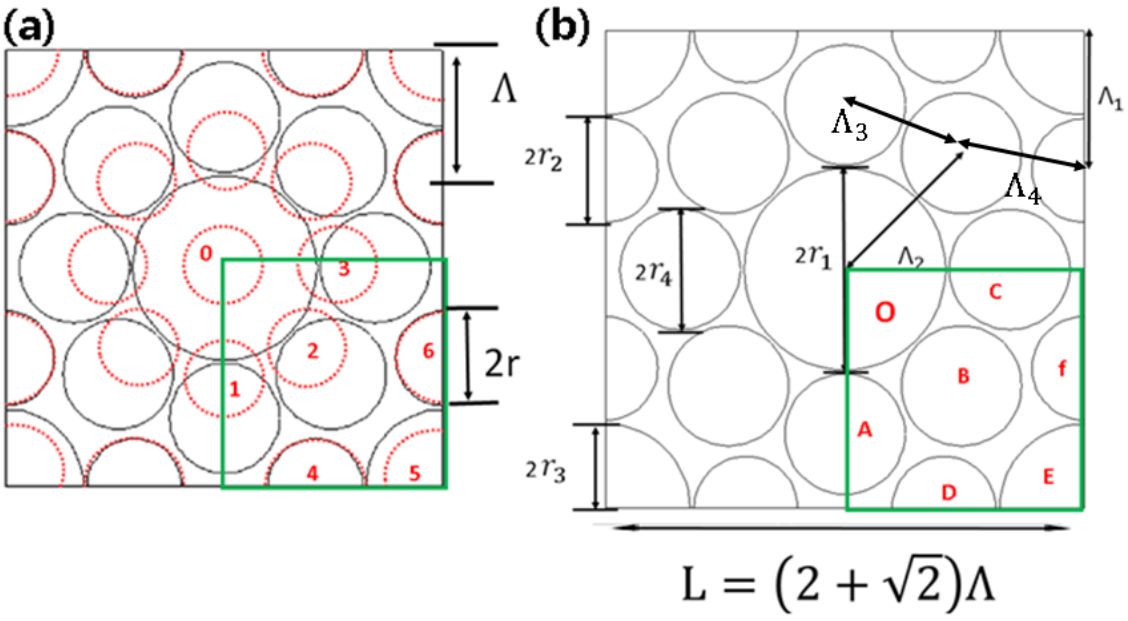

Figure 6. 12: (a) overlap of Ammann-Beenker structure (red dotted lines), and M8-fold as solid black structure. (b) Geometrical details of M8-fold and M8-fold approximant.

Table 6.1 representing all changes we applied on original 8-fold to obtain modified 8-fold (M8-fold). We choose only a quarter of structure (green square), because, due to rotational symmetry all of mentioned dimensions and sizes repeat rotationally. We labeled the holes of pristine structure with numbers and M8-fold structure with letters. (We chose Λ_1 as the reference of metrics, since $\Lambda_1 = \Lambda$ for both 8-fold and M8-fold).

8-fold hole	Radius of hole	Position of hole	M8-fold	Radius of hole	Position of hole
1	0.37Λ	(0,-Λ)	A	0.43 Λ	1.2×(0,-Λ)
2	0.37Λ	$(sin\left(\frac{\pi}{4}\right),- sin\left(\frac{\pi}{4}\right))$	B	0.43 Λ	$1.2 \times (sin\left(\frac{\pi}{4}\right),- sin\left(\frac{\pi}{4}\right))$
3	0.37Λ	(Λ, 0)	C	0.43 Λ	1.2×(Λ, 0)
4	0.37Λ	$(\sin(\frac{\pi}{4}),-(1+\cos\left(\frac{\pi}{4}\right)))$	D	0.37 Λ	$(\sin(\frac{\pi}{4}),-(1+\cos\left(\frac{\pi}{4}\right)))$

5	0.37Λ	(1+cos $\left(\frac{\pi}{4}\right)$,-(1+cos $\left(\frac{\pi}{4}\right)$))	E	0.60 Λ	(1+cos $\left(\frac{\pi}{4}\right)$,-(1+cos $\left(\frac{\pi}{4}\right)$))
6	0.37Λ	((1+cos $\left(\frac{\pi}{4}\right)$), $-\sin(\frac{\pi}{4})$)	F	0.37 Λ	((1+cos $\left(\frac{\pi}{4}\right)$), $-\sin(\frac{\pi}{4})$)
0	0.37Λ	(0,0)	O	0.72 Λ	(0,0)
$S_{AFF} = 0.52\%$			$S_{AFF} = 0.78\%$		

Table 6. 1: The comparison of position and radius of geometrical component of 8-fold structure and M8-fold lattice.

As a results of modification, as the modified 8-fold (M8-fold) unit cell is plotted in figure 12.(b), it is clear that in the modification process we will have different pitches $\Lambda_1, \Lambda_2, \Lambda_3$ *and* Λ_4 with some relationship in between such as $\Lambda_4 < \Lambda_1 = \Lambda < \Lambda_2$ and $\Lambda_3 < \Lambda$ and 4 different radii r_1, r_2, r_3, and r4 (see table 6.1 and figure 6.12 (b), In this work we apply the changes and increase the size of capillaries as much as possible, redefining four different radii as $r_1 = 0.72\Lambda, r_2 = 0.37\Lambda, r_3 = 0.6\Lambda$, and r_4=0.43Λ, Consequently these changes improve air filling up to S_AFF=78.3%, slightly lower than the 12-fold one.

The cross section of M8-fold fiber in figure 6.13 (a) is constructed by replicating a big portion of M8-fold structure as it is depicted. While the air core is achieved by the removal few capillaries with core radii of R=1.38Λ in figure 6.13.

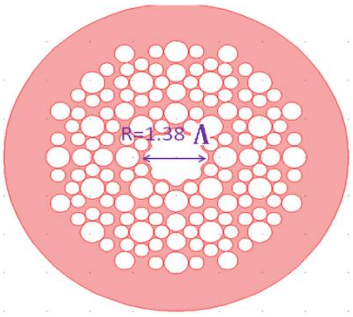

Figure 6. 13: Cross section of M8-fold HC-PQF, with core radius of R=1.38Λ.

6.3.2 Band gap calculation for M8-fold design

In this section we present the band analysis of M8-fold lattice. The approximant to analysis band structure is defined as shown in figure 6.12 (b), the geometrical details of the structure has been defined comprehensively, in previous section. In what follows, the band structure are considered for M8-fold structure with mentioned approximant

(which contains 14 cylinders) and the approximant size is a square with the edge size of L=2+√2 as shown in figure 6.12 (b).

The photonic band structure of a crystal based on such approximant is calculated by applying periodic boundary condition at the sides of square approximant. The periodicity is defined by $R = l_1\, a_1 + l_2\, a_2$ where l_1 and l_2 are integers and $a_1 = (L, 0), a_2 = (0, L)$ are translational vectors.

The photonic bandstructure of a QC based on mentioned approximant in figure 6.12 (b) has been calculated by applying periodic boundary conditions at the edges of the square unit cell and using Bloch theorem. It should be mentioned that the resulting structure is not pure quasicrystalline, but rather pure periodic one, actually a short-range eight-fold rotational symmetry within the approximant is reflected. On the other hand a sort of aperiodicity is added to structure inherited from different capillaries size.

Study of photonic Bandgap for optical fibers requires to calculate band structure of a 2-D quasicrystal with present of out of plane wave vector which is well discussed in chapter 4 and 5. The M8-fold case has been analyzed via FEM and results of band structures is presented in figure 6.14(a), (b), for $\frac{k_z\, \Lambda}{2\pi} = 1.45$ and $\frac{k_z \Lambda}{2\pi}$=1.65 respectively.

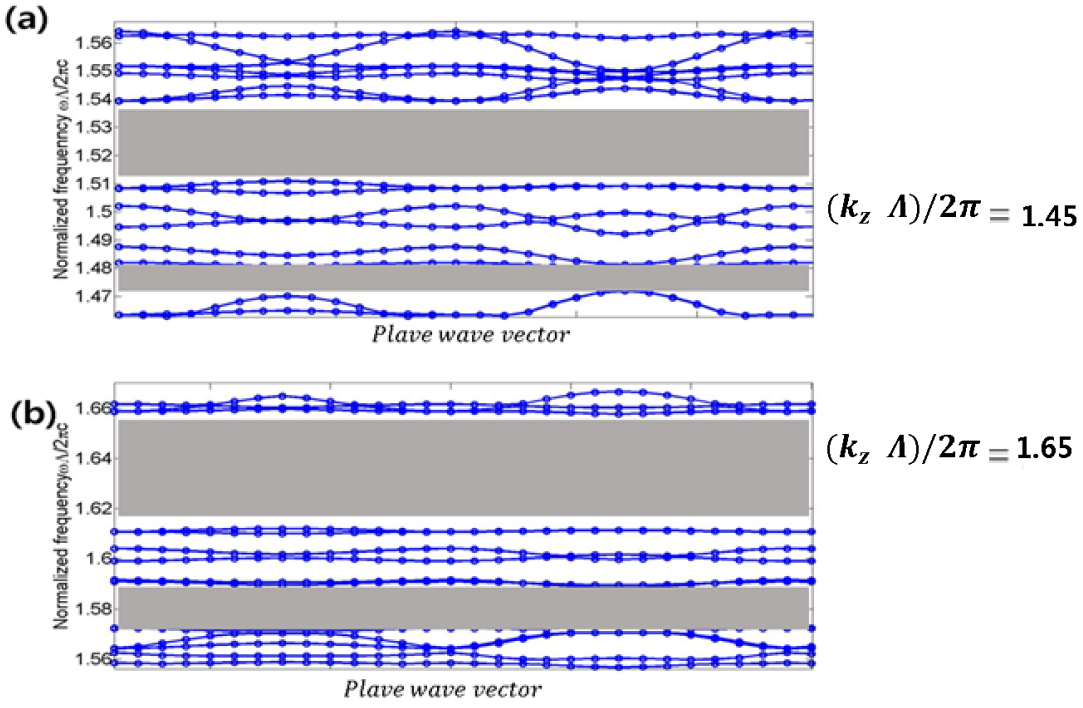

Figure 6. 14: Band structure of a 2-D, M8-fold symmetry with employing a square approximant for different out of plane wave vector, (a) $\frac{k_z\, \Lambda}{2\pi} = 1.45$(*b*) $(k_z\ \Lambda)/2\pi = 1.65$.

Our calculations show that band-gap's width (shaded regions in figure 6.14(a), (b)) increases, while the out of plane wave vector increase. The gaps which are detectable in figure 6.13 (a) with $\frac{k_z \Lambda}{2\pi} = 1.45$ and we can observe the increase of band gap with increasing the out of plane wave vector in figure 6.14 (b) corresponding$\frac{k_z \Lambda}{2\pi} = 1.65$.

The FEM method used in the calculation of the bandstructure of figure 6.14 permits to calculate of the electromagnetic field profiles of individual eigenfrequencies. Figure 6.15 shows examples of such profiles. In figure 6.15, the electromagnetic field profile is shown for the approximant of containing 14 cylinders. The particular state is shown at the $k_x = 0.5, k_y = 0.5 \; and \; k_z = 1.9$ point in reciprocal space, and have frequencies of $\frac{\omega \Lambda}{2\pi c} = 2.19$, $\frac{\omega \Lambda}{2\pi c} = 1.92$, $\frac{\omega \Lambda}{2\pi c} = 2.04$ in figure 6.15 (a), (b), (c) respectively. Different fields profile, are approving 8-fold symmetry. In case of bands where they represent the majority of electromagnetic energy on the edges, which means the electromagnetic waves consider edges of structure as defects of quasicrystal.

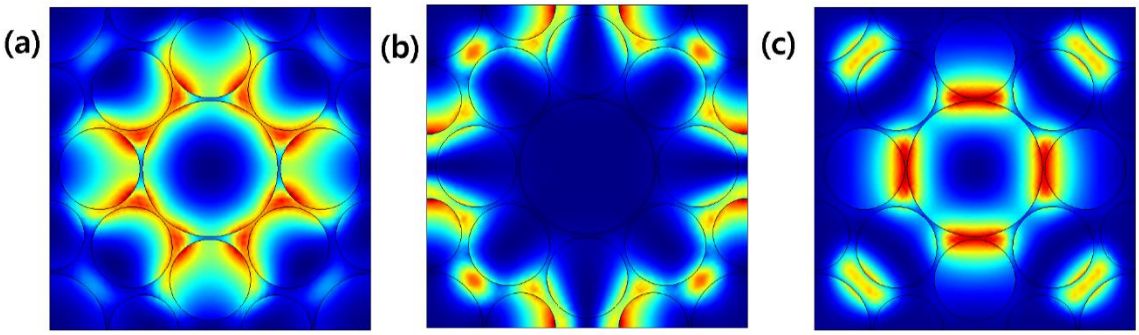

Figure 6. 15: Electromagnetic field profile calculated for a structure with 14 cylinders with $S_{AFF} = 82\%$. the field profiles are belong to eigenfrequencies of (a) ωΛ/2πc=2.19, (b) ωΛ/2πc=1.92, (c) ωΛ/2πc=2.04 at certain reciprocal vector k=(0.5,0.5,1.9).

Band gap map of the M8-fold structure as a function of out of plane wave vector has been calculated for wavelength range with $\frac{\lambda}{\Lambda} < 1$ and it is illustrated in figure 6.16. Two different presentation of band map as a graph of effective index vs. normalized wavelength in figure 6.16 and normalized frequency vs. out of plane wave vector (inset) are shown. It is worth noting that there are two PBGs (shaded regions figure 6.16) in $\frac{\lambda}{\Lambda}$<1.

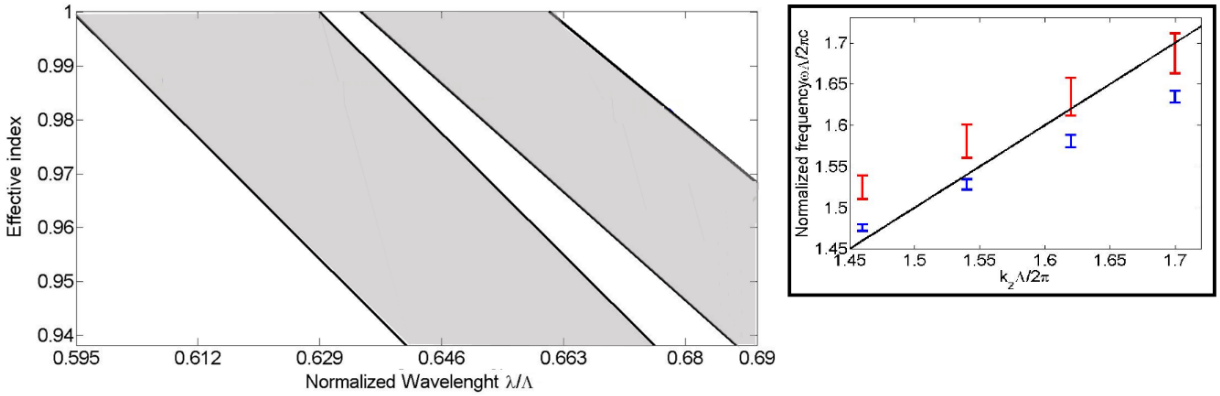

Figure 6. 16: The band map as a function of effective index and (inset) band map with eigenfrequeny presentation (blue and red error bars represent bandgap).

6.3.3 Modal analysis and results of M8-fold HCPQF

M8-fold HC-PQF is designed and investigated. Fundamental mode for the HC-PQF with the core size of R=1.38Λ has obtained throw FEM method. Figure 6.17 depicting effective index of fundamental mode confined in the core. The results representing a good confinement due to dispersion curve close to air line and a quasi-linear behavior.

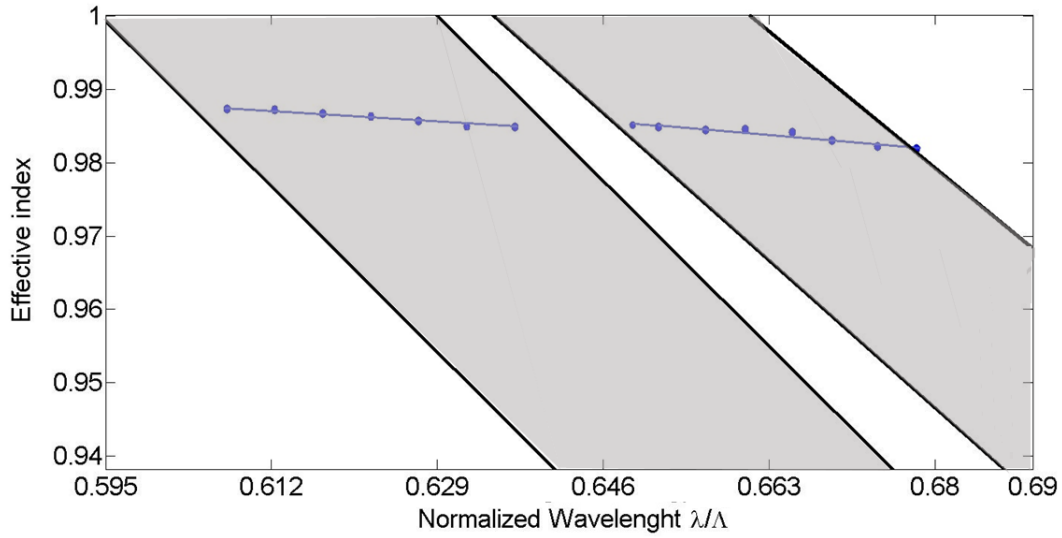

Figure 6. 17: Represent effective index of fundamental mode of M 8-fold HC-PQF.

6.3.4 Electromagnetic field profile for M8-fold

The intensity of electromagnetic field of the fundamental mode of M8-fold HC-PQF in both photonic bandgaps, are depicted as the measure of poynting vector. The intensity

of electromagnetic profile in both photonic bandgaps, for λ/Λ=0.628 and λ/Λ =0.671, are plotted in figure 6.18 (a) and 6.18(b), respectively.

As it is presented the fields are well confined in the air core and, especially in M8-fold, the field profile surface is not approaching the edge of the core-cladding interface. M8-fold fibers there is no surface mode observable and the circularity of the fundamental modes is remarkable.

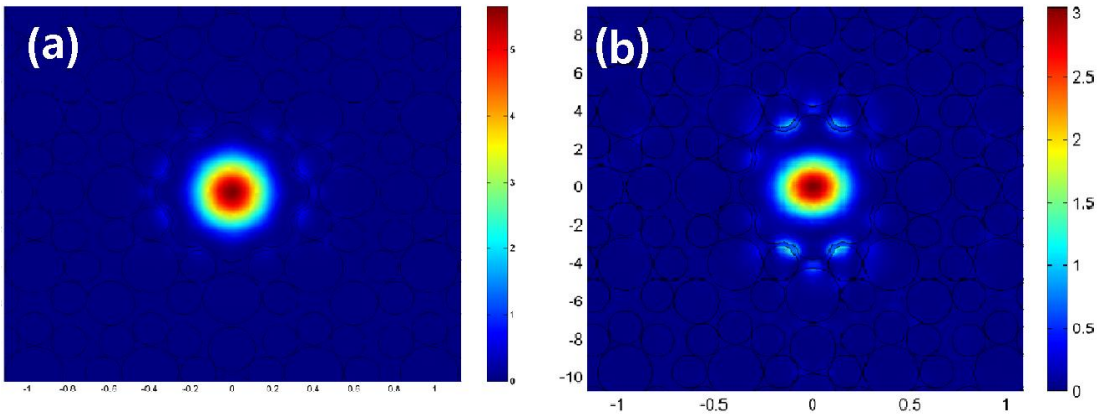

Figure 6. 18: The field profile of the fundamental mode in case of M8-fold fiber at (a) λ/Λ=0.628, (b) λ/Λ =0.671.

6.3.5 Confinement loss for M8-fold HC-PQF

The confinement loss of fundamental mode of the fiber in both PBG are calculated by the full-vector finite- element method (FEM) with considering a circular perfectly matched layer (PML) [12]. Due to finite numbers of air holes in the cladding, modes always suffers by some leakage loss. Figure 6.19 illustrates the leakage loss of fundamental mode as a function of normalized wavelength for HC-PQF for modified 8-fold HC-PQF. The confinement loss in complete agreement with bandgap behavior. increasing the number of layers are so important to heal this unfortunate, since the loss decreases almost linearly on a logarithmic scale with respect to cladding ring number [12]. We can see that there are two lowest loss central frequencies in the PBG region. Therefore, we can obtain simultaneous guidance of two span wavelengths with low loss in a single fiber.

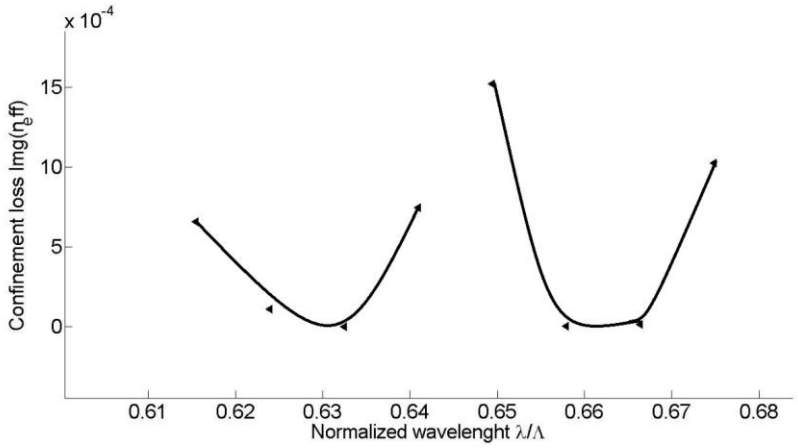

Figure 6. 19: represents confinement loss for M8-fold HC-PQF.

6.4 Summary

In conclusion, we have proposed two new kinds of HC-PQFs, with air holes arranging in 12-fold (from paper [12]) and properly modified 8-fold quasi-periodic structures. Both fibers have presented two major PBGs in the range $\lambda/\Lambda<1$. We have analyzed bandgap formation and dispersion curves of the fundamental mode as well as the intensity of electromagnetic profile of the fundamental mode. Confinement loss has been studied.

Bibliography

1. P. V. Kaiser, H. W., Astle, “Low-loss single material fibers made from pure fused silica,” Bell Syst. Tech. J. 53(6), 1021-1039 (1974).
2. J. C. J Knight, T. Birks, P.st.J. Russell, and D. M. Atkin, “All-silica single-mode fiber with photonic crystal cladding,” Opt. Lett. 21(19), 1547-1549 (1996).
3. A. Cusano, D. Paladino, andA. Iadicicco, “Microstructured Fiber Bragg Gratings,” Journal of Lightwave Technology 27(11), 1663-1697 (2009).
4. L. Vincetti, F. Poli, and S. Selleri, “Confinement loss and nonlinearity analysis of air-guiding modified honeycomb photonic crystal fibers,” IEEE Photonics Technology Letters 18(3), 508–510 (2006).

5. P. Ghenuche, H. Rigneault, and J. Wenger,"Hollow-core photonic crystal fiber probe for remote fluorescence sensing with single molecule sensitivity," Optics Express 20(27), 28379-28387 (2012)
6. A.Iadicicco, S. Campopiano, A. Cusano., "Long-Period Gratings in Hollow Core Fibers by Pressure-Assisted Arc Discharge Technique," IEEE Photonics Technology Letters 23(21), 1567-1569 (2011)
7. M. E. Zoorob,M.D.B Charlton,G. J. Parker,J. J. Baumberg, and M.C. Netti, "Complete photonic bandgaps in 12-fold symmetric quasicrystals," Nature 404, 740-743 (2000)
8. M. Florescu, S. Torquato, and P. J. Steinhardt,"Complete band gaps in two-dimensional photonic quasicrystals," Physical Review 80, 155112 (2009).
9. A. Ricciardi,I. Gallina, S. Campopiano,G. Castaldi,M. Pisco,V. Galdi,V. , A. Cusano, "Guided resonances in photonic quasicrystals," Opt. Express 17,6335-6346 (2009)
10. A. Ricciardi, M. Pisco, A. Cutolo, A. Cusano, "Evidence of guided resonances in photonic quasicrystal slabs," Phys. Rev. B 84, 085135 (2011).
11. S. Kim, C. Kee., and J. Lee, "Novel optical properties of six-fold symmetric photonic quasicrystal fibers," Opt. Express 15, 13221–13226 (2007)
12. X. Sun, and D.J.J Hu, "Air Guiding With Photonic Quasi-Crystal Fiber," IEEE Photonics Technology Letters 22(9), 607-609 (2011)
13. S. Light, F. Couny, Y.Y Wang, N.V. Wheeler, P.J. Roberts. , and. Benumbed, "Double photonic bandgap hollow-core photonic crystal fiber," Opt. Express 17, 16238–16243 (2009).

Chapter 7

Conclusion

In this thesis we defined two different road to reach single goal “Enhancement and Improvement of chemical optical fiber sensors”.

The work was divided into two general activity. The first one was aimed to experimentally demonstrate a novel technique based on UV assisted procedure to integrate a special class of functionalized materials such as porphyrin derivate with optical fiber technology. Here the sensing potentialities of novel fiber optic devises for environmental monitoring were presented. .

The second activity was aimed to design and analyze a new class of hollow core optical fibers where the micro-structured cladding region, responsible of the photonic bandgap, were based on quasicrystal patterns of hole-silica running along the fiber. We focalized our activity to photonic bandgap calculation and modal study of HC-PQF as function of the geometrical features.

In the very beginning we were motivated and excited with optical properties of porphyrin molecule, therefore an approach to employ optical properties of porphyrin pops in our minds. Consequently we started our work experimental on deposition technique for deposition of porphyrin by assistance of UV-light. We developed and designed an optical setup for adopting UV-assisted technique of deposition with optical fiber technology.

Two general molecule of porphyrin TpyP4 and TPPS were studied. Our microscopic observation admit the presence of thin film well-aligned to the fiber core. We characterize deposited film via reflectance spectroscopy. In both molecules and different UV-irradiation time. We claim the film thickness increases as time increases. We proof the possibility for deposition of different porphyrin molecule on optical fiber technology, obtaining a novel in fiber device for sensing Applications. Therefore the

deposited fiber with TPPS thin film is studied and investigated for acid vapor and alkaline sensing.

The reflectometry analysis for the deposited film trough optical fiber, leads to detection of J-and H-aggregate's spectral features. A strong intense peak at ~ 490 nm as spectral evident of J-aggregate. J-band and hence resonance light scattering presented a good selectivity for sensing of acid and base vapors. Dynamic response time of sensor represents order dynamic response of 1 minutes for acid detection and ~ 4s for base detection. Eventually sensing abilities of film with study of fluorescence features of thin film has been studied, the distinctive spectral features in acid and base vapor is investigated.

Finally as another investigation of in first part of my activity, we develop and modified the UV-induced technique to obtain a thin film of silver with a simple and effective procedure on the fiber end, the results depicting that uniform self-aligned film on distal end of fiber.

In second part of this thesis, we were wondered how with employing a hole-silica quasicrystal can be developed as optical fiber. On the other hand HC-PCF has proven new propagation mechanism. We studied at the beginning HC-PCF numerically and we presented simulation results for bandgap and modal study of an HC-PCF formed by a triangular lattice via finite element method.

Subsequently we designed two different Hollow core photonic quasicrystal fiber (HC-PQF) of 12-fold and modified 8-fold symmetry. It is worth highlighting, we proof in this thesis, 8-fold symmetry does not satisfy conditions for PBG propagation, and therefore the mentioned modified 8-fold is designed.

We proceed to band calculation for planar quasicrystal with non-zero out of plane wave vector... Results of this study represents optical fiber can be realized by 12-fold quasicrystal structure and modified8-fold due to band gaps opening at $\frac{\lambda}{\Lambda} < 1$. We would like to report two spectral windows opening for both modified 8- and 12-fold structures. This phenomenon is not achievable as easily in simple HC-PCFs while in quasicrystal studied structures it is happened properly. Modal study of modified 8-fold and 12-fold HC-PQF are studied and calculated.

I would like notice, which different method from bandgap calculation and modal study was employed, the result of propagated mode and bandgap meet each other.

The confinement loss is calculated for the fundamental mode with the same modal study. The results of confinement method shows an order of minimum loss for modified 8-fold is 10 times less than 12-fold structure.

I would like to conclude, a new class of, low loss, HC-PQF is possible to develop and lead to dual bandgap guiding mechanism. Several potential application is expected from new structures. We are proceeding to fabricate the new HC-PQFs and integrating porphyrin molecule in order to achieve another novel optoelectronic device for sensing application.

List of publications and scientific Production

Journal:

1. **Abolfazl Bahrampour,** Agostino Iadicicco, Giovanna De Luca, Michele Giordano, Anna Borriello, Antonello Cutolo, Andrea Cusano, and Luigi Monsù Scolaro,"Porphyrin Thin Films on Fiber Optic Probes through UV-light Induced Deposition", ***Optics & Laser Technology* , 49, 279-283,2013.**
2. A.R. Bahrampoura, M. Bathaeea, S. Tofighia, **A. Bahrampour,** F. Farmana, M. Valia, "Polarization maintaining optical fiber multi-intruder sensor", ***Optics & Laser Technology***, Volume 44, Issue 7, 2026–2031, October 2012, 2026–2031
3. **A. Bahrampour,** A. Iadicicco, A. Cutolo, A. Cusano "Novel quasi crystal hollow core fiber", **Optics Express ,** (in preparation)

International Conference:

- **A. Bahrampour**, A. Iadicicco, G. De Luca, M. Giordano, A. Cutolo, L. Monsù Scolaro, and A. Cusano, "Sensing Characteristics to Acid Vapors of a TPPS Coated Fiber Optic: a Preliminary Analysis" **proceeding** World Academy of Science, Engineering and Technology **Venice,November 2012**, https://www.waset.org/journals/waset/v71/v71-2.pdf
- **Abolfazl Bahrampour**, Agostino Iadicicco, Giovanna De Luca, Michele Giordano,Anna Borriello, Antonello Cutolo, Andrea Cusano, and Luigi Monsù Scolaro,"Porphyrin coated Fiber Optic Probes for Acid Vapor Detection," for poster presentation, European Workshop on Optical Fibre Sensors, 5th EWOFS'2013, 19 – 22 May 2013, Krakow, POLAND.
- **Abolfazl Bahrampour,** Agostino Iadicicco , Ali Reza Bahrampour, Stefania Campopiano, Antonello Cutolo, Andrea Cusano "Design and Analysis of Photonic Quasi-Crystal Hollow Core Fibers ," for poster presentation,European Workshop on Optical Fibre Sensors, 5th EWOFS'2013, 19 – 22 May 2013, Krakow, POLAND

Thesis Co-Totur:

Massimo Saviano, "***Sensori in Fibra Ottica con Strati Sottili di Porfirina: Studio di Fattibilità",*** *Corso di* ***Laurea Magistrale*** *in Ingegneria delle*

Telecomunicazioni Università degli Studi di Napoli "Parthenope" Facoltà di Ingegneria. Relatori: Stefania Campopiano, Agostino Iadicicco, Correlatori:Dott.ssa Giovanna de Luca, ***Abolfazl Bahrampour.***